SPRINGER BRIEFS IN
APPLIED SCIENCES AND TECHNOLOGY

Wilson Acchar
Eduardo J.V. Dultra

Ceramic Materials from Coffee Bagasse Ash Waste

Springer

SpringerBriefs in Applied Sciences and Technology

More information about this series at http://www.springer.com/series/8884

Wilson Acchar · Eduardo J.V. Dultra

Ceramic Materials from Coffee Bagasse Ash Waste

Springer

Wilson Acchar
Department of Physics Campus
Universitario, S-N
Federal University of Rio Grande do Norte
Natal, RN
Brazil

Eduardo J.V. Dultra
Campus Eunapolis
Instituto Federal de Educação
Ciência e Tecnologia da Bahia
Eunapolis, BA
Brazil

ISSN 2191-530X ISSN 2191-5318 (electronic)
SpringerBriefs in Applied Sciences and Technology
ISBN 978-3-319-15280-6 ISBN 978-3-319-15281-3 (eBook)
DOI 10.1007/978-3-319-15281-3

Library of Congress Control Number: 2015930730

Springer Cham Heidelberg New York Dordrecht London

Printed on acid-free paper

Springer International Publishing AG Switzerland is part of Springer Science+Business Media (www.springer.com)

Contents

Chapter 1
Introduction

Abstract This chapter presents the main topics that will be discussed in the book.

Keywords Porcelain tile · Coffee industry · Coffee hush ash · Properties

Porcelain stoneware tile is the class of ceramic coatings of highest added value in the market of floors and coatings due to its excellent technical characteristics. This condition allowed manufacturers of porcelain stoneware tiles to invest in technology for control and automation of the manufacturing process of their products. Strict criteria in the selection and purchase of raw materials have also been established. The commercial value of a product, in any situation, is crucial for its marketing; however, in relation to porcelain stoneware tile, product quality is also critical to its acceptance in the consumer market.

Seeking better competitiveness, manufacturers invest in research to better understand the factors and processes that influence the properties of the final product and to control them in order to obtain the desired microstructure. The challenge is to produce porcelain stoneware tiles in an economically viable way, and within the quality standards required by regulatory agencies.

Many researchers concentrated efforts to find a flux material, with technical and economic feasibility to allow its use in the manufacture of porcelain stoneware tiles. Flux material play an important role in the final microstructure of the ceramic coating. During firing, these materials form a liquid phase that fills the pores, decreasing porosity and water absorption, promoting the thermodynamic conditions for the growth of mullite crystals in acicular shape and contributing to increase the mechanical strength. However, to promote the desired effects, it is necessary that the liquid formed during burning has adequate amount and viscosity characteristics. Currently, feldspar is the flux material most widely used by porcelain manufacturers, since it is responsible for obtaining products with excellent technical and aesthetic properties. Costs with the purchase of feldspar significantly contribute to the final product price. According to some studies, some flux materials can keep the technical properties or even improve them, but compromise the

W. Acchar and E.J.V. Dultra, *Ceramic Materials from Coffee Bagasse Ash Waste*, SpringerBriefs in Applied Sciences and Technology,
DOI 10.1007/978-3-319-15281-3_1

aesthetic of the product, restricting its use only in glazed porcelain tiles. When the aesthetic factor is essential, such as the manufacture of polished porcelain tiles, the proportion of feldspar in the ceramic mass can reach 50 % by mass. Flux materials that allow decreasing this ratio without impairing the technical properties and favorable regarding the availability and costs of acquisition are well accepted by manufacturers. Thus, many industrial and agricultural wastes have potential to be investigated in order to assess its use in ceramic masses in general and also in the manufacture of porcelain stoneware tiles. Thus, the environmental is also favored, since besides the recovery of waste, once discarded, the extraction of a natural raw material is reduced.

Brazil is the largest coffee producer in the world, responsible for over 30 % of world's production. The process of coffee processing produces waste and the main and of largest amount produced is the coffee bark. Domestic production generated approximately 2,668,780 tons of coffee husks in the 2011 harvest, since for each kg of processed coffee 1 kg of husk is obtained. Coffee husk ashes are obtained when the husks are burned to generate heat for drying the fruit. These ashes are produced in large amounts by farms that use mechanical dryers, and use coffee husks as fuel. Coffee husk ashes are usually discarded by farmers randomly, without proper treatment and in places near the farms, often at roadsides, rivers and streams. Coffee husk ash has large amounts of potassium oxide (K_2O), and to a lesser extent, calcium oxide (CaO) and magnesium (MgO). Together, these alkali oxides and earth alkaline account for almost 95 % of the material, giving it flux characteristic, that is, it melts at lower temperature when compared to clay minerals.

The aim of this book is to show the possibility of reducing the consumption of feldspar in the production of porcelain stoneware tiles by adding coffee husk ash byproducts as flux material in the industrial ceramic mass. This book is divided in nine chapters (Introduction, Porcelain Tile, Solid Waste Materials, Coffee Industry in Brazil, Using CBA in Ceramic Formulations, Theoretical Analysis of Crystalline Phases, Physical and Mechanical Properties of CBA incorporated Materials, Mullite and Leucite formation), where results and discussion about this probability were shown.

The raw materials investigated were collected directly in a manufacturer of glazed porcelain tiles located in the municipality of Dias d' Ávila, state of Bahia. The compacting pressure, firing temperature and holding time parameters were the same as those used in the company. For comparison purposes, a standard mass (SM) with raw materials in the same proportion used by the company and with no addition of the coffee waste were analyzed.

Chapter 2
Porcelain Tile

Abstract This chapter described all features and characteristics of the porcelain tile such as the raw materials and the ceramic processing to produce the porcelain as well as some properties defined by the norms. Some aspects of pressing, drying and fire are also presented.

Keywords Porcelain tile · Ceramic processing · Norms

Porcelain stoneware tile is without doubt the class of ceramic coating which most evolved in recent decades, both in terms of technical properties as in relation to marketing. According to Heck (1996), porcelain stoneware tile emerged in the 1980s, being basically used in industrial and commercial flooring with very few color options and manufactured in small formats. The author mentions two important changes in the porcelain industry that allowed this evolution. The first was the replacement traditional tunnel ovens by modern roller ovens, allowing the manufacture of products with large formats, the most significant change was the transformation of porcelain stoneware tile in a modern and versatile material through the polishing process and the introduction of decorating techniques.

Porcelain tile is certainly a product of higher quality compared to traditional stoneware, resulting from the use of carefully selected raw materials and processing procedures accurately controlled. The emergence of the porcelain tile is partly associated with a conceptual and technological development in all the phases of the production process, from the reformulation of masses to the redefinition of the firing cycles, and also to the development of coloring and decorating techniques (Oliveira 1998).

The porcelain designation is sufficient to define the origins and characteristics of the product. Indeed, in the ceramic terminology stoneware indicates a very compact material composed of various crystalline phases dispersed in a glassy matrix, while the adjective porcelain has an etymological root in the term porcelain, the noblest ceramic material in evidence and appreciated for centuries (Oliveira 1998). According to Biffi (2002), porcelain tile is the product that offers the highest

W. Acchar and E.J.V. Dultra, *Ceramic Materials from Coffee Bagasse Ash Waste*, SpringerBriefs in Applied Sciences and Technology,
DOI 10.1007/978-3-319-15281-3_2

possible interventions on the production lines and with which ceramic technicians have acquired the pleasure of "making pottery" because they can invest in this product all the expertise they have. Therefore, large sums are invested in research for product innovation and process innovation for ceramic plates of porcelain tiles. According to Heck (1996), porcelain tiles stand out due to the following features:

- High abrasion strength;
- Resistance to frost;
- Resistance to acids and alkalis;
- Uniformity of colors;
- Waterproofing;
- Easy maintenance;
- Various composition possibilities.

It is noteworthy that the excellent technical properties of porcelain tiles are achieved through careful control of the entire ceramic processing, which starts in the careful selection of raw materials and final inspection for packaging and shipping of the product. All that is required to obtain the desired microstructure, which should be as compact as possible, with minimum porosity and exclusively closed, i.e., any existing pores must be closed without interconnection with the outside of the ceramic body. Thus, with the desired microstructure, the desired properties and quality of the manufactured product are maximized. The accurate control of ceramic processing with a firing temperature ranging from 1,200 to 1,250 °C, are the factors responsible for the high added value of porcelain tiles.

In Brazil, ceramic coatings are classified according to NBR 13817 using solely water absorption (WA) as a parameter for the classification of ceramic coating as described in Table 2.1.

According to NBR 13817, porcelain tile belongs to the ceramic group Bla, with AA less than or equal to 0.5 %.

WA is a property that measures the amount of water that the ceramic body is able to absorb within a normalized period of time. To be determined through an extremely practical test and also reveal a notion of the ceramic body behavior in relation to porosity, WA was for a long time, the main parameter to classify a ceramic plate. Intuitively, the lower the WA, the more compact and dense the material microstructure; this was the way the porcelain quality was assessed until the NBR 15463 entered into force in February 2007. This standard is specific for porcelain tiles and determines the minimum values of the main properties that the product should achieve. According to ANFACER, NBR 15463 is the

Table 2.1 Classification of ceramic tiles according to NBR 13817

Water absorption (%)	Extruded	Presssed	Others
WA < 0.5	Al	Bla	Cl
0.5 < WA < 3		Blb	
3 < WA < 6	Alla	Blla	Clla
6 < WA < 10	Allb	Bllb	Cllb
WA < 10	Alll	Blll	Clll

Table 2.2 Classification of porcelain tiles according to NBR 15463

Physical properties		Units	Product area < 50 cm^2		Product area > 50 cm^2	
			Technical	Glazed	Technical	Glazed
Water absorption	Mean	%	≤0.1	≤0.5	≤0.1	≤0.5
	Individual (max)	%	0.2	0.6	0.2	0.6
Flexural strength	Mean	MPa	≥45		≥45	≥37
	Individual (min)	MPa	42		42	35
Rupture load	*e < 7.5 mm	N	≥1,000		≥900	≥900
	*e ≥ 7.5 mm	N	Not applied		≥1,800	≥1,500
Abrasion resistance (not glazed)		mm^3	≤140	Not applied	≤140	Not applied

**e* thickness

first specific standard for porcelain tiles in the world and aims to raise the quality of products and protect consumers from misuse of the term "porcelain tile" about products whose characteristics do not comply with the new Brazilian standard. This standard defines "porcelain tile" as: "Ceramic plates for coating consisting of clays, feldspars, and other inorganic raw materials. It is intended to coat floors and walls, and can be shaped by pressing, extrusion, or other processes. The manufacturing process involves a high degree of grinding, high content of fluxing raw materials and high densification upon firing, resulting in products with low porosity and high technical performance. It can be glazed or not, polished or natural, rectified or not. Porcelain tile may have various dimensions: Small (product area < 50 cm^2), intermediate (50 cm^2 < Product area < 2,500 cm^2) or large size (product area > 2,500 cm^2)".

NBR (Brazilian Norm) 15463 divided porcelain tiles into two categories: technical porcelain tile and glazed porcelain tile and also added other technical properties such as "performance evaluators," apart from water absorption (wa). Table 2.2 shows the main properties and characteristics of porcelain tiles according to NBR 15463.

Therefore, NBR 15463 undoubtedly provides the classification of porcelain tiles using physical properties (water absorption, flexural strength, abrasion resistance, and tensile strength) and chemical properties and parameters (resistance to staining and to chemicals) and geometry of plates (side straightness, orthogonally, central and lateral bending, and twist).

2.1 Ceramic Processing of Porcelain Tiles

2.1.1 Raw Materials

Ceramic coverings are manufactured by ceramic processing from the dust, where a mixture of raw materials, known by ceramists as "ceramic mass," undergoes a sintering process (Petzold 1992). A ceramic mass for porcelain tile production

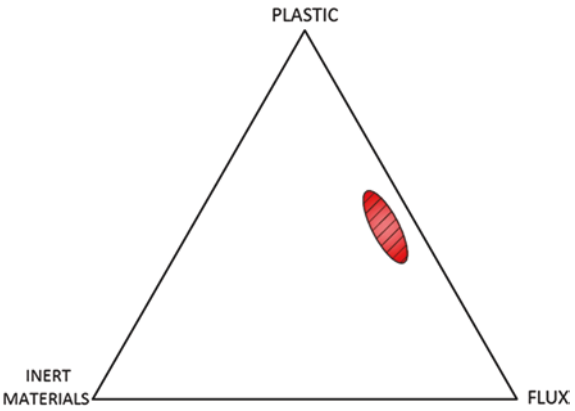

Fig. 2.1 Ternary diagram highlighting the region of compositions of a ceramic mass

consists of raw material of distinctive characteristics, which can be classified into three main groups: (a) plastic, (b) fluxing agents and (c) inert materials, with compositions ranging within the region shown in the ternary diagram of Fig. 2.1.

The plastic materials used are clay and kaolin, which main function is to provide plasticity to the mass and therefore green resistance to the pressed body. The main flux materials used are feldspar, talc and pyrophyllite, whose main role is to produce liquid phase during sintering. As inert raw materials, quartz is undoubtedly the most common due to its immense availability, and as inert materials, they essentially remain inert during the firing cycle and are used mainly for the purpose of improving the dimensional stability after firing. Detailed information and features of each raw material are described below.

Every ceramist knows that a classical whiteware must have clay (50 %), feldspar (25 %), and flint (25 %). The main function of the clay is to provide plasticity and workability to form different suitable shapes. The feldspar acts as a flux during firing and the flint, usually quartz is inert filler, providing strength to the dried and fired specimens (Brownell 1976; Acchar 2006).

2.1.2 Clay

According to Santos (1989), clay is a natural, earthy and fine-grained material, which generally acquires certain plasticity when moistened with water; chemically, clays are composed of hydrated silicates of aluminum, iron and magnesium, containing certain amounts of alkali and alkaline earth elements. There is considerable variation in the terminology of clay minerals in various scientific and technological fields that use this material. As described above, plasticity is the main reason for the use of clays for ceramic masses, and according to Santos (1989), plasticity in clays is mainly a result of attraction forces between clay particles and the lubricant action of water between anisometric lamellar particles. It could be assumed

that plasticity develops when clay has enough water to cover the entire accessible surface of clay minerals with a film that acts as a lubricant facilitating the sliding of the plates on each other when a shear stress is applied. Como-oriented water molecules are trapped on the surface of the clay minerals through hydrogen bonds, they also serve to bind clay particles to each other in the wet clay form, giving rise to various forms of mechanical strength of the green clay.

Biffi (2002) states that in addition to plasticity, clays used in ceramic masses for porcelain tiles need to present additional features as below:

- To provide light coloring during firing;
- To provide rheological properties facilitating flow;
- To provide with the flux characteristics a good density in firing;
- To provide excellent mechanical characteristics in firing.

To meet the characteristics described above, especially in relation to the light coloring during firing, kaolinite clays are preferably used, evaluated as little plastic as compared to the group of illite and montmorillonite clays.

2.1.3 Kaolin

The kaolin name derives from Kau-ling, China location from which the first samples were extracted. Kaolin is mainly composed of kaolinite. Kaolinite is a clay mineral whose chemical formula is $Al_2O_3{\cdot}2SiO_2{\cdot}2H_2O$ and has highly refractory behavior after firing (Biffi 2002).

In many situations, kaolin used in the production of porcelain tile in Brazil is obtained from the processing of kaolinite clays in order to increase the percentage of kaolinite and reduce the content of impurities. Importantly, the main characteristic of kaolin for use in ceramic masses for the manufacture of porcelain tiles is its whiteness. This feature directly influences the market value of the product as it is a great indicator of the material purity, and the higher its whiteness, the brighter the appearance of the ceramic mass after firing. According to Biffi (2002) in addition to providing whiteness to the ceramic mass, kaolinite is a basic supplier of aluminum oxide (Al_2O_3), which during the glazing phase of the ceramic mass, becomes a regulator of the equilibrium of reactions. In fact, alumina can take part in the formation of a silicon aluminous glassy phase in association with alkaline fluxing elements or also found predominantly at the end of the firing process as mullite ($3Al_2O_3{\cdot}2SiO_2$), which due to its needles morphology, acts as a "skeleton" to products obtained contributing to increase the mechanical strength.

The light color of the porcelain tile samples is desired by manufacturers and is caused by the interaction of Fe_2O_3 and TiO_2 with pigments and dyes, resulting in deviations in color of glazed samples. According to Moraes et al. (2007), ceramic kaolin must have kaolinite content between 75 and 85 % and absence of minerals affecting the firing color such as hematite (Fe_2O_3), whose content should be less than 0.9 %, so that the whiteness index after firing is within the range from 85 to 92.

2.1.4 Feldspar

According to Biffi (2002), feldspars are defined as silicon aluminates of alkali and alkaline earth metals. From the chemical point of view, they are classified into the following types:

- Orthoclase $K(AlSi_3O_8)$ potassium feldspar;
- Albite $Na(AlSi_3O_8)$ sodium feldspar;
- Anorthite $Ca(Al_2Si_2O_8)$ calcium feldspar.

Feldspars play a fundamental role in ceramic masses for porcelain tile production. In fact, these minerals provide high vitrification and mechanical strength at the end of the firing process.

To achieve accurate water absorption and mechanical strength values, which characterize porcelain tiles, it is necessary to suppress open porosity and reduce closed porosity after firing. For this purpose, the use of fluxing raw materials in the ceramic mass is necessary, so that a liquid phase is formed before maximum firing temperature is reached. This liquid formed during firing must have adequate quantity and viscosity to promote the filling of the pores present in the ceramic body and also improve the reactivity between elements, so that the onset of sintering occurs at lower temperatures. The most characteristic behavior of this mineral is the remarkable fusibility and the formation, with other elements, of eutectic elements that enable achieving vitrification even at relatively lower temperatures. The basic element for the fluxing properties is the content of alkali in the mineral. The theoretical values of K_2O and Na_2O, respectively, in potassium and sodium feldspars are 16.9 and 11.8 %. The more the alkali content approaches the theoretical value, the higher the commercial value of the feldspar.

2.1.5 Pyrophyllite

Ceramic pyrophyllite or only pyrophyllite, is a very fine metasedimentary rock primarily composed of sericite, kaolinite and quartz, with alkali content of about 7 %, giving it fluxing characteristics. Due to its mineralogical and chemical nature, pyrophyllite shows no plastic and plastic properties and can compose up to 50 % of many ceramic masses of wet process, especially in industries in the state of São Paulo, favored for its relative abundance in the southern state (Motta et al. 1998).

2.1.6 Talc

Talc is not always present on ceramic masses to porcelain stoneware tiles. Talc is a magnesium silicate of formula $3MgO{\cdot}4SiO_2{\cdot}H_2O$ used in ceramic masses in varying amounts up to 4 % increased fusibility due to the formation of an eutectic

between talc and feldspar, giving better results in terms of resistance to staining and flexural modulus. P. Grosjean 1995 reports that the use of talc led to the following improvements:

- Resistance to stains (from values above 1.6 %);
- Improvement of the flexural modulus up to 30 %;
- It seems to favor the polishing operations when microporosity is minimal;
- Lowers the thermal expansion coefficient;
- Increased whiteness when in the presence of zirconium.

2.1.7 Quartz

Also known as 'sand,' quartz (SiO_2, with crystalline structure) is added to ceramic masses for porcelain tiles with the function of maintaining a siliceous skeleton in the mass when, due to the increasing temperature, the other components such as clay, kaolin, and feldspars soften. In addition, it is an important regulator of correct ratio between SiO_2 and Al_2O_3 to form mullite ($3Al_2O_3{\cdot}2SiO_2$). It can also play the role of regulator of contraction and deformations during firing when it forms a structure of grains that are slightly attacked by the surrounding mass (Biffi 2002).

Quartz is also present in the mineralogical composition in other raw materials: clays, kaolin, and feldspars. Thus, some attention should be given to the allotropic change that occurs during heating around 573 °C, when quartz shifts from α to β, and also in the cooling step when submitted to the same temperature and the inverse transformation occurs. During these allotropic transformations, expansions and contractions occur due to changes in the crystalline structure of quartz, resulting in internal defects such as microcracks. The α-quartz has rhombohedral structure and β-quartz form has hexagonal structure.

2.1.8 Dosage and Grinding

Dosage is performed at the time of preparing the load to be ground. To obtain the desired product, dosage is performed based on formulation developed at the laboratory (Barbosa et al. 2008).

Depending on the moisture content (wet basis) of each of the raw materials, the wet weight required is calculated (according to the formulation) and the scale is programmed. The addition of each raw material is manually performed with mechanical shovels up to the wet weight indicated by the scale. Plastic and nonplastic materials are alternately added to facilitate the discharge operation (Barbosa et al. 2008).

In the grinding operation, there is reduction of the particle size of raw materials. The result of this ceramic processing step influences not only the properties and

behavior of the mass in the following manufacturing steps, but also the quality of the final product after firing due to the close relationship with the sinterability of the ceramic mass.

In most industrial plants, porcelain tile manufacturing uses the wet process through discontinuous grinding (Ribeiro and Abrantes 2001; Barbosa et al. 2008). The particle size distribution of raw materials specifies the size of balls in the mill (large, medium, and small). The volume of balls is controlled by the addition of large- and medium-sized balls based on measurements of the level every month. This level is indirectly measured as the difference between the diameter of the mill and void space height. The grinding efficiency is checked usually after 5 h from start of batch production—through sieving of samples taken from the mill, and depends on the measurement of the percentage of residue on the sieve, bulk density, and flow time (Barbosa et al. 2008).

In the grinding step by wet method, the ceramic mass is called "slip" and viscosity must be such as to allow the total discharge from the mill by injecting compressed air. To control the slurry viscosity, deflocculants are added at the beginning of the charge of the mill. After milling, the slip follows to homogenization and to storage tanks.

2.1.9 Spraying

Briefly, it could be assumed that spraying is the transformation of an aqueous suspension of solid particles (slip) into dried particles by spraying the suspension inside a heated chamber. The sprayed slip droplets acquire a spherical shape by the action of strong pressure exerted and by the surface tension, and undergo rapid water evaporation (Ribeiro and Abrantes 2001). Currently, mixed flow atomizers are used, where the slip is sprayed first countercurrent to the hot air, and then in parallel, with capacity of 16,000 kg of dust/hour. Air heated by natural gas and forced circulation are used to extract water vapor and finer powder (Barbosa et al. 2008).

At this stage of processing, the homogeneity of moisture and particle size of the sprayed powder should be controlled because these variables can affect the uniformity and regularity of the ceramic body packaging after pressing and may cause changes in color and dimensions from one batch to another. According to Barbosa et al. (2008), defects in the final product such as twisted square, loop, black heart, peeling, dirty stamping, size variations, and cracks due to low mechanical strength may be associated with these variables.

The moisture content of the atomized powder is controlled by adjusting the inlet air temperature, pressure in the slip pump, or flow of the exhausting air through the exchange of worn pads. Negre et al. (2000) state that variations in the moisture content of the atomized powder is mainly responsible for small changes in the density of the green body, and consequently, differences in the dimensions of the fired product. The particle size is manually controlled using as measuring

devices, manual or electromechanical sieves. The atomized powder is continuously produced through conveyor belts to storage silos. The material remains in silos for at least 24 h in order to obtain homogeneous moisture.

2.1.10 Pressing

At this stage, the ceramic body is formed and assumes its final shape, taking into account the shrinkage after firing. So, as in all stages of the porcelain tile processing, the pressing stage has its importance because the positive or negative effects will be observed in the behavior of the material pressed in the following steps, and especially in the microstructure of the final product. The characteristics of the atomized powder, particularly particle size and moisture content can influence packaging during pressing. The highest possible packaging is desired in order to maximally reduce intergranular porosity, i.e., voids between particles. According to the literature, the higher the density of the green body, the greater the reactivity during firing. It could be inferred that the more particles are in contact with each other (high density values), the largest contact surface and then higher the possibilities of severe reactions during firing.

The conformation of the material is made by double-action differential uniaxial pressure. In the production of porcelain tiles, hydraulic presses with capacity of 2,000 tons with four cavities are used. The press has its own automatic pressure control and verifications are hourly performed (Barbosa et al. 2008). According to Biffi (2002), the compression pressure for the production of porcelain tiles must be between 350 and 450 kg/cm^2 because the density of particles must allow, during firing, oxidation of organic substances and removal of gases that are generated. Compaction pressures higher than 500 kg/cm^2, in some cases, can cause internal defects and thus increased porosity of the fired body.

2.1.11 Drying

Before the firing step, the green ceramic body must be dried, i.e., its moisture content should be reduced from approximately 5.5–6 % to less than 0.5 %. This is due to the very high heating rate to which pressed bodies are submitted. Moisture contents above this parameter would cause cracks, warps, and eruptions on the surface of the ceramic body due to rapid loss of water. According to Brownell (1976) and Barbosa et al. (2008), the drying operation is performed with vertical dryers by hot air circulating, which generates the required gradients, both for mass transfer and for heat transport.

The temperature at the dryer outlet, in general, ranges from 180 to 210 °C and then the pressed part is directed to glazing and decorating processes when it comes to the production of glazed and/or decorated porcelain tile. The heat transferred to

the green ceramic body assists in the drying step helps the impregnation and adhesion of the ceramic glaze, and especially the soluble salts used for decoration. In the production of polished porcelain tiles, the pressed material is not submitted to glazing and decorating steps, going straight from the dryer to the firing furnace.

2.1.12 Firing

As previously mentioned all stages of porcelain tile processing have their importance and influence the final characteristics of the product. However, the firing stage is undoubtedly the watershed of ceramic processing because the ceramic sintering, responsible for all changes in the microstructure of the material, occurs in this stage. It is also necessary to mention the vitrification phenomena through the formation of the liquid phase that flows to interstices filling the pores and when cooling, promotes the formation of a glass that results in a dense and durable body. The vitrification degree depends on temperature and cooking time, as well as on the composition of the body. The temperature at which the liquid phase is formed is reduced by adding fluxing agents such as feldspar. During firing, as the temperature increases, the ceramic body contracts, with consequent decrease in porosity, making it denser or sintered (Castro and Benthem 2013). At this stage, constriction occurs along the contact between neighboring particles. With the advancement of sintering, the pores tend to decrease and acquire more spherical shape. The sintering of clay minerals is conducted at temperature below the melting temperature, so that in general (without the use of fluxing agents), a liquid phase is present. Mass transport is achieved through diffusion of atoms from the particles within the material to constriction regions.

It should be accentuated that both sintering and vitrification occur by heating at high temperatures, but glazing cannot occur during sintering of a ceramic mass. Vitrification is directly related to the formation of the liquid phase and in the presence of elements that produce liquid phase at temperatures lower than the maximum firing temperature. These elements are commonly known as fluxes. Both phenomena result in densification and reduced porosity, favoring the mechanical properties.

Manufacturing ceramic bodies with maximum densification, extremely low water absorption, high resistance to flexure, abrasion, and stain are only achieved by adding fluxing elements to the ceramic mass, because the sintering of clays and kaolin is not enough to drastically reduce the porosity of ceramic bodies. The formation of liquid phase during heating with adequate characteristics of quantity and viscosity, minimal addition to filling the pores, anticipates and enhances chemical reactions and changes of phase and mass transport, i.e., the sinterability, and also promotes vitrification of the ceramic body. This is the difference between porcelain tiles and other ceramics classes for coating.

Another approach that should be highlighted refers to the formation of mullite from kaolinite. When heated at about 450 °C, kaolinite begins to lose structural

water, turning into metakaolin. This process occurs up to temperature of 600 °C, approximately. According to literature, with continued heating, close to 980 °C, metakaolin turns into a Si–Al spinel ($2Al_2{\cdot}O_3{\cdot}3SiO_2$) and nonreactive silica. If heating reaches temperatures between 1,000 and 1,100 °C, the spinel begins to transform into orthorhombic mullite 3:2 ($3Al_2O_3{\cdot}2SiO_2$), known as primary mullite. When the temperature exceeds 1,250 °C, the spinel disappears and the appearance of a 3:2 mullite begins to be observed at acicular or needle shape, called secondary mullite (Restrepo and Dinger 2003; Santos et al. 2006). Restrepo and Dinger (2003) reports that mullite developed from Al–Si spinel, called primary mullite, forms large blocks and lamellar crystals and little contributes to increase the mechanical strength of porcelain parts. The crystallized mullite from the amorphous aluminum silicate phase, called secondary mullite grows in the shape of needles and help strengthen the system in the same way as fibers reinforce composites. The author also reports the secondary mullite crystals in the shape of needles only form from the melt material or in the presence of liquid phase.

It should be observed that the presence of flux materials in the ceramic mass also allows the crystallization of secondary mullite at lower temperatures (from 1,100 °C), since the liquid phase necessary for mullite crystallization in acicular format will be present before the maximum firing temperature is reached and, therefore, before the merger of clay minerals (Noni et al. 2010).

Currently, for the production of porcelain tiles, horizontal roller ovens with length of about 120 m are used, as well as natural gas as fuel to generate heat are used. The oven is divided into regions along its length, each of which has a thermocouple and a servomotor as actuator to automatically modify the air/fuel ratio in the corresponding burner (Barbosa et al. 2008). According to Biffi (2002), roll ovens allow a number of adjustments performed with the aid of microprocessors, able to avoid temperature differences between the center and sides of the oven, obtaining products with great geometric features. The firing cycle of porcelain tiles decreased considerably if compared to the cycles used in the mid 1990s, time at which there was a great production expansion and marketing of porcelain tiles.

The current firing cycles used by manufacturers of porcelain tiles comprise time intervals ranging from 40 to 60 min, with holding time from 6 to 8 min at

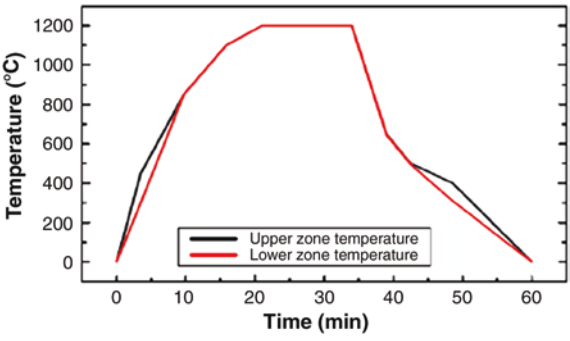

Fig. 2.2 Typical firing curve for porcelain tile

maximum firing temperature, between 1,190 and 1,230 °C, and according to Biffi (2002), this temperature may reach 1,250 °C for "super white" products containing refractory elements such as zirconium silicate and alumina. Figure 2.2 shows a typical firing curve of porcelain tile production, where heating, plateau, and cooling are observed.

2.1.13 Polishing

This step is performed only on unglazed porcelain tiles. Polishing step is an innovation in the production of ceramic tiles. Brightness is a feature quite sought by coating consumers, because besides the esthetic effect, it also facilitates cleaning.

During grinding and polishing, a layer with about 0.5–1.0 mm of thickness is removed (Oliveira 1998). However, parts submitted to polishing are more susceptible to staining because the removal of this layer exposes pores that were previously closed. According to Oliveira (1998), the existence of irregularities on the surface of a ceramic body causes particles to adhere to its surface and makes them more difficult to be removed. Relatively large pores (>60 μm) facilitate cleaning of the product but determine loss of esthetic appearance on the product surface, since these pores can be viewed with the naked eye. Other studies point out the pore diameter as the main cause for the incidence of stains on polished porcelain tiles (Arantes et al. 2001; Amorós et al. 2007). Alves and Baldo (1998) assessed which class of pore sizes was responsible for making the polished surface of the porcelain tile more susceptible to the staining phenomenon and found that parts that had the highest percentage of pores with diameters ranging from 5 to 20 μm were more susceptible to staining. The authors state that for surfaces with greater presence of pores with diameters below this range, the penetration of staining agents is more difficult, and for surfaces with greater presence of pores with diameters above this range, the removal of staining agents is facilitated.

References

Acchar W (2006) Materiais Cerâmicos: Caracterização e Aplicações. Ed. UFRN, Natal-RN

Alves WA, Baldo JB (1998) O Potencial de Utilização de um Resíduo Argiloso na Fabricação de Revestimento Cerâmico Parte I—Caracterização. Revista Cerâmica Industrial 3(1/2):34–46

Amorós JL, Orts MJ, García-Ten J, Gozalbo A, Sánchez E (2007) Effect of green porous texture on porcelain tile properties. J Eur Ceram Soc 27:2295–2301

Arantes FJS, Galesi DF, Quinteiro E, Boschi AO (2001) O Manchamento e a Porosidade Fechada de Grês Porcelanato. Revista Cerâmica Industrial 6(3):18–25

Barbosa DS, Silva JE, Machado RAF, Hotza D (2008) Controle e Automação na Indústria Cerâmica: Estudo de Caso na Fabricação de Porcelanato no Brasil. Revista Cerâmica Industrial 13(4):23–30

Biffi GO (2002) Grês Porcelanato: Manual de Fabricação e Técnicas de Emprego. Ed. Faenza Editrice do Brasil

Brownell WE (1976) Structural clay products. Springer, New York
Castro RHR, Benthem K (2013) Sintering, mechanisms of convention nanodensification and field assisted process. Springer, New York
Heck C (1996) Grês Porcelnato. Cerâmica Industrial 4:21–24
Moraes MLVN, Paskocimas CA, Nascimento RM (2007) Aproveitamento de Resíduo de Beneficiamento do Caulim na Produção de Porcelanato Cerâmico. Tese de Doutorado. Universidade Federal do Rio Grande do Norte, Natal-RN
Motta JFM, Júnior MC, Tanno LC (1998) Panorama das Matérias primas Utilizadas na Indústria de Revestimentos Cerâmicos: Desafios do Setor Produtivo. Revista Cerâmica Industrial 3(4–6):30–38
Negre F, Jarque JC, Feliu C, Enrique JE (2000) Estudo da Operação de Secagem por Atomização de Pós Cerâmicos em Escala Industrial: Seu Controle e Automação. Revista Cerâmica Industrial 5(2):47–52
Noni JRA, Hotza D, Soler VC, Vilches ES (2010) Influence of composition on mechanical behaviour of porcelain tile. Part I: microstructural characterization and developed phases after firing. Mater Sci Eng A 527:1730–1735
Oliveira APN (1998) Grês Porcelanato: Aspectos Mercadológicos e Tecnológicos. Revista Cerâmica Industrial 3:35–41
Petzold A (1992) Anorganisch-nichtmetallische Werkstoffe. Deutscher Verlag fuer Grundstoffindustrie
Restrepo JJ, Dinger DR (2003) Controle da Deformação Piroplástica em Massas de Porcelanas Triaxiais Usando a Análise Dilatométrica. Revista Cerâmica Industrial 8(4):37–48
Ribeiro JMPM, Abrantes JCC (2001) Moagem em Moinho de Bolas: Estudos de Algumas Variáveis e Otimização Energética do Processo. Revista Cerâmica Industrial 6(2):7–11
Santos PS (1989) Ciência e tecnologia das argilas, 2 edn., vol 1. Edgard Blucher, São Paulo, 408 pp
Santos HS, Kiyohara P, Coelho ACV, Santos PS (2006) Estudo por Microscopia Eletrônica das Transformações Durante a Queima de Argilas Altamente Aluminosas Brasileiras. Cerâmica 52:125–137

Chapter 3
Solid Waste Materials

Abstract In this chapter is described the definition and classification of the solid residues as well as an overview of the current Brazilian legislation and a summary of the use of residues in the ceramic industry.

Keywords Solid residues · Brazilian legislation · Ceramic industry

According to estimates of the United Nations (UN), the world population reached 5 billion on July 11, 1987, and reached 6 billion people on October 12, 1999. This rapid and continued expansion of human impression on a planet that seems increasingly smaller has serious implications in almost every aspect of life. Now, 10 years later, it was estimated to be approximately 7 billion (Dultra and Acchar 2010).

It is not difficult and even intuitive to realize that the consequences of this growth directly affect the environment. The famous sustainability and the desired sustainable growth are still far from our current reality. However, we are reaching critical levels of environmental degradation and its effects and consequences can already be perceived in our lives. On the other hand, there is a world tendency to increase the stringency of environmental protection policies upgrading and improving laws and legal provisions.

The productive sectors of different countries are increasingly incorporating costs related to environmental issues, implying need for significant changes in production, trade, and consumption patterns. These changes are the response to strict legal control norms (national and international) associated with a new consumer profile (FIESP 2004).

The proper management of solid residues leads to the idea that reduction in waste generation results in the economy of raw materials and reduced operating costs (Coelho et al. 2011).

W. Acchar and E.J.V. Dultra, *Ceramic Materials from Coffee Bagasse Ash Waste*, SpringerBriefs in Applied Sciences and Technology,
DOI 10.1007/978-3-319-15281-3_3

3.1 Definition and Classification of Solid Residues

For the perfect understanding of the subject, it is necessary to differentiate terms "solid residues" and "waste". According to law 12.305/10, solid residue is any material, substance, or object resulting from human activities in society, whose final destination proceeds, is proposed to proceed or is required to proceed, in solid or semi-solid state, as well as gases and liquids in containers whose characteristics make it impossible to be released into public sewage systems or water bodies, or that require technically or economically unviable solutions in the light of best available technology. This definition is similar to that adopted by the Brazilian Association of Technical Standards (ABNT) through NBR 10004: 2004. Wastes are solid residues that after exhausting all possibilities of treatment and recovery by available and economically viable technological processes, will not present another possibility that the environmentally sound disposal (Law No. 12.305/10). Thus, solid residues should be referred to a process for reuse and/or recycling, and only after "exhausted all possibilities," and with the nomenclature of "waste" be forwarded to the "environmentally sound final disposal."

ABNT through NBR 10004: 2004 ranked solid residues as:

- Class I residues—Hazardous: residues that due to their physical, chemical, or infectious properties may offer:

  (a) Risk to public health, causing mortality, diseases, or increase their incidence;
  (b) Risk to the environment when improperly managed.

- Class II residues—Non-hazardous: These are subdivided into:

  – Class II A residues, not inert;
  – Class II N residues, inert.

According to NBR 10004: 2004, residues may be classified as Class II B and thus considered inert when not belonging to Class I (hazardous waste) and also when submitted to dynamic and static contact distilled or deionized water at room temperature, according to NBR 10006, do not present any of their solubilized constituents at concentrations higher than drinking water standards, except for appearance, color, turbidity, hardness, and taste.

3.2 Overview of Current Brazilian Legislation

In Brazil, trends of increasing environmental protection, from the point of view of legislation, may be evidenced by citing Law No. 12.305, published on August 2, 2010, which established the National Policy on Solid Wastes (PNRS) that among other requirements, establishes in its Article 54, the deadline of 4 years from the date of publication, that the environmentally sound disposal of waste through a "shared responsibility for the lifecycle of product" is implemented. For the

purposes of this law, the shared responsibility for the lifecycle of products includes manufacturers, importers, distributors and retailers, consumers, and holders of those responsible for urban sanitation and solid waste management.

One of the principles of PNRS (Law No. 12.305/10) is the recognition of reusable and recyclable solid waste as an economic good with social value, which generates jobs and income and promotes citizenship. Among the many goals of PNRS included in Article 7, the following are worth mentioning:

IV—adoption, development, and improvement of clean technologies in order to minimize environmental impacts;
VI—encouragement of the recycling industry, aimed at promoting the use of raw materials and inputs derived from recycled and recyclable materials;
XV—promotion of environmental labeling and sustainable consumption.
As instruments of PNRS described in Article 8, to ensure that objectives are achieved, the following should be highlighted:
VII—scientific and technological research;
IX—fiscal, financial, and credit incentives.

The law also provides in Articles 15, 16, and 18, the elaboration of Solid Waste Management Plans in federal, state, and municipal levels and determines the period of 2 years from the date of publication for states and municipalities to do so as a condition for access to federal funds aimed at businesses and services related to solid waste management services, or to be benefited by incentives or financing from federal credit entities or encouragement for such purpose. It also provides in Article 20 that the Solid Waste Management Plans are developed by the waste generator and establishes in Article 24 that it should be an integral part of the environmental licensing process of the project or activity.

In Brazil, the waste generator is responsible for the waste generated and the waste generator's responsibility for managing the waste generated is described in Article 10 of the National Policy on Solid Wastes (Law No. 12.305/10). Preferably, industrial waste should be treated and stored at the site where they were generated and have proper disposal in accordance with the legal norms and current techniques (Governo Federal 2011).

3.3 Use of Residues in the Ceramic Industry

The ceramic industry stands out in the recycling of industrial and urban wastes due to its high production volume that enables the consumption of large amounts of waste and that, allied to the physicochemical characteristics of ceramic raw materials and the particularities of ceramic processing, it allows the incorporation of a reasonable amount of such waste without impairing the properties of the final product. In addition, it obtains advantages in the production process with the incorporation of waste, reducing the consumption of high-quality raw materials, increasingly scarce and expensive, reducing energy consumption, and therefore reducing costs.

Segadães (2006) highlights a very important feature in the manufacture of ceramic products that are the high firing temperatures, usually equal to or greater than 1,000 °C, which can promote the blanketing of hazardous waste, which make the ceramic industry make an excellent welcoming of waste with distinct characteristics. According to Santos (1989), another feature is that some residues have composition similar to raw materials and often have elements that not only are compatible with the desired products but also bring benefits to the manufacturing process of ceramic materials.

In general, residues with potential use in the ceramic industry can be classified according to the role played in the manufacturing process such as: (a) fuel, with high levels of organic matter, which gives them high calorific value; (b) fluxes, which assist in the sintering of ceramic bodies (forming the glassy phase); (c) controlling plasticity, which influence the characteristics of the green body (Menezes et al. 2007; Segadães 2006). Segadães (2006), reports that most often, a residue produces one of the dominant effects described above; however, in some cases, the use of a residue can influence other features, in addition to its dominant effect.

According to Pinto (2004), for the recovery of a residue by the ceramic industry, some basic requirements are important:

- Selective and temporary storage in order to obtain batches of significant size and free from other types of waste;
- Mixing different batches in order to ensure good homogeneity;
- Pretreatment when needed, which usually involves simple operations such as milling, drying, deferrization, and calcination.

It is worth mentioning that a residue will only be used if the application brings significant benefits to the manufacturing process, either by reducing costs, either by facilitating any stage of the production process, or even by improving some characteristic of the manufactured product. Only the environmental "appeal" is not enough for the industrial sector to use waste as a raw material. However, the trend of environmental policies for environmental protection through legal provisions (such as Law No. 12.305/10), and greater awareness of the consumer class, result in a preference for environmentally friendly products can change this reality. Thus, the environmental labeling of a product can bring benefit such as "greater acceptance" in the market. Casagrande et al. (2008) claim that the concern for the environment has grown in recent years and several factors indicate this growth, among which: the increasing interest of the general public that gradually will make environmental label a marketing argument, the increase in the amount and level of civil society organizations dedicated to the subject, and the demand for environmental certification for Brazilian exporters, leading to changes even in the domestic industry. In this context, a product that uses waste to partially replace some natural raw materials has doubled environmental effect: first, its manufacture recovers waste, avoiding its disposal and environmental consequences, and second, there is the preservation of deposits of natural raw materials, decreasing the extraction volume and again, environmental consequences.

References

Casagrande CC, Sartor MN, Gomes V, Della VP, Hotza D, Oliveira APN (2008) Reaproveitamento de Resíduos Sólidos Industriais: Processamento e Aplicações no Setor Cerâmico. Revista Cerâmica Industrial 13(1/2):34–42

Coelho HMG, Lange LC, Jesus LFL, Sartori MR (2011) Proposta de um Índice de Destinação de Resíduos Sólidos Industriais. Eng Sanit Ambient 16(3):307–316

Dultra EJV, Acchar W (2010) Incorporação de Cinzas da Casca de Café na Produção de Placas Cerâmicas para Revestimento. Dissertação de Mestrado. UFRN-PPGEM, Natal

FIESP—Federação das Indústrias do Estado de São Paulo (2004) Indicadores de Desempenho Ambiental da Indústria. FIESP, São Paulo-SP. Disponível em: http://www.fiesp.com.br/indices-pesquisa-e-publicaoes/indicadores-de-desempenho-ambiental-da-industria-2004

Governo Federal, Ministério do Meio Ambiente (2011) Plano Nacional de Resíduos Sólidos, Brasília

Menezes RR, Almeida RR, Santan LNL, Ferreira HS, Neves GA, Ferreira HC (2007) Utilização do Resíduo do Beneficiamento do Caulim na Produção de Blocos e Telhas Cerâmicos. Revista Matéria 12(1):226–236

Pinto FAR (2004) Resíduos Sólidos Industriais: Caracterização e Gestão. O Caso do Ceará. Dissertação de Mestrado, Universidade Federal do Ceará

Santos, PS (1989) Ciência e tecnologia das argilas, 2 edn., vol 1. Edgard Blucher, São Paulo, 408 pp

Segadães AM (2006) Use of phase diagrams to guide ceramic production from wastes. Adv Appl Ceram 105(1):46–54

Chapter 4
Coffee Industry in Brazil

Abstract This chapter presented the state of the coffee industry in Brazil. Brazil has a great production of coffee and causes a huge amount of waste. In the productive sector, the main residue is coffee husk, obtained after processing of coffee fruits. Information of the coffee processing and refining as well as details about the waste from the coffee production are described.

Keywords Coffee industry · Coffee waste

Brazil has a prominent position in the world coffee production. The country is the world's largest producer and its production exceeds the sum of the production of the other top five of the list, as shown in Fig. 4.1.

According to the Brazilian Institute of Geography and Statistics (IBGE), the national coffee production in the 2011 harvest was approximately 2,668,780 tons of processed coffee. Figure 4.2 shows the percentage of domestic production by state. The state of Minas Gerais is the main coffee producer, with approximately half the national production, followed by the states of Espírito Santo, São Paulo, Bahia, Paraná, and Rondônia.

In Brazil, plants of species *Coffea arábica*, known as Arabica coffee, and *Coffea canephora*, mostly conillon variety, also known as Robusta coffee, are grown. The species Arabica is better adapted to regions of higher altitudes, between 1,000 and 2,000 m in relation to sea level and cooler temperatures, with annual averages between 18 and 22 °C. The species Robusta easily adapts to lower regions, close to sea level areas, and higher temperatures, with annual averages between 22 and 26 °C. The fruit of the Arabica species results in a more refined drink in terms of aroma and flavor, a condition that substantially affects the commercial value of the product. However, Robusta has high contents of soluble solids and therefore is preferred by manufacturers of instant coffee and by pharmaceutical and food industries due to the interest in caffeine as a raw material. Figure 4.3 shows the percentage of state wise domestic production of both species of plants according to IBGE.

W. Acchar and E.J.V. Dultra, *Ceramic Materials from Coffee Bagasse Ash Waste*, SpringerBriefs in Applied Sciences and Technology,
DOI 10.1007/978-3-319-15281-3_4

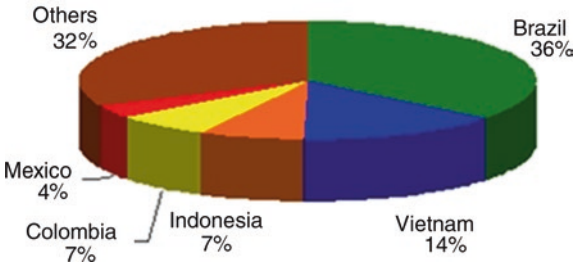

Fig. 4.1 World coffee production. *Source* International Coffee Organization

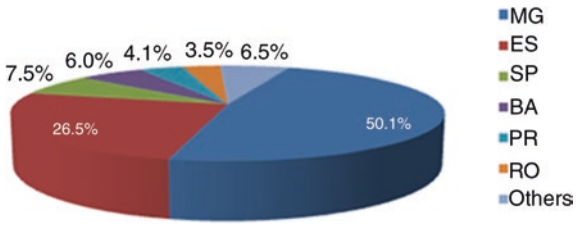

Fig. 4.2 National coffee production by state. *Source* IBGE (2012)

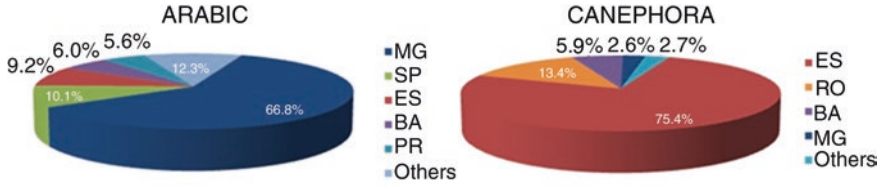

Fig. 4.3 Brazilian coffee production by variety of species—2011. *Source* IBGE (2012)

The state of Minas Gerais, the largest coffee producer in Brazil, figures as the main producer of species Arabica, with approximately 67 % of the national production. The state of Espírito Santo is the main producer of species Robusta, followed by the state of Rondônia. Figure 4.4 shows the main coffee growing regions by species.

In Bahia, of the 160,033 tons of coffee produced in the 2011 harvest, 74.5 % were of the species *Coffea arabica* and 25.5 % were of the species *Coffea canephora* (IBGE 2012). The western, northern, and mid-eastern regions of the state are producers of the species Arabica, while Robusta is grown in the southern coast. According to Bessa (2012), in Bahia, the most significant growth occurred in the Cerrado region (high technology, fully irrigated), with growth rate around 20 %

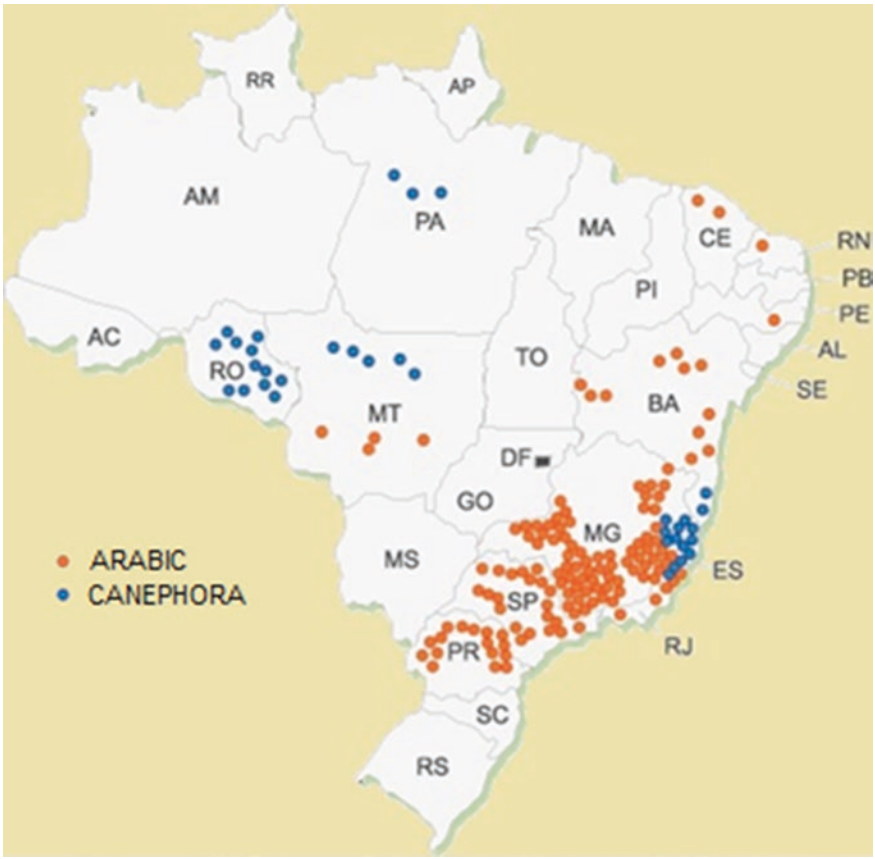

Fig. 4.4 Main coffee growing regions in Brazil by species. *Source* Markcafe

per year. Recently, this growth is also occurring in the Conillon region (Robusta coffee), called "Atlântico," with a growth rate of 10 % per year. Therefore, one could conclude that coffee production in Bahia is currently under expansion.

4.1 Coffee Processing and Refining

After harvest, the coffee fruit undergoes processing for the removal of impurities, as well as bark, parchment, and separation of the grain, which is the commercial product, from unused parts for manufacture of the beverage. Figure 4.5 shows a schematic drawing of the coffee fruit structure.

Coffee processing and refining can be performed by two different methods for drying fruits: wet or dry process. Both begin with the step of separating and classifying the fruit by maturation stage: green, cherry, or dry. Thus, the

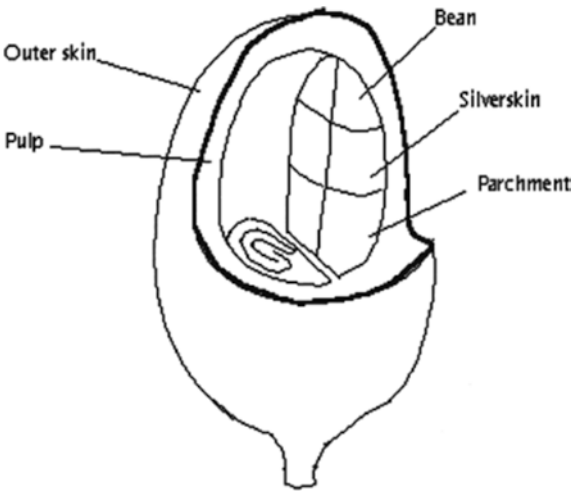

Fig. 4.5 Schematic drawing of the coffee fruit structure (Saenger et al. 2001)

manufacturer has greater control of the processes, since for each maturation stage, there are different characteristics in the drying step.

Drying agricultural grain means improving its condition to be stored at room temperature, maintaining its characteristics with the best cost–benefit ratio. Then, after drying, the moisture content should present the maximum value with which the product can be stored for predetermined periods at room temperature without any damage that could reduce the quality (Palacin et al. 2005).

Drying as a step in processing and beneficiation is considered critical for providing heat stresses, developing undesirable fungi, adding odors from fumes or other contaminants in fruits and grains, depending on the technique used in the operation (Palacin et al. 2009; Oliveira, 1998). Many researchers claim that the drying conditions of the fruit influence the quality of commercial coffee and hence the value of the final product (Machado et al. 2003; Palacin et al. 2009). Drying in yards, with natural air, is possible in environments with low relative humidity and low cloud conditions. The main advantage of this method is energy saving, but it has disadvantages such as requiring large areas and dependence on climatic factors, which are not favorable, slow the process, and compromise the quality of the final product. In Brazil, a predrying step in yards with mechanical dryers for additional drying is common (Machado et al. 2003).

Artificial drying in mechanical dryers has the advantages of reducing the drying time, use in humid regions and periods of rain, reducing the climate influence on the quality of coffee, and allowing the reduction of the area of yards and hand labor, despite requiring better professional qualification. Thus, the literature classifies artificial drying by mechanical dryers as advantageous from the technical point of view due to the reasons above. Still according to the literature, the main disadvantage is the higher drying cost compared with outdoor natural drying. However, due to the smaller influence from climatic factors and the less likely action of fungi

and bacteria, and also their influence on the quality and therefore the price of the product, the cost–benefit ratio at the end of processing may be favorable to the use of mechanical dryers.

This review on the use of mechanical dryers is important for it is at this stage, with the use of such equipment, that coffee hush ashes are produced (resulting from burning coffee husks), the residues used in this study. From the point of view of coffee production in Brazil, it is difficult to estimate and quantify the use of mechanical dryers. There are a few studies of regional coverage, for example, carried out by Freitas et al. (2000) which evaluated the characteristics of the production processes of coffee in southern Minas Gerais. In this study, 170 farms classified as small, medium, and large were analyzed. According to the authors, approximately 82 % of farms used mechanical driers in the drying process of grains. Of these, 90 % were medium (with area between 10 and 50 acres) and large (above 50 ha of area), that is, most of the farms that did not use mechanical dryers were classified as small (less than 10 ha). It is noteworthy that this study was conducted over 10 years, and many investments in improvements of processing conditions have been made by small producers, for example, through associations, causing this percentage to be currently higher. In a recent study, (Sater et al. 2011) reported that virtually all drying of the production in the state of Espírito Santo is made with the use of mechanical dryers. After the drying step, the coffee grains are packaged and stored, and later marketed.

4.2 Waste from Coffee Production

Due to their high production, the coffee industry in Brazil generates huge amounts of waste. In the productive sector, the main residue is coffee husk, obtained after the processing of coffee fruits.

Coffee husk is derived from the cleaning of coconut coffee, composed of epicarp (husk), mesocarp (pulp or mucilage), and endocarp (parchment). The pulp is the residue of wet pulping the cherry coffee, composed of epicarp and mesocarp (Matiello 1991). The amount of husks produced in a harvest season is huge. According to several authors, in the processing of coconut coffee, approximately 50 % is grain and 50 % is husk (Badocha et al. 2003; Giomo et al. 2006; Rocha et al. 2006). Thus, in the 2011 harvest season, about 2,668,780 million tons of coffee and therefore the same amount of husks were produced.

A small part of the coffee husks is used in farms as fodder for coffee plants (Badocha et al. 2003). There are differences between authors on the use of this waste as animal feed. So, large amounts are discarded, most often, inappropriately. The inadequate disposal of wastes generate serious environmental problems such as pollution and siltation of rivers, air pollution due to burning, and use of areas for the storage of this material that could be aimed for other purposes, and waste of raw materials entering the industry.

The most interesting use in terms of use of coffee husk is the production of thermal energy from biomass (Vale et al. 2007). Due to the growing world concern to increase the use of renewable energy, wastes of various origins emerge as interesting energy alternatives (Protásio et al. 2012). Studies have shown the excellent energy viability of coffee husk to produce heat (Saenger et al. 2001; Vale et al. 2007; Oliveira et al. 2008; Protásio et al. 2012). This conclusion is mainly based on the calorific value of coffee husk, with values between 3,990 and 4,393 kcal/kg, rated as excellent in terms of biomass residue from agriculture. Vale et al. (2007) compared results of the combustion of coffee husk with *Cedrelinga catenaeformis* residue (shavings) and concluded that coffee husk, despite having lower calorific value than *Cedrelinga catenaeformis* (3,933 and 4,932 kcal/kg, respectively), has higher bulk density (567,965 kcal/m^3 for coffee husk and 470,463 kcal/m^3 for shavings), resulting in higher energy output per unit volume, optimizing the use of burning appliances. The authors emphasize the possibility of manufacturing charred briquettes from coffee husk for the production of thermal energy, with viability for use in thermoelectric power plants. Other studies have also suggested this possibility (Saenger et al. 2001; Oliveira et al. 2008; Sater et al. 2011; Protásio et al. 2012). Coffee husk is an excellent fuel for industries that use furnaces. Many coffee producing farms use this residue as fuel for their mechanical dryer, maintaining energy autonomy in the drying process, as shown in Fig. 4.6. Burning the coffee husks results in residual ash, which is discarded by farmers.

According to Dultra and Acchar (2010), in many cases, the ash is disposed in areas close to producing farms, on roadsides, or near rivers and streams without treatment and may contaminate soil or water. Figure 4.7 shows an example of the improper disposal of coffee husk ashes.

Coffee husk ash, currently of no commercial value, is rich in alkali (K_2O) and alkaline earth metals (CaO and MgO). Dultra and Acchar (2010), concluded that

Fig. 4.6 Coffee husks used as fuel

Fig. 4.7 Improper disposal of coffee husk ashes

Fig. 4.8 Coffee husk ash

it is possible to incorporate this residue into masses for the production of ceramic tiles. In this study, the author evaluated as satisfactory results for water absorption and mechanical strength obtained by ceramic bodies with 10 % added residue, without the use of other fluxes. According to the author, the residue contributed to the formation of liquid phase, or vitrification, improved sintering and, consequently, increased the densification of the ceramic body. Figure 4.8 shows coffee husk ash obtained in a producing farm in Eunápolis—Ba.

The fact is that coffee husk ash comes from coffee cultivation, its offer is submitted to the harvest period, which begins in late March and continues until early October, according to the Ministry of Agriculture. However, if one considers that: (a) the annual production of coffee husks (and its improper disposal) is abundant, (b) the current situation in the search for renewable energy sources, along with policies to encourage the use of residues may contribute so that more industries make use of coffee husks as a source of energy, the amount of ash generated from burning coffee husks tends to steadily increase, allowing the accumulation of strategic reserves of this residue.

A positive factor highlighted by Dultra and Acchar (2010), regarding the use of coffee husk ashes by the ceramic industry is the geographical location of both producers. Coffee cultivation is very strong in the states of São Paulo, Paraná, Minas Gerais, and Espirito Santos (as can be seen in Fig. 4.4), and the major states of ceramic coatings production are Sao Paulo and Santa Catarina, where there is a higher concentration of manufacturers. Thus, geographically, obtaining the residues by ceramic tile manufacturers is facilitated.

References

Badocha TE, Costa RSC, Leônidas FC (2003) Casca de Café: Um Importante Insumo para a Agricultura Orgânica. In: Anais (ed) III Simpósio de Pesquisa dos Cafés do Brasil, Porto Seguro-BA

Bessa F (2012) Tecnologias Fazem da Bahia o Quarto produtor de Café no Brasil. Embrapa Café

Dultra EJV, Acchar W (2010) Incorporação de Cinzas da Casca de Café na Produção de Placas Cerâmicas para Revestimento. Dissertação de Mestrado. UFRN-PPGEM, Natal

Freitas RF, Chalfoun SM, Mourão Júnior M, Pereira MC (2000) Características das Lavouras e Infraestrutura Empregada na Pós Colheita do Café Amostradas no Programa de Regionalização da Qualidade do café da Região Sul de Minas Gerais. In: Anais (ed) Simpósio de Pesquisa dos Cafés do Brasil, Embrapa Café, Poços de Caldas-MG

Giomo GS, Nakagawa J, Gallo PB (2006) Beneficiamento de Sementes de Café Arabica e Efeitos na Qualidade Física

IBGE—Instituto Brasileiro de Geografia e Estatística (2012) Levantamento Sistemático da Produção Agrícola—LSPA, Fevereiro

Machado MC, Sampaio CP, Silva JS (2003) Estudo Comparativo de Sistemas de Secagem do Café: Aspectos Técnico-Econômicos. In: Anais (ed) Simpósio de Pesquisa dos Cafés do Brasil, Porto Seguro-Ba

Matiello JB (1991) O Café: do Cultivo ao Consumo. Ed. Globo, São Paulo

Oliveira APN (1998) Grês Porcelanato: Aspectos Mercadológicos e Tecnológicos. Revista Cerâmica Industrial 3:35–41

Oliveira WE, Franca AS, Oliveira LS, Rocga SD (2008) Untreated coffee husks as biosorbents for the removal of heavy metals from aqueous solution. J Hazard Mater 152:1073–1081

Palacin JJF, Lacerda Filho AF, Melo EC, Silva JS, Donzeles SML (2005) Boas Práticas para Produzir Café com Qualidade. In: Anais (ed) IV Simpósio de Pesquisa dos Cafés do Brasil, Londrina, PR

Palacin JJF, Lacerda Filho AF, Melo EC, Teixeira EC (2009) Secagem Combinada de Café Cereja Descascado. Revista Engenharia na Agricultura 17(3):244–258

Protásio TP, Bufalino L, Mendes RF, Ribeiro MX, Trugilho PF, Leite ERS (2012) Torrefação e Carbonização de Briquetes de Resíduos do Processamento dos Grãos de Café. Revista Brasileira de Engenharia Agrícola e Ambiental 6(11):1252–1258

Rocha FC, Garcia R, Freitas AWP, Souza ALS, Gobbi KF, Valadares Filho SC, Tonucci RG, Rocha GC (2006) Casca de Café em Dietas para Vacas em Lactação: Consumo, Digestibilidade, produção e Composição de Leite. Revista Brasileira de Zootécnica 35:2163–2171

Saenger M, Hartger EU, Werther J, Ogada T, Siagi G (2001) Combustion of coffee husks. Renewable Energy 23:103–121

Sater O, Souza ND, Oliveira EAG, Elias TF, Tavares R (2011) Estudos Comparativos da Carbonização de Resíduos Agrícolas e Florestais Visando a Substituição da Lenha no Processo de Secagem de Grãos de Café. Revista Ceres 58(6):717–722

Vale AT, Gentil LV, Gonçalez JC, Costa AF (2007) Caracterização energética e Rendimento da Carbonização de Resíduos de Grãos de Café. Cerne, Lavras 13(4):416–420

Chapter 5
Using CBA in Ceramic Formulations

Abstract This chapter describes formulations investigated in this book (clay with coffee husk ash), methodology adopted in the performance of tests and procedures. Physical characteristics of these formulations such as particle size, mixing, homogenization, thermal analysis, sintering and also mineralogical analysis by X-ray diffraction (XRD) are presented.

Keywords Clay · Coffee husk ash · Characterization of the mixtures

This chapter describes all the materials used as well as the standards and methodology adopted in the performance of tests and procedures. To better clarify the procedures, Fig. 5.1 shows the flowchart of the experimental phase.

5.1 Raw Materials

A Brazilian ceramic company provided clay, kaolin, quartz, feldspar, pyrophyllite, and talc used in this work. The raw materials used in the manufacture of glazed porcelain tiles were directly collected from the storage silos of the company.

Coffee husk ash was collected in its raw state in a coffee farm located in Eunápolis, southern state of Bahia. Importantly, this farm uses solely coffee husks as fuel for the production of heat to be used in drying ovens and coffee processing. Residues 1 and 2 are byproducts obtained from a physical treatment performed in coffee husk ash in its original state. The main purpose of this coffee husk ash treatment was to decrease the amount of charred matter contained in fresh ashes as a way to mitigate the negative effects caused during firing (excessive weight loss and gas formation), as reported by Dultra and Acchar (2010).

The treatment consists of adding distilled water to the fresh ash in the ratio of 3:1 by weight (water and ash). About 500 g of ash was used and after mixing with distilled water, part of the charred matter migrated to the surface of the mixture and was removed with the aid of sieves. After removal of the excess charred matter, the

W. Acchar and E.J.V. Dultra, *Ceramic Materials from Coffee Bagasse Ash Waste*, SpringerBriefs in Applied Sciences and Technology,
DOI 10.1007/978-3-319-15281-3_5

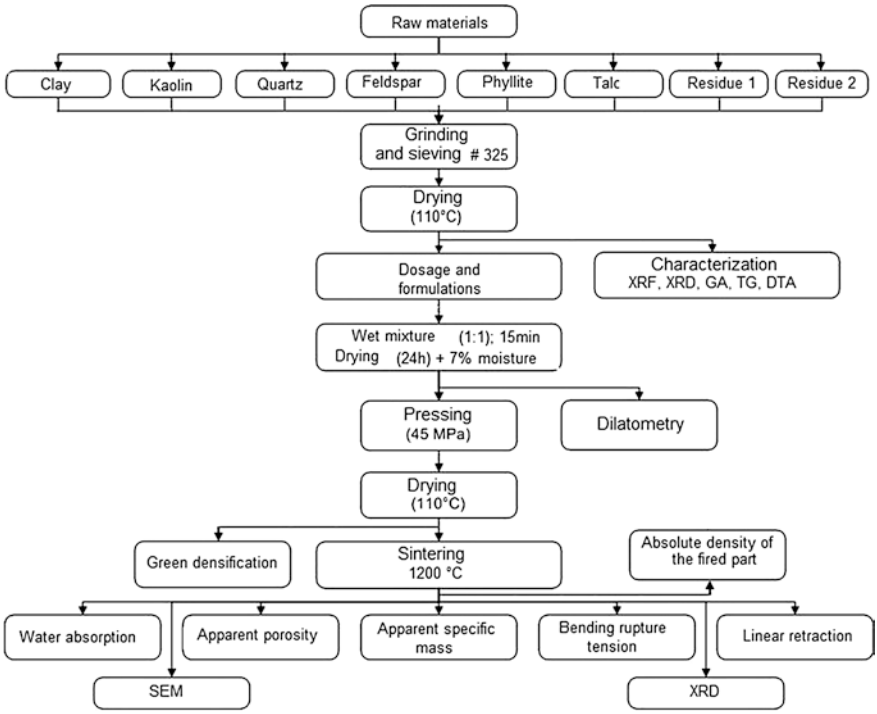

Fig. 5.1 Flowchart of the experimental methodology adopted

mixture was stirred and placed for decantation for 3 h. After this time, the surface was composed of a yellowish liquid and the ash particles were at the bottom. The liquid portion was collected and the procedure with the remaining material was repeated two more times. Then, the yellow liquid solution was transferred to another container, which was filtered on filter paper to eliminate impurities. After filtering, the solution was dried in oven so that all the water was eliminated. After this procedure, 148 g was left in the container, i.e., 29.6 %, approximately, of a white particulate material, hereinafter, for the purposes of this study, will be referred to as residue 1 (R1). The solid material of gray color that remained after decantation, was dried in an oven to obtain a mass of 308 g, i.e., 61.6 %, approximately, hereinafter, for the purposes of this study, will be referred to as residue 2 (R2). Figure 5.2 shows residues R1 and R2.

All raw materials from the supplier company were previously ground and sieved through 325 mesh sieve (0.044 mm). Residue R1 was not submitted to grinding for being completely soluble in water. Residue R2 was ground and sieved through 200 mesh sieve (0.075 mm). The material was ground in a ball mill for 3 h (each batch), and then the materials were sieved. Sieving was carried out in wet method where excess water was removed after decantation and the remaining water was removed by drying in an oven at 110 °C for 24 h.

Fig. 5.2 Residue R1 and residue R2

5.2 Formulations

In this book, two residues R1 and R2 were used separately (in total or partial replacement of fluxing materials) and added to the glazed porcelain mass used by a given industry. For each formulation, 5 specimens were made, and for MP, MB, and MB+6.7F+6.7R2 formulations, 10 specimens were made.

5.3 Standard Formulation of Supplier Company

The formulation used by the company to produce glazed porcelain tile was provided together with the raw materials, provided the wording, designated in this work with MP. Table 5.1 describes the percentage by weight of the standard MP mass and MB mass, free from fluxes.

The MP formulation was used as a comparison parameter in relation to the properties for formulations with the addition of residues.

The MB mass, whose acronym stands for basic mass, is a mixture of clay, kaolin, and quartz in the same proportions of MP, where the same ratios between the amounts of clay and kaolin, and between clay and quartz were kept, but without fluxing materials (feldspar, talc, and pyrophyllite). Residue R1, residue R2, and feldspar were added to the MB mass to obtain formulations in Table 5.1.

Table 5.1 Standard MP and MB formulation

Material	MP (%)	MB (%)
Clay	31	44.93
Kaolin	33	47.83
Quartz	5	7.25
Feldspar	11	0
Phyllite	15	0
Talc	5	0

5.4 Formulations with Residue R1

Formulations containing residue R1 were determined based on the amount of residue needed to compensate for the removal of the fluxing material from the standard formulation with respect to the sum of elements: K_2O, Na_2O, CaO, and MgO. For this, the X-ray fluorescence results of each raw material were used and the percentage by weight of components (K_2O, Na_2O, CaO, and MgO) present in the standard mass was determined. Then standard mass of feldspar, pyrophyllite, and talc was disregarded, and the mass of clay, kaolin, and quartz was kept (in the same proportion as the standard mass, i.e., keeping constant the clay/kaolin and clay/quartz ratios) and calculating the percentage of residue R1 needed for the percentage of elements K_2O, Na_2O, CaO, and MgO, combined, reached the same percentage present in the standard mass. Based on this principle, it was concluded that with the addition of 7.67 % of residue R1 to the mass containing clay, kaolin, and quartz (in the same proportion as the standard mass), the percentage of elements K_2O, Na_2O, CaO, and MgO, together, would be the same. Thus, we took as a reference for adding residue R1, the percentage of 8 % and formulations with higher and lower percentages of residue R1 were also used, as shown in Table 5.2.

Where MB, for the purpose of nomenclature of formulations used in this work, refers to the mixture of clay, kaolin, and quartz in the same proportions as the standard mass, as described in Table 5.1. Masses containing clay, kaolin, quartz (in the same proportions as the standard mass—MB), residue R1, and feldspar were also formulated, as described in Table 5.3.

Table 5.2 Formulations with the addition of residue R1

Formulation	Clay (%)	Kaolin (%)	Quartz (%)	R1 (%)
MB+2R1	44.03	46.87	7.10	2
MB+4R1	43.13	45.91	6.96	4
MB+6R1	42.23	44.96	6.81	6
MB+7R1	41.78	44.48	6.74	7
MB+8R1	41.33	44.00	6.67	8
MB+9R1	40.88	43.52	6.59	9
MB+10R1	40.43	43.04	6.52	10
MB+12R1	39.54	42.09	6.38	12
MB+14R1	38.64	41.13	6.23	14

Table 5.3 Formulations with the addition of residue R1 and feldspar

Formulation	Clay (%)	Kaolin (%)	Quartz (%)	R1 (%)	Feldspar (%)
MB+17.5F+2.25R1	35.94	38.26	5.80	2.25	17.50
MB+17.5F+4.5R1	35.04	37.30	5.65	4.50	17.50

Table 5.4 Formulations with the addition of residue R2

Formulation	Clay (%)	Kaolin (%)	Quartz (%)	R2 (%)
MB+5R2	42.68	45.43	6.88	5
MB+10R2	40.43	43.04	6.52	10
MB+15R2	38.19	40.65	6.16	15
MB+20R2	35.94	38.26	5.80	20

Table 5.5 Formulations with the addition of residue R2 and feldspar

Formulation	Clay (%)	Kaolin (%)	Quartz (%)	R2 (%)	Feldspar (%)
MB+6.7F+6.7R2	38.91	41.42	6.28	6.7	6.7
MB+10F+10R2	35.94	38.26	5.80	10	10

5.4.1 Formulations with Residue R2

For formulations containing residue R2, masses with percentages of materials were mixed according to Table 5.4. To determine the percentage of addition of residue R2 in MB mass, the results obtained by Dultra and Acchar (2010) in experiments with coffee ash in ceramic masses were analyzed.

Mixtures containing clay, kaolin, quartz (in the same proportions as the standard mass—MB), residue R2, and feldspar were also formulated, as described in Table 5.5.

5.5 Formulations with Feldspar

To evaluate and compare the fluxing effect of both residues in the ceramic mass, mixtures with clay, kaolin, quartz, (in the same proportions as the standard mass—MB) and feldspar were formulated, as shown in Table 5.6. The amount of feldspar was determined to obtain increasing percentage up to 35 % by weight. This maximum feldspar percentage was defined according to the main aim of this work, i.e., the possible reduction in the consumption of feldspar for the manufacture of porcelain tiles. Reviewing the vast literature, it was found that the percentage of feldspar porcelain masses vary between 35 and 50 % by weight when the feldspar is the only fluxing material in the composition. Thus, the minimum amount of feldspar used in the composition of porcelain tiles was taken as reference.

5.5.1 Preparation of Ceramic Masses

Raw materials were previously dried in oven at 110 °C for 24 h. Then, amounts specified for the formulations used were weighed. For this, a Mettler Toledo® digital scale model AL204, with accuracy of 0.0001 g, calibrated with standard weights of 20 and 50 g was used.

Table 5.6 Formulations with the addition of feldspar

Formulation	Clay (%)	Kaolin (%)	Quartz (%)	Feldspar (%)
MB+10F	40.43	43.04	6.52	10
MB+17.5F	37.07	39.46	5.98	17.5
MB+20F	35.94	38.26	5.80	20
MB+35F	29.20	31.09	4.71	35

5.5.2 Mixing and Homogenization

After dosing, the raw materials were mechanically mixed and homogenized by eccentric rotation in ceramic containers with alumina balls, using a mill. Distilled water was added in the ratio of 1:1 (water/solid material). The stirring time was approximately 15 min. Then, the mixed and homogenate material was placed in an oven at 110 °C for 24 h. After this time, the material was disaggregated in a mortar and then placed in plastic bags. About 7 % of distilled water was added as a lubricant in order to obtain a better distributed packing and increased green strength, according to Santos (1989), and then the material was manually crushed still inside the bags. The material remained at rest for 24 h to standardize humidity.

5.5.3 Pressing

The pressing of specimens was performed in uniaxial hydraulic press with capacity of 15 tons, using SAE 1045 steel with internal dimensions of 60 × 20 mm. For molding, 15 g of material was used, which resulted in specimens with thicknesses between 5.7 and 6.1 mm. The load applied was of 5.6 tons and maintained for a period of 1 min to accommodate particles, resulting in compaction pressure of 45 MPa. After pressing, the specimens were placed in an oven for 24 h and then weighed on a Mettler Toledo® digital scale model AL204, with accuracy of 0.0001 g and its dimensions were measured using Mitutoyo® digital caliper with precision of 0.01 mm.

5.5.4 Firing

The firing of specimens was performed in muffle-type EDG® electric oven with heating capacity of up to 1,200 °C. Since it is a comparison with the standard mass of a ceramic industry, the final firing temperature used was 1,200 °C, which is the same as that used by the ceramic industry that provided the raw materials. To be as close as possible to the firing conditions of the ceramic industry, the

highest possible heating rate respecting the limitations of the equipment was used. The heating rate was 25 °C/min up to 700 °C, 15 °C/min between 700 and 900 °C, and 7.5 °C/min from 900 °C up to the final temperature. The plateau time at the final temperature was 8 min, according to the ceramic industry that provided the raw materials. After reaching the plateau time, cooling followed the natural conditions of the furnace. To ensure the desired firing characteristics, all the cycles were externally monitored with a thermometer model TH-060 (Thermometer®), along with a K-type thermocouple. The thermocouple thermometer set was calibrated on the water–ice thermal equilibrium (0 °C) and in boiling water (100 °C).

5.6 Characterization of Raw Materials

5.6.1 Chemical Analysis by X-Ray Fluorescence (XRF)

In this analysis, Shimadzu® X-ray spectrometer model EDX-700 was used in a vacuum atmosphere using a semiquantitative method to determine the elements present in the sample. Before analysis, samples were classified by sieving in particle size less than 0.074 mm, corresponding sieve No. 200 of ABNT, and dried in oven at 110 °C for 24 h. The equipment does not detect elements with atomic number less than 9.

Table 5.7 shows the XRF results of raw materials. The results are in the form of equivalent oxides. It is possible that the main constituents of clay and kaolin are SiO_2 and Al_2O_3, as expected. The amounts of Fe_2O_3 and TiO_2 in clay are close to the limits (Biffi 2002) for clear firing. For kaolin, it is recommended that the sum

Table 5.7 XRF of raw materials supplied by the company

Oxides	Concentrations by weight (%)					
	Clay	Kaolin	Quartz	Feldspar	Phyllite	Talc
SiO_2	54.17	66.15	94.65	68.87	56.48	54.91
Al_2O_3	38.61	32.03	4.89	23.68	24.69	11.23
K_2O	2.28	0.59	0.06	1.47	8.67	0.38
Fe_2O_3	1.53	0.37	0.04	0.11	6.72	1.12
TiO_2	0.63	0.73	0.07	0.01	1.44	0.17
MgO	2.69	–	–	–	1.82	31.77
P_2O_5	–	–	–	0.15	–	–
Na_2O	–	–	–	5.42	–	–
SO_3	0.05	0.09	0.20	0.07	0.06	–
CaO	–	–	–	0.18	–	0.38
SrO	–	–	–	–	0.01	–
Outros	0.04	0.04	0.09	0.04	0.15	0.04

Table 5.8 XRF of fresh ash and of residues

Oxides	Concentrations by weight (%)		
	Received ash	R1	R2
SiO_2	0.60	0.74	5.30
Al_2O_3	–	–	–
K_2O	72.33	95.18	31.00
Fe_2O_3	0.43	–	0.73
TiO_2	–	–	0.10
MgO	3.16	–	18.66
P_2O_5	1.66	0.34	14.98
Na_2O	–	–	–
SO_3	1.41	3.68	0.77
CaO	20.27	–	28.18
SrO	0.09	–	0.12
Outros	0.05	0.06	0.16

of Fe_2O_3 and TiO_2 is below 0.90 % (Biffi 2002). These elements are responsible for the dark color of products after firing. Quartz, as expected, has essentially SiO_2 in the crystalline form. Feldspar has a high SiO_2 content (68.87 %) and, to a lesser extent, Al_2O_3 (23.68 %). The predominant fluxing element in feldspar is Na_2O, which characterizes it as sodium feldspar (albite). Table 5.8 shows the XRF results of fresh ash and residues. It can be observed that the main constituent of fresh ash is K_2O, which represents more than 72 % of constituents detected by the machine. Significant amounts of CaO were detected in this residue (20.27 %), low amounts of MgO (3.16 %) were also detected. These constituents are alkali and alkaline earth metals that fluxing characteristics in relation to clay minerals, or its reaction with increasing temperature results in liquid phase at lower temperature than that of melting.

After treatment carried out with fresh ash residues R1 and R2 were obtained, as explained previously. In residue R1, it was observed that the presence of K_2O is large, with over 95 % of the elements detected. The percentage of SO_3 is considered high for raw materials used in the production of ceramic tile because in significant amounts, the vaporization of sulfur can accumulate in the upper part of the furnace and drip onto parts. Since R1 and R2 are residues, it is expected that the added amounts of residue R1 in the ceramic mass are small, so that such an effect does not occur.

Residue R2 features more balanced percentage of K_2O (31.00 %), CaO (28.18 %), and MgO (18.66 %). From the point of view of fluxing elements, this can be interesting because K_2O has characteristics of energetic fluxing, while CaO and MgO have characteristics of moderate fluxing. This ratio has a direct influence on the amount, and mainly on the viscosity of the liquid formed during firing, and both the amount and the viscosity of the liquid influence the microstructure and hence the physical properties of the product after firing.

5.7 Mineralogical Analysis by X-Ray Diffraction (XRD)

This analysis was performed on a Shimadzu® diffractometer model XRD-6000, using Cu–Ka radiation with $\lambda = 1.54056$ Å, voltage of 40 kV, current of 30 mA, and scanning angle from 5° to 80° corresponding to 2θ, speed of 2°/min, and step of 0.02°. The identification of crystalline phases was made by comparing the peaks generated by the diffraction patterns with charts using the JCPDF software registered in the ICDD (International Centre for Diffraction Data). Both raw materials as sintered samples were characterized by XRD as described above. Figure 5.3 shows the graph with the XRD results for clay and kaolin.

According to the XRD pattern, the phases present in clay are: quartz, kaolinite, and halloysite. In kaolin, quartz and kaolinite phases are present, as expected. Figure 5.4 shows the XRD patterns of feldspar and talc. The phases present in feldspar are quartz and albite, confirming that it is sodium feldspar. Talc is composed of a hydrated magnesium silicate, characteristic of this type of material. Figure 5.5 shows the XRD pattern of pyrophyllite, with peaks related to phases quartz (SiO_2), halloysite ($Al_2Si_2O_3(OH)_4 \cdot 2H_2O$), and potassium aluminum silicate ($KAl_3 \cdot Si_3 \cdot O_{11}$), responsible for the fluxing effect of pyrophyllite.

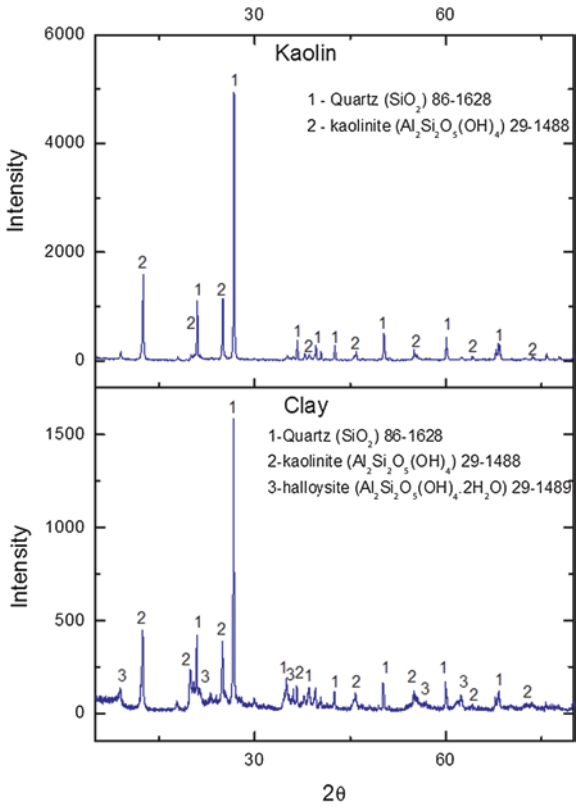

Fig. 5.3 XRD results for clay and kaolin

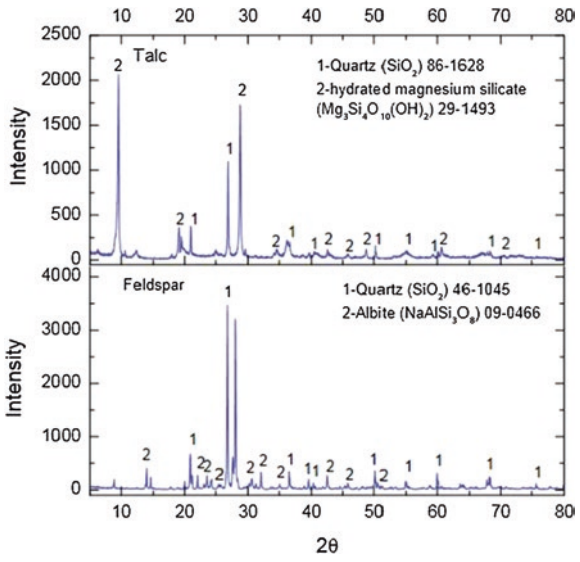

Fig. 5.4 XRD pattern of feldspar and talc

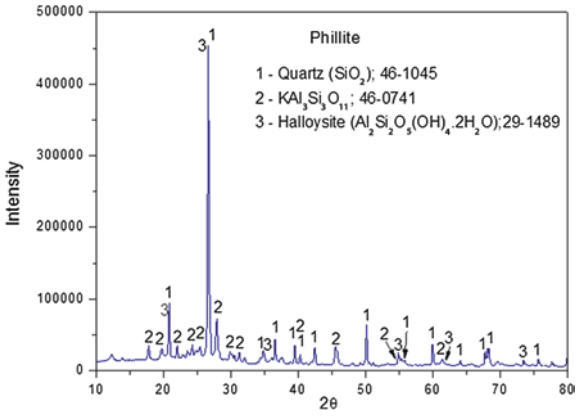

Fig. 5.5 XRD pattern of pyrophyllite

Figure 5.6 shows the XRD pattern of residue R1, where the main peaks are related to the phase of hydrated potassium carbonate ($K_2CO_3(H_2O)_{1.5}$). The presence of potassium carbonate may explain the fact that the sample is highly hygroscopic. As the sample was referred to X-ray diffraction test shortly after a period of 24 h in an oven at 110 °C, it is likely that water has been absorbed during the preparation and handling before the test. Therefore, the water absorbed was not sufficient for the reaction of potassium carbonate with water to form potassium bicarbonate ($KHCO_3$) plus potassium hydroxide (KOH), as diffraction peaks related to these phases were not detected. In the X-ray diffraction, potassium oxide (K_2O) peaks also appear, increasing the fluxing effect of the material. Figure 5.7 shows the graph with the X-ray diffraction of residue R2. Peaks of the following

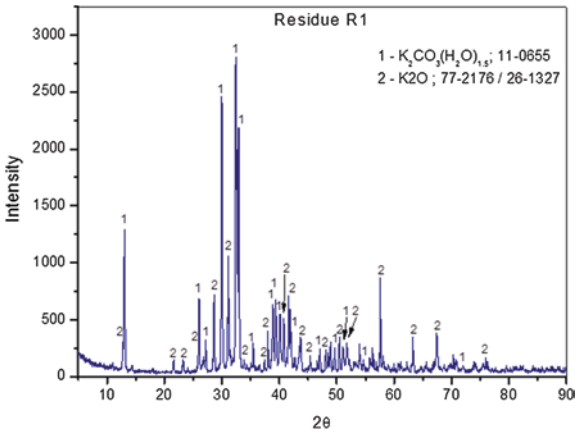

Fig. 5.6 X-ray diffraction of residue R1

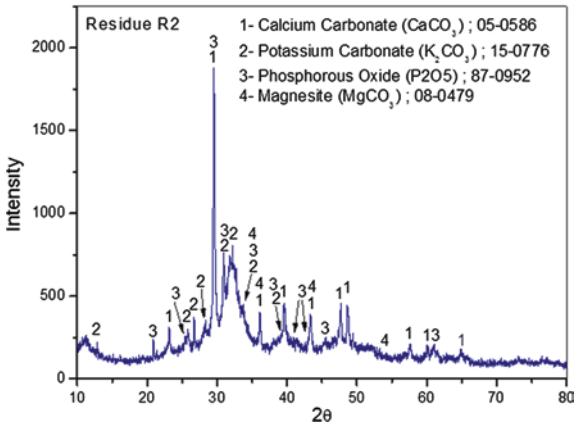

Fig. 5.7 X-ray diffraction of residue R2

phases were identified: Calcium carbonate ($CaCO_3$), potassium carbonate (K_2CO_3), phosphorous oxide (P_2O_5), and Magnesite ($MgCO_3$).

Figure 5.8 shows the XRD pattern of residue R2 after heating at temperatures of 600, 800, 950, and 1050 °C. At temperature of 600 °C, the presence of peaks relating to fairchildite phase ($K_2Ca(CO_3)_2$) is detected. It is common to find fairchildite in ash originating from the burning of biomass fuels (Navrotsky et al. 1997). Liodakis et al. (2005) identified the presence of fairchildite when analyzing the mineralogical composition of ashes originated from the combustion of forest wood in Greece. The presence of calcium carbonate ($CaCO_3$), a double potassium and calcium phosphate ($KCaPO_4$), and magnesium (MgO) and potassium oxide (K_2O) was also observed.

According to the XRD pattern, as the temperature increases, the peaks relating to the fairchildite, calcium carbonate and double potassium and calcium phosphate phases lose intensity, becoming more discrete, suggesting a reduction in amounts. With respect to fairchildite phase ($K_2Ca(CO_3)_2$) and double calcium and

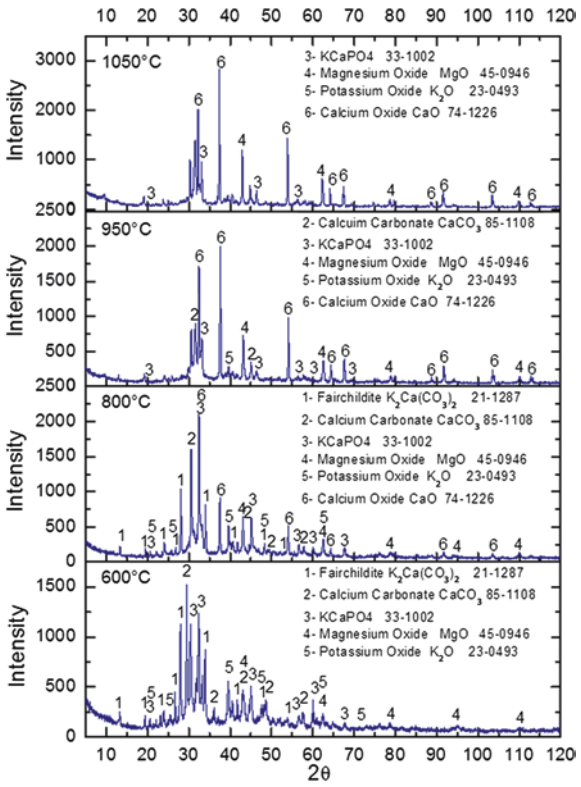

Fig. 5.8 XRD pattern of residue R2 at temperatures of 600, 800, 950, and 1,050 °C

potassium phosphate ($KCaPO_4$), the reduction of intensity of peaks is certainly related to the decomposition of carbonate and phosphate. With increasing temperature, the process of fairchildite decomposition occurs, individualizing both carbonates, and thus, potassium carbonate decomposes into $K_2O + CO_2$, leaving calcite residues ($CaCO_3$), which also decompose. As a result, peaks related to the calcium oxide phase, with increasing temperature, become more intense. The decomposition of calcium carbonate ($CaCO_3$), which begins between 720 and 840 °C (Liodakis et al. 2005), originates the calcium oxide stage (CaO)—with consequent release of CO_2—whose peaks become more intense with increasing temperature. The peaks relating to the magnesium oxide phase (MgO) have slight increase as the temperature increases.

5.8 Thermal Analysis

Thermogravimetric analysis (TGA) was performed using a Shimadzu® thermal analyzer model TGA-60 from the Laboratory of Physical Properties of Ceramic Materials—LaPFiMC, with sample weight of about 15.0 mg, heating rate of

10 °C/min under argon flow at flow rate of 50 ml/min, reaching final temperature of 1,150 °C. The analysis of results was performed using TA-60 software supplied by Shimadzu®. Simultaneously to the thermogravimetric analysis, Thermal Differential Analysis (DTA) was performed. The analysis of results was performed using TA-60 software supplied by Shimadzu®.

For best viewing of the thermal analysis results, the TGA curves (Thermogravimetric Analysis), the curve derived from TGA (DrTG) and the DTA curve (Differential Thermal Analysis) were plotted on the same graph, for each material. Figure 5.9 shows the graph with TGA, DTA, and DrTG curves of clay. The initial weight loss up to 200 °C (1.875 %) is associated with an endothermic peak (52.30 °C) in the DTA curve and was due to the loss of adsorbed water and zeolite water from the mineral.

At temperatures between 400 and 650 °C, higher mass loss rate followed by endothermic peak in the DTA curve at temperature of 508.14 °C was observed. This can be explained by the fact that in this temperature range, the kaolinite structure loses water and transforms into metakaolin. The mass loss continues during heating, however, the loss rate decreases, ending the cycle with approximately 9 % loss. The endothermic peak at 957.44 °C is related to the initial formation of the Si–Al spinel from metakaolin. Figure 5.10 shows the graph with TGA, DrTG, and DTA curves of kaolin. It is easy to perceive the similarity between the thermal analysis of clay and kaolin. This similar behavior confirms the results of the chemical and mineralogical composition of both materials. The endothermic peak at 574.98 °C is due to the allotropic transformation of α-quartz into β-quartz. This transformation was more noticeable in kaolin in relation to clay due to the greater amount of quartz present in the kaolin sample.

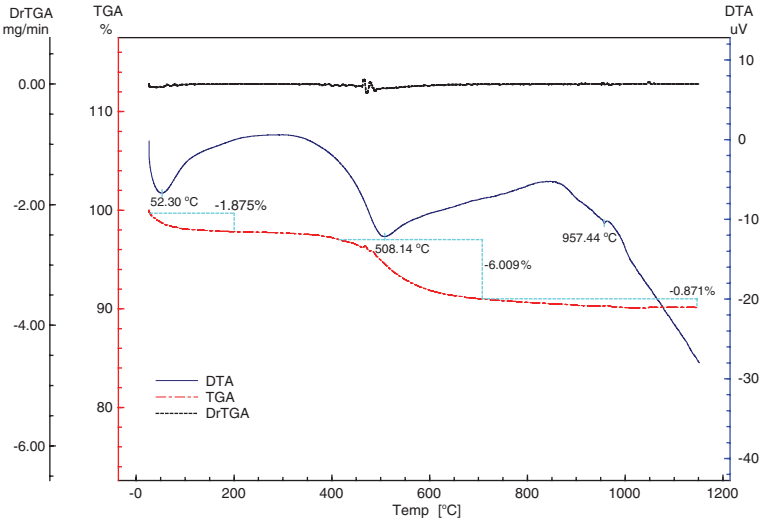

Fig. 5.9 DTA/TGA thermal analysis of clay

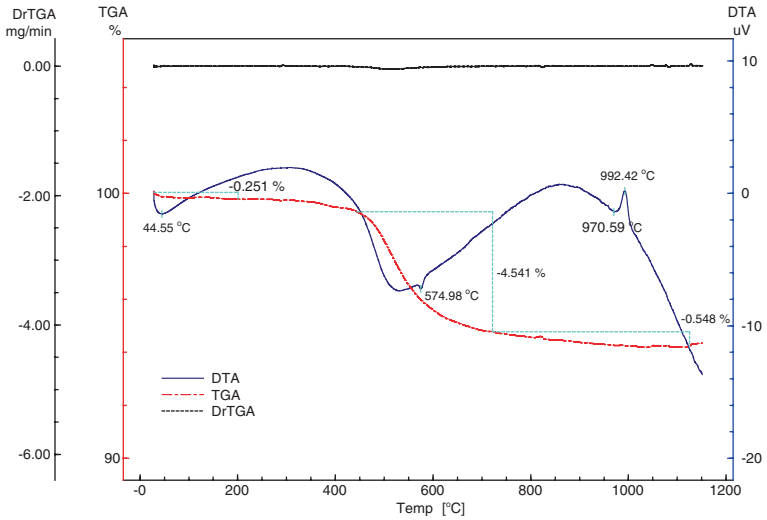

Fig. 5.10 DTA/TGA thermal analysis of kaolin

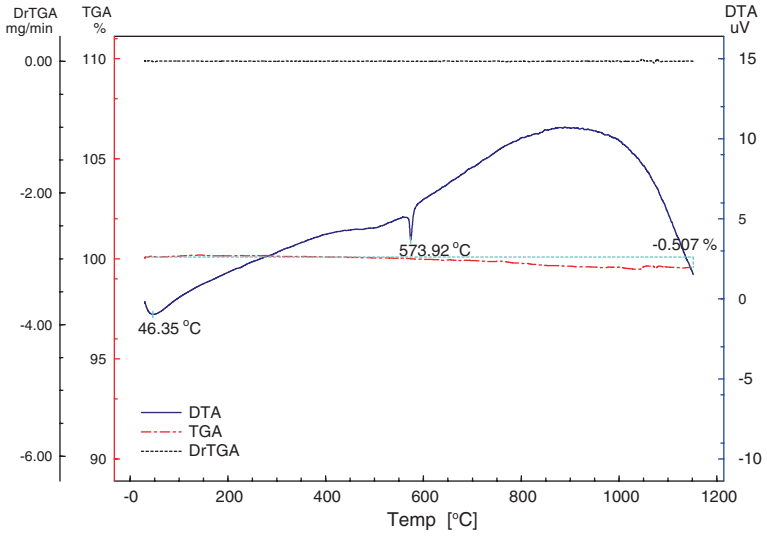

Fig. 5.11 DTA/TGA thermal analysis of quartz

The peak at 992.42 °C in the DTA curve refers to the formation of the Si–Al spinel, and is more evident in kaolin due to the greater amount of kaolinite present in kaolin in relation to clay. Figure 5.11 shows the graph with TGA, DrTG, and DTA curves of quartz.

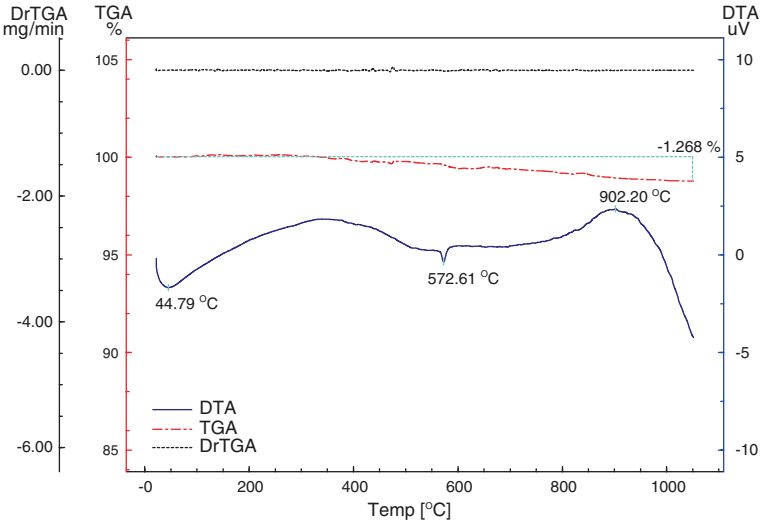

Fig. 5.12 DTA/TGA thermal analysis of feldspar

The excellent thermal stability of quartz in relation to mass loss during heating can be observed. The allotropic transformation of α-quartz into β-quartz can also be observed.

Figure 5.12 shows the graph with TGA, DrTG, and DTA curves of feldspar. The maximum temperature of the thermal analysis of feldspar was 1,050 °C due to the possibility of melting the material and hence loss of the crucible. Overall, the material exhibited stable behavior in relation to mass loss up to the end of the test with a little more than 1.2 % variation. The endothermic peak at 572.61 °C is due to the allotropic transformation of α-quartz into β-quartz.

Figure 5.13 shows the graph with TGA, DrTG, and DTA curves of pyrophyllite. Relatively low mass loss of about 2.6 % may be observed up to 850 °C. In the DTA curve, in turn, the peak at 42.55 °C refers to the loss of water adsorbed by particles of the material, and peak at 575.65 °C is related to the allotropic transformation of quartz shown above.

Between 800 and 900 °C, the mass loss of 2.577 % is followed by endothermic peak at temperature of 847.79 °C, which is likely to be related to the formation of a new phase involving MgO and SiO_2 (Fig. 5.14). According to the binary diagram of the MgO–SiO_2 system and taking into consideration only the composition of the talc used in this work (36.6 % MgO and 63.4 % SiO_2, for 100 % MgO and SiO_2), the formation of the enstatite phase ($MgO{\cdot}SiO_2$) is more likely to occur, since the formation of the fosterite phase (Mg_2SiO_4) occurs for compositions with higher MgO contents. However, in this case, only the composition with percentages of MgO and SiO_2 of one of the raw materials is not enough to identify with accuracy which phase was formed due to the interference from the other components. Figure 5.15 shows the graph with TGA, DrTG, and DTA curves of residue R1.

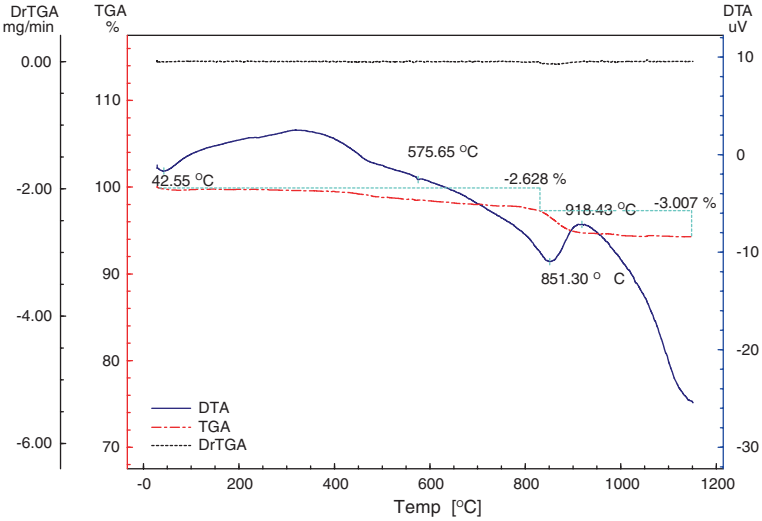

Fig. 5.13 DTA/TGA thermal analysis of pyrophyllite

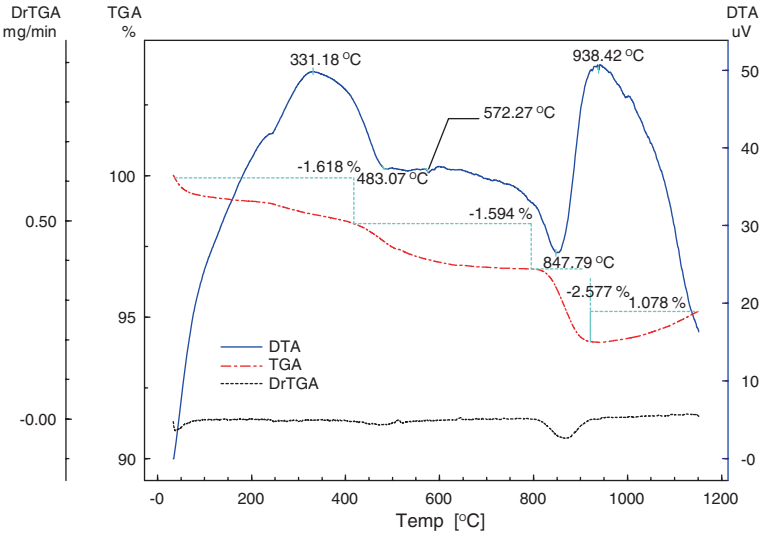

Fig. 5.14 DTA/TGA thermal analysis of talc

It is possible to observe a mass loss of about 8.95 % up to 200 °C. This mass loss is accompanied by an endothermic peak in DTA curve (108.20 °C), which results from the loss of adsorbed water and zeolitic water, confirming the presence of hydrate component (K_2CO_3) that will be confirmed latter in the X-ray diffraction pattern.

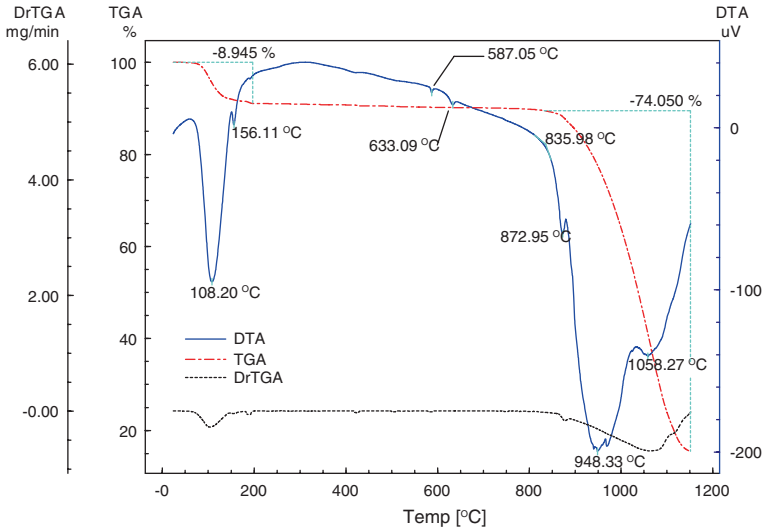

Fig. 5.15 DTA/TGA thermal analysis of residue R1

Then, the sample remains virtually constant mass up to temperature of 835.98 °C, when, thereafter, began to lose mass until the end of the heating cycle. It was observed that the mass loss was very significant in the temperature range from 850 to 1,150 °C, where the sample has lost more than 70 % of its original mass. The mass loss in this temperature range is characteristic of carbonates, a fact which once again confirms the presence of K_2CO_3 in the sample. K_2CO_3 decompose to form $K_2O + CO_2$, where CO_2 is removed in the form of gas and K_2O tends to volatilize upon decomposition of K_2CO_3 (Liodakis et al. 2005). It is possible that this feature makes the use of this residue in the manufacture of porcelain tiles unfavorable, because considering the firing temperature, the effects of eliminating these gases along with the high mass loss will certainly be observed in the microstructure of the final product. Safronova (2009), reports that at high temperatures, the decomposition of potassium carbonates may contribute to obtaining a material with greater porosity.

Figure 5.16 shows the graph with TGA, DrTG, and DTA curves of residue R2. Mass loss, along with endothermic peaks at the beginning of heating cycle up to 200 °C, relates to the loss of adsorbed water and zeolitic water. The mass loss up to 600 °C may be associated with the presence of organic matter in the sample.

The increased mass loss rate observed in the temperature range from 600 to 750 °C, with a peak at 739.84 °C in the DrTG curve is mainly related to the decomposition of calcium carbonate ($CaCO_3$), as according to Winbo et al. (1998), the experimental value of the temperature at which the decomposition of $CaCO_3$ occurs is 697 °C at atmospheric pressure. The endothermic peak in the DTA curve (735.84 °C) confirms the effect of this decomposition. In the range from 800 to 900 °C, slight increase in the mass loss rate is observed. In this temperature range,

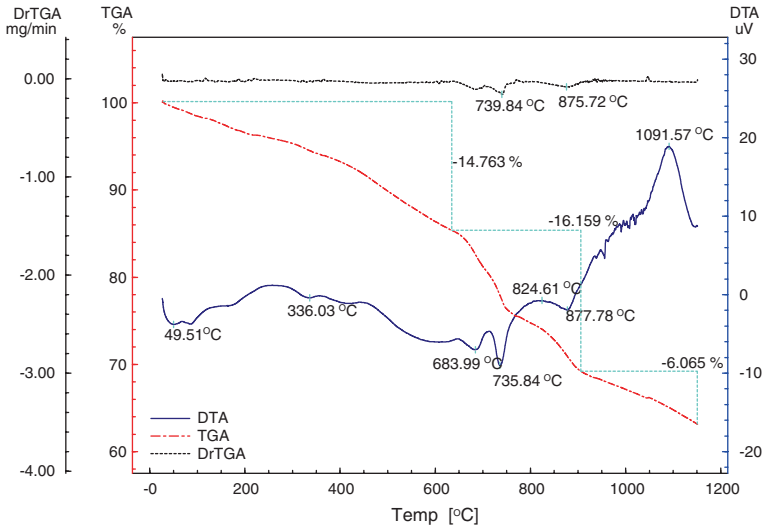

Fig. 5.16 DTA/TGA thermal analysis of residue R2

fairchildite begins decomposition process, with formation of liquid phase plus residual calcite ($CaCO_3$) (Navrotsky et al. 1997; Winbo et al. 1998).

5.9 Particle Size Analysis

The particle size analysis of raw materials was performed by classification of particle size by laser diffraction on a CILAS® laser granulometer model 1180, coupled to an ultrasound system. About 2 g of sample was used in 10 ml of distilled water without addition of dispersing agent. The dispersion occurred at 60 s.

The result of the analysis was provided by The Particle Expert® software. The device provides the corresponding diameters of particles from the flow trapped in the fractions of interest, and also the mean diameter (Dmean) and the granulometric distribution curves of particles.

The size of the particles plays an important role in the preparation of raw materials for the production of porcelain tiles. Biffi (2002), highlights the role that particle size plays in the vitrification and densification reactions during firing and that the smaller the particle size of the ceramic mass, the higher its reactivity during firing. The author also states that the residue of grinding ceramic masses for porcelain tile production shall be between 0.5 and 1.0 % in 325 mesh (44 μm) and, for this, the average particle diameters should be between 15 and 20 μm.

Figure 5.17 shows the particle size curves of clay and kaolin. In clay, the particle size is between 0.04 and 25 μm, with mean diameter Dmean = 4.65 μm, D10 = 0.86 μm, D50 = 3.34 μm, and D90 = 10.67 μm.

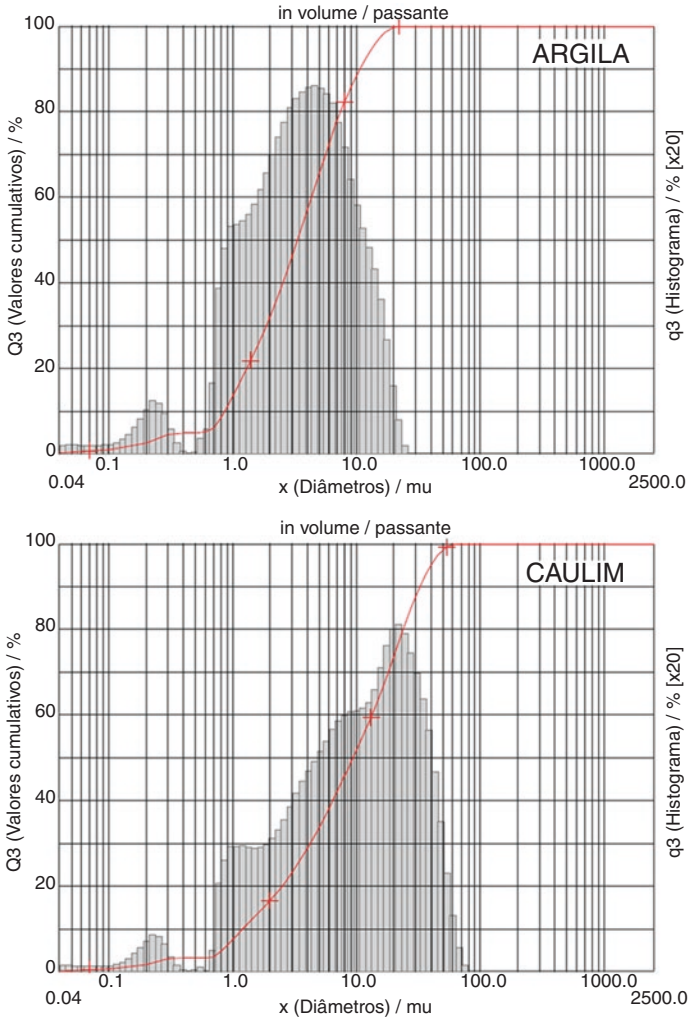

Fig. 5.17 Particle size analysis of clay (**a**) and kaolin (**b**)

For kaolin, the particle size is between 0.04 and 71 μm, with mean diameter Dmean = 13.61 μm, D10 = 1.21 μm, D50 = 9.34 μm, and D90 = 32.53 μm. Particles in kaolin with diameter greater than 44 μm (325 mesh) represent only 2.72 % and may be associated with impurities acquired after sieving. The smaller particle size of clay was expected due to the characteristics of materials. Clays have a higher clay fraction (particles with diameter < 2 μm), which is primarily responsible for the clay sintering due to the particle size and predominance of clay materials (Vieira et al. 2007).

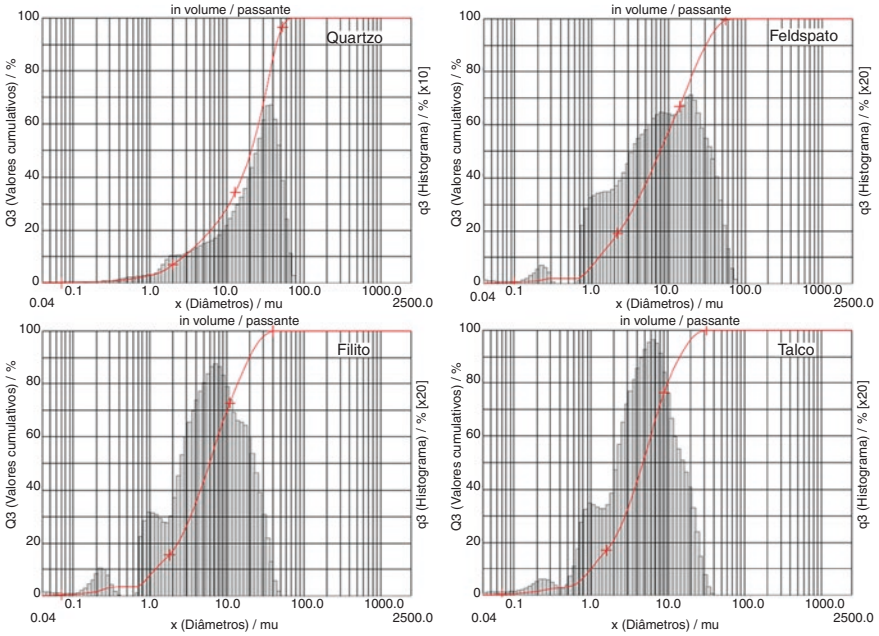

Fig. 5.18 Particle size analysis of quartz (**a**), feldspar (**b**), phyllite (**c**), and talc (**d**)

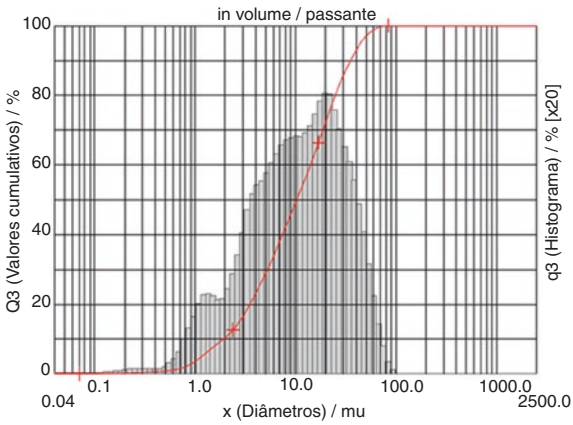

Fig. 5.19 Particle size analysis of residue R2

Figure 5.18 shows the particle size analysis of quartz, feldspar, phyllite, and talc. In quartz, the particle size is between 0.04 and 63 μm, with mean diameter Dmean = 22.54 μm, D10 = 2.73 μm, D50 = 21.01 μm, and D90 = 44.55 μm. For feldspar, particle size is between 0.04 and 63 μm, with mean diameter Dmean = 12.42 μm, D10 = 1.25 μm, D50 = 7.82 μm, and D90 = 30.96 μm.

For phyllite, the particle size is between 0.04 and 40 μm, with mean diameter Dmean = 8.50 μm, D10 = 1.17 μm, D50 = 5.98 μm, and D90 = 19.83 μm. For talc, the particle size is between 0.04 and 32 μm, with mean diameter Dmean = 6.43 μm, D10 = 1.00 μm, D50 = 4.77 μm, and D90 = 14.51 μm. Figure 5.19 shows the particle size analysis of residue R2. This residue was sieved in 200 mesh because it is a highly hygroscopic material, greatly reducing the sieving efficiency on 325 mesh. The residue R2 showed particle sizes from 0.04 to 85 μm and mean diameter Dmean = 15.05 μm, D10 = 1.92 μm, D50 = 10.29 μm, and D90 = 35.40 μm. Although the sieving of residue R2 was performed in mesh greater than those used for the other raw materials, the material showed adequate particle size after the grinding process.

In the analysis of residue R1, equipment did not detect solid particles because the material is water soluble. With respect to particle size analysis, all raw materials are within characteristics reported in literature for the manufacture of porcelain tiles.

The results after the sintering process will be discussed in the next chapters.

References

Biffi G (2002) O Grês Porcelanato: Manual de Fabricação e Técnicas de Emprego. Ed. Faenza Editrice do Brasil

Dultra EJV, Acchar W (2010) Incorporação de Cinzas da Casca de Café na Produção de Placas Cerâmicas para Revestimento. Dissertação de Mestrado. UFRN-PPGEM, Natal

Liodakis S, Katsigiannis G, Kakali G (2005) Ash properties of same diminant Greek forest species. Thermochim Acta 437:158–167

Navrotsky A, Putnam RL, Winbo C, Rosén E (1997) Thermochemistry of double carbonates in the K_2CO_3-$CaCO_3$ system. Am Mineral 82:546–548

Safronova TV (2009) Phase composition of ceramic based on calcium hidroxyapatite powders containig by products of the synthesis reaction. Glass Ceram 66(3–4):136–139

Santos PS (1989) Ciencia e tecnologia das argilas, vol 12. Edgard Blucher, Sao Paulo

Vieira CMF, Terrones LA, Sánches R, Monteiro SN (2007) Características e Efeito da Fração Granulométrica < 2 μm no Comportamento de Queima de uma Argila. Cerâmica 53:249–254

Winbo C, Rosén E, Heim M (1998) Thermal analytical study of the decomposition of $K_2Ca_2(CO_3)_3$. Acta Chem Scand 52:431–434

Chapter 6
Theoretical Analysis of Crystalline Phases

Abstract This chapter makes a theoretical analysis of the promising crystalline phases using the phase's diagram of the principal components. Phase diagrams of the SiO_2–Al_2O_3–K_2O, leucite–SiO_2–mullite and SiO_2–CaO–Al_2O_3—systems are used to analyze the promising crystalline phases.

Keywords Crystalline phases · Phase diagram

To allow a view of the general behavior of formulations, the ternary diagram of the Si–Al–K system was chosen. The phase diagrams are developed taking into account the condition of thermodynamic equilibrium, and in current firing cycles of porcelain tile production, this equilibrium does not occur. However, according to Segadães (2006), even in cycles where thermodynamic equilibrium does not occur, the phase diagram of a system can provide important information about the trends of chemical reactions. According to Segadães (2006), it was considered that the sum of percentage of K_2O, Na_2O, CaO, and MgO elements should be placed in the vertex of K_2O due to the similarity of the fluxing effect between them. Figure 6.1 shows the phase diagram of the SiO_2–Al_2O_3–K_2O system. Whereas virtually all formulations are located in the compatibility triangle region $K_2O{\cdot}Al_2O_3{\cdot}6SiO_2$–$SiO_2$–$3Al_2O_3{\cdot}2SiO_2$ (Potassium feldspar–SiO_2–Mullite), the leucite–SiO_2–Mullite subsystem ternary diagram was used and positioned in formulations. Thus, the information obtained from the diagram becomes more evident (Dultra and Acchar 2010).

In all diagrams, MB (fluxing-free mass) and MP (standard mass) formulations are positioned for comparison purposes. Figure 6.2 shows the ternary diagram related to leucite–SiO_2–Mullite subsystem with formulations containing residue R1 as single fluxing and formulations with the combination of residue R1 and feldspar.

MP and MB masses (points 1 and 2, respectively) are located in the triangle of mullite–feldspar potassium–SiO_2 compatibility, in the primary field of the mullite region. However, the chemical composition of the MP mass sets it into a more

W. Acchar and E.J.V. Dultra, *Ceramic Materials from Coffee Bagasse Ash Waste*, SpringerBriefs in Applied Sciences and Technology,
DOI 10.1007/978-3-319-15281-3_6

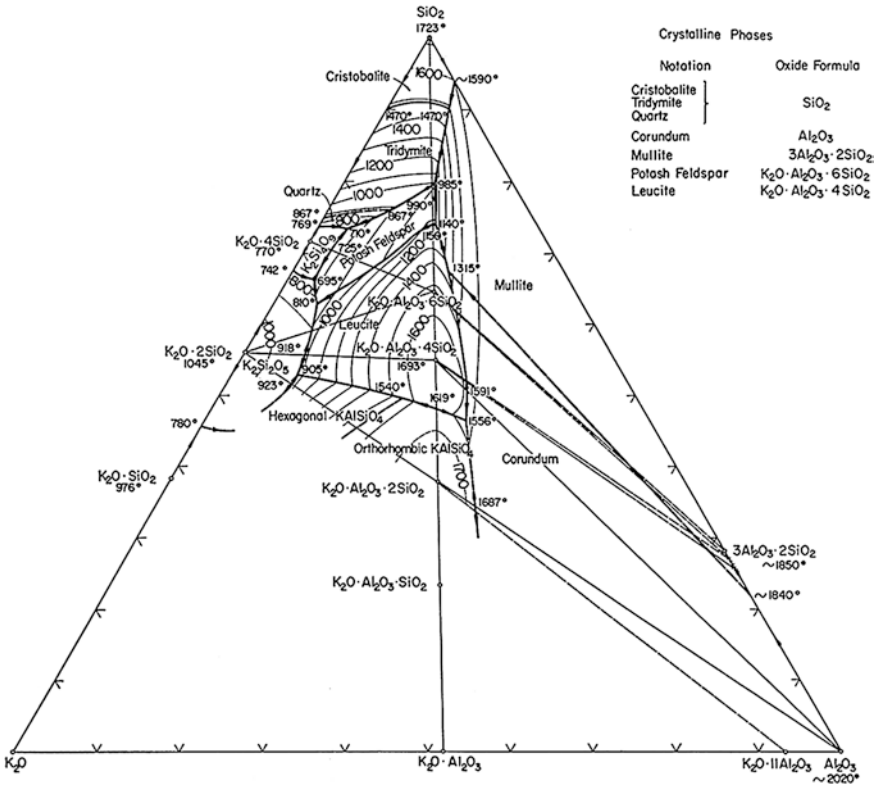

Fig. 6.1 Phase diagram of the SiO_2–Al_2O_3–K_2O system

interesting region of the diagram, since the secondary phase formed in the diagram will be potassium feldspar ($K_2O{\cdot}Al_2O_3{\cdot}6SiO_2$). In the case of the MB sample, the secondary phase is cristobalite (SiO_2). Based on the phase diagram and according to the calculation methodology described by Segadães (2006), the positions of MP and MB masses in the diagram suggest that at temperature 1,200 °C (maximum firing temperature of samples of this study), the MP sample presents higher amount of liquid than the MB sample. At the start of cooling outside the thermodynamic equilibrium, the liquid solidifies forming this glassy phase and thus the ceramic body resulting from the MP mass tends to become more vitrified compared with the MB sample.

It could be clearly observed that the addition of residue R1 shifted the formulation toward the leucite vertex. Regarding the mechanical strength, the mullite region is more favorable. The spherical shape of leucite crystals does not improve the mechanical strength. It is found that the addition of feldspar to formulations 10 and 11 caused no significant shift, and the formulations remained in the primary mullite field.

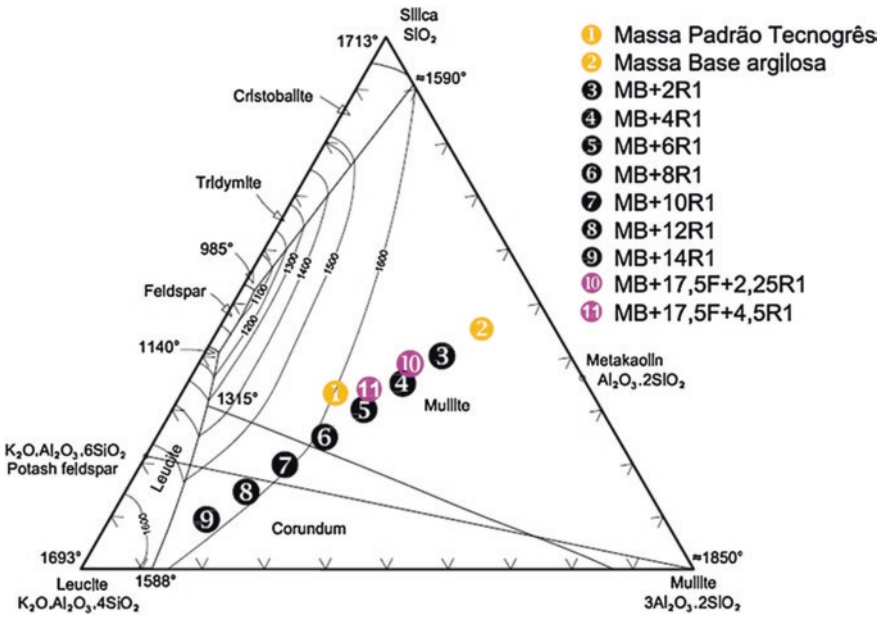

Fig. 6.2 Phase diagram of the leucite–SiO_2–mullite subsystem containing formulation added of residue R1

It is noteworthy that, according to the XRF results, residue R1 has 95 % K_2O and this means that when larger amounts of residue R1 are added, displacement toward the leucite vertex is practically real because it should be recalled that the K_2O vertex is represents the sum of K_2O, Na_2O, CaO, and MgO elements.

Figure 6.3 shows the ternary diagram related to the leucite–SiO_2–mullite subsystem with the position of formulations containing residue R2 as a single fluxing agent, and formulations with the combination of residue R2 with feldspar. Similar to formulations containing residue R1, the addition of residue R2 also causes displacement towards the leucite vertex, but we must consider that residue R2 contains more balanced amounts of K_2O, CaO, and MgO. Although the diagram indicates a trend to displace the leucite vertex, a smaller amount of this phase will be obtained since the real amount of K_2O is smaller in residue R2. As residue R2 is added to the mass, the formation of phases involving MgO, CaO, SiO_2, and Al_2O_3, like anorthite ($CaAl_2Si_2O_8$) and cordierite ($Mg_2Al_4Si_5O_{18}$) is also possible, as these are located in nearby regions, but in their respective CaO–SiO_2–Al_2O_3 and MgO–SiO_2–Al_2O_3 systems.

The MB+5R2 mass is located in the primary field of mullite, while MB+10R2 mass is located near the boundary line between mullite and corundum, but already in the primary field of corundum.

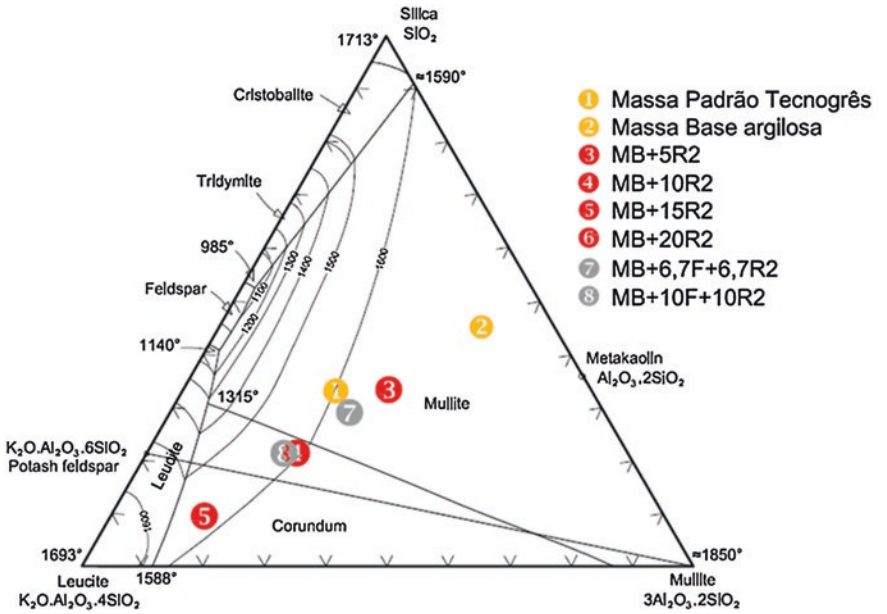

Fig. 6.3 Phase diagram of the leucite–SiO_2–mullite subsystem containing formulation with the addition of residue R2

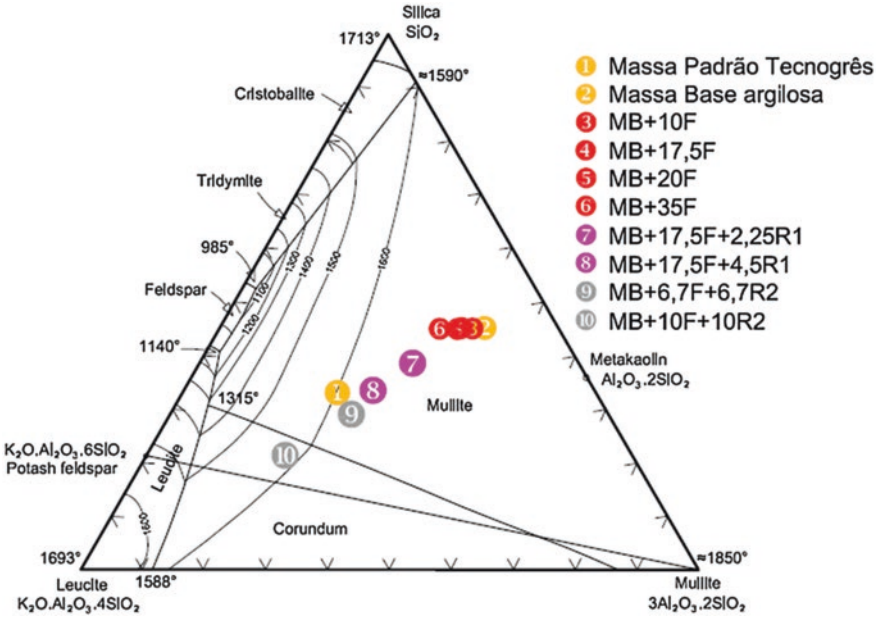

Fig. 6.4 Phase diagram of the leucite–SiO_2–mullite subsystem containing formulation added of feldspar

The MB+5R2 mass is located at the primary field of corundum, in the leucite–potassium feldspar–mullite compatibility triangle, near the border line with leucite. The MB+20R2 mass is located outside the system of Fig. 6.3. Thus, as larger amounts of residue R2 are added, the diagram reading indicates less formation of mullite in favor of leucite and as mentioned above, of anorthite and cordierite. The MB+6.7F+6.7R2 mass (point 7) is located in the primary field of mullite, near the location of the MP mass.

Figure 6.4 shows the ternary diagram related to the leucite–SiO_2–mullite subsystem with the position of formulations containing feldspar as a single fluxing agent along with formulations in association with feldspar residues R1 and R2 residue with feldspar. It could be observed that the addition of feldspar caused displacement in parallel direction to the opposite side of the SiO_2 vertex, or the amount of SiO_2 in the chemical composition of the mass remained constant with the addition of feldspar. All formulations added to feldspar as a single fluxing

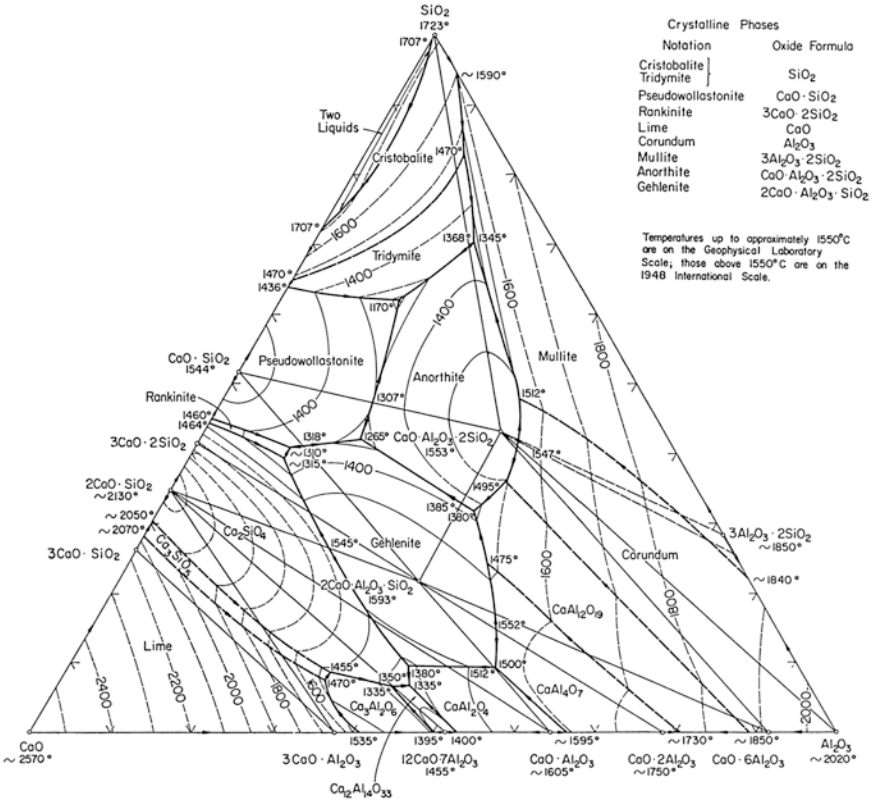

Fig. 6.5 SiO_2–CaO–Al_2O_3 system

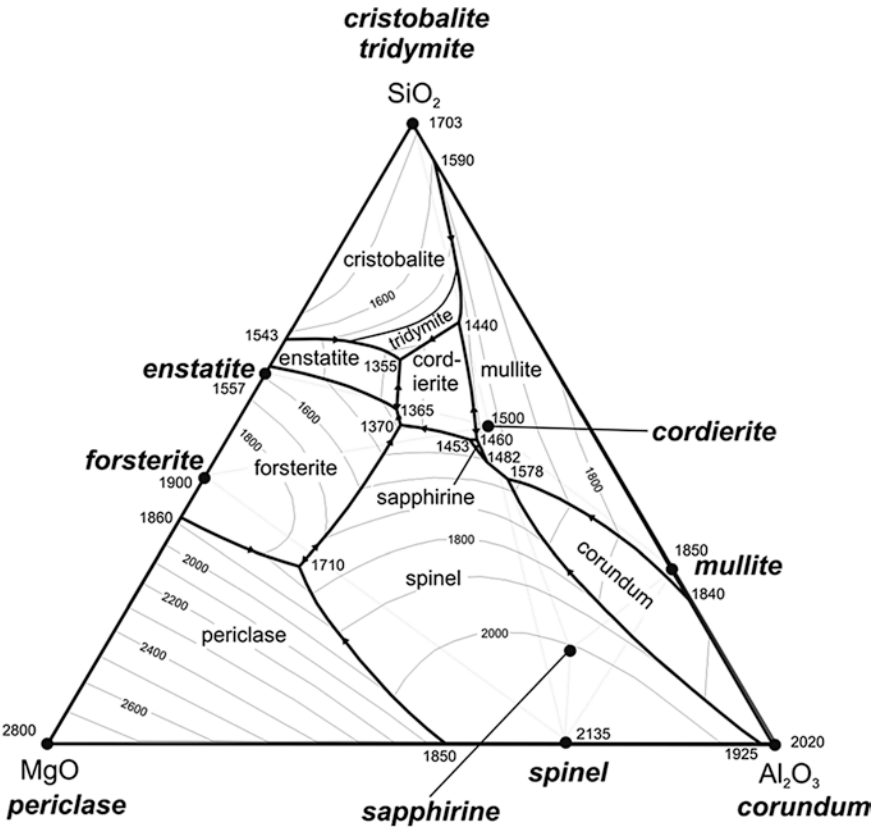

Fig. 6.6 Cristobalite–corundum–periclase system

agent are in the region of mullite and mullite formation in the presence of liquid phase favors the growth of acicular crystals, called secondary mullite. This characteristic is desired, since it will lead to better mechanical performance of parts.

Figures 6.5 and 6.6 show another phase diagram in the SiO_2–CaO–Al_2O_3 and cristobalite–corundum–periclase system that may be useful to identify and compare the crystalline phases formed during the sintering process.

The crystalline phases formed during the sintering process as well as the theoretical previous will be discussed in another chapter.

References

Dultra EJV, Acchar W (2010) Incorporação de Cinzas da Casca de Café na Produção de Placas Cerâmicas para Revestimento. Dissertação de Mestrado. UFRN-PPGEM, Natal

Segadães AM (2006) Use of phase diagrams to guide ceramic production from wastes. Adv Appl Ceram 105(1):46–54

Chapter 7
Physical and Mechanical Properties of CBA Incorporated Material

Abstract This chapter shows the physical and mechanical properties after the sintering process. Dilatometric analysis and X-ray diffraction after firing as well as the water absorption, porosity and bending strength values are described and compared with the Brazilian norms.

Keywords Physical properties · Mechanical properties · Clay with coffee husk ash

7.1 Dilatometric Analysis

The dilatometric analysis is evaluated for expansion and contraction of sample as a function of temperature (heating) and time. Through the analysis of results, it is possible to determine the thermal expansion coefficient at different temperature ranges.

For practical purposes, on ceramic masses, the main response obtained is the temperature where the sintering of the ceramic body starts to occur, since it is known that sintering is accompanied by volume shrinkage, as explained in Sect. 2.1.12. This information is important for evaluating the thermal cycle in the manufacture of ceramic products.

Figure 7.1 shows the dilatometric curve of masses containing residue R1 as fluxing. The flux-free MB mass curve is also shown.

For temperatures little above 200 °C, there was volumetric contraction seen in masses containing residue R1. The occurrence of this type of effect at this temperature range is not common. As residue R1 is excessively hygroscopic, it is possible that the sample has absorbed significant amounts of water, especially in the region near the surface. The removal of this surface water due to the increase in temperature could have caused such initial contraction. From 200 °C, samples containing residue R1 are expanding, where a volumetric expansion peak can be observed due to allotropic shift of α-quartz to β-quartz around 573 °C and from this temperature, contraction begins to occur. It was observed that, at the temperature range from 573 to 858 °C, the contraction became more discrete in samples with

W. Acchar and E.J.V. Dultra, *Ceramic Materials from Coffee Bagasse Ash Waste*, SpringerBriefs in Applied Sciences and Technology,
DOI 10.1007/978-3-319-15281-3_7

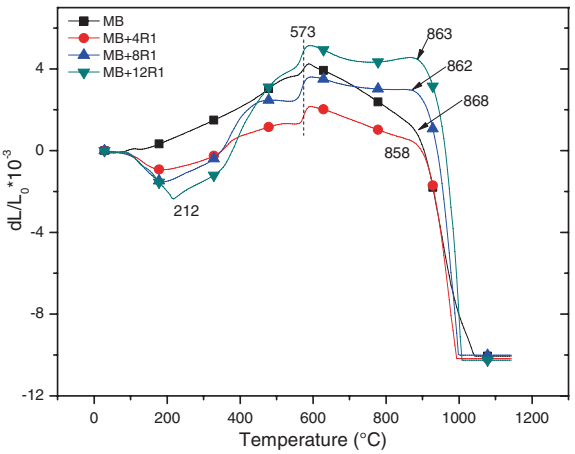

Fig. 7.1 Dilatometric analysis of masses containing residue R1

a higher percentage of residue R1, and for MB+12R1 formulation with 12 % of residue R1, contraction instead of expansion was observed, considering the same temperature range. This effect is certainly related to the increased content of carbonates in the formulations with higher percentage of residue R1, whose decomposition (and subsequent release of gas) causes a typical volumetric expansion.

Contraction significantly increased at temperature range from 858 to 868 °C, characterizing the onset of sintering. It was observed that the temperature of onset of sintering is within a rather narrow range for masses containing residue R1. According to the analysis of data, it was found that the addition of residue R1 influenced the temperature of onset of sintering in relation to mass MB. Mass MB begun sintering at 868 °C, while masses with residue R1 started sintering at 858, 862, and 863 °C, respectively, according to the increasing amount of residue added.

Figure 7.2 shows the curves of dilatometric analyses of masses containing residue R2 and flux-free mass (MB). It was also observed that samples with addition of residue R2 showed contraction at the beginning of heating to 200 °C. This contraction was more evident as the content of residue R2 increased. Residue R2 is hygroscopic and it is quite possible that this initial contraction is due to this fact.

It was observed that residue R2 obtained better contribution in relation to the earlier start of sintering when compared to residue R1. In temperature ranges from 573 to 850 °C, contraction is observed in MB, MB+5R2, and MB+10R2 samples. At this stage of the heating cycle, early signs of softening particles will melt first, i.e., the microstructure of the material is thermodynamically preparing to the beginning of the sintering process. It was also observed that the contraction tended to be lower as the amount of residue R2 is increased due to the higher content of carbonates in the formulation, whose decomposition (and consequent release of gas) causes a typical volumetric expansion.

In MB+15R2 and MB+20R2 samples, no contraction was observed in this temperature range, where instead of contracting, samples showed volumetric

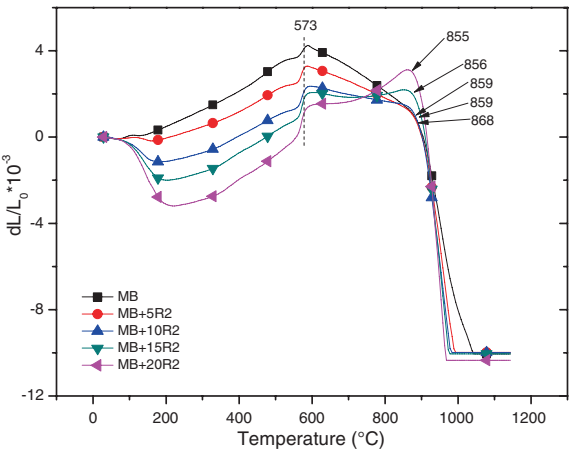

Fig. 7.2 Dilatometric analysis of masses containing residue R2

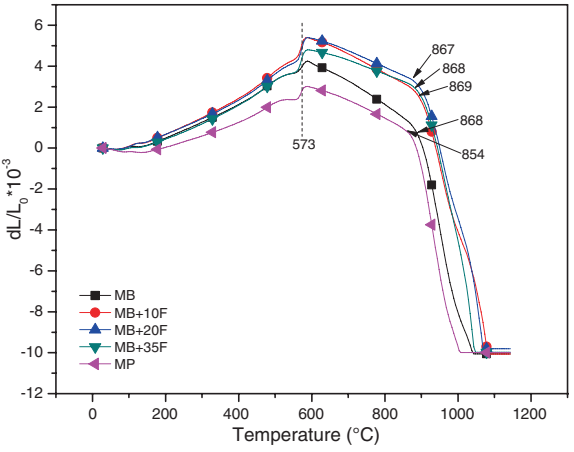

Fig. 7.3 Dilatometric analysis of masses containing feldspar

expansion. As previously mentioned, the decomposition of carbonates causes a typical volumetric expansion due to the elimination of gases. If these gases remain trapped within the ceramic mass it will cause the appearance of closed pores inside the sample enhancing volumetric expansion. Thus, for residue R2 content equal to or greater than 15 %, increasing the amount and possibly the larger size of closed pores inside the sample caused an increase in volume of the ceramic mass, within the heat range considered.

The MB mass began sintering at 868 °C, while the mass with the highest content of residue R2 (MB+20R2) started sintering at 855 °C. Mass with the lowest levels of residue R2 (MB+5R2) started sintering at 859 °C.

Figure 7.3 shows the dilatometric analysis of the masses containing feldspar as fluxing, along with flux-free mass (MB) used by the supplier company as raw material (MP), whose formulation is described in Table 2.3.

It was observed that the initial contraction at temperature of up to 200 °C does not occur in samples with feldspar. This confirms that the cause of this effect involves a simultaneous feature present in residues R1 and R2. According to the results, feldspar contributed little to the earlier start of sintering when compared to the MB mass. The onset of sintering occurred virtually at the same temperature for all masses containing feldspar as fluxing in comparison with the MB mass, unlike expectations. It is possible that the liquid formed at this temperature range has very high viscosity, thus making the wetting of particles that remained solid difficult. MP mass started sintering at 854 °C, and this anticipation was certainly due to the presence of pyrophyllite and talc in the ceramic mass.

7.2 Characterization of Specimens After Firing

In this step, the mineralogical characterization of crystalline phases, the physical properties, and microstructure will be assessed.

7.2.1 X-Ray Diffraction (XRD)

Figure 7.4 shows the graph with the X-ray diffraction pattern of sintered MB and MP samples. MB Sample showed diffraction peaks related to quartz and mullite phases. In MP sample, diffraction peaks related to quartz, cordierite, and mullite phases were identified. The cordierite phase present in the MP sample comes from the talc used as raw material. The results confirm expectations indicated by the phase diagram for both MB and MP samples. The presence of fluxes in the MP sample caused a displacement to the leucite region. However, it should be recalled that the sum of K_2O, CaO, Na_2O, and MgO elements was considered to position formulations in the diagram. Then, hydrated magnesium silicate present in talc promoted the formation of the cordierite phase in MP sample.

Figure 7.5 shows the graph with the X-ray diffraction pattern of sintered MB+4.5R1 and MB+12R1 samples. In MB+4.5R1 sample, diffraction peaks related to quartz and mullite phases were identified. In MB+12R1 sample, diffraction peaks related to quartz, mullite, and leucite phases were identified. The leucite arises due to the greater amount of residue R1, confirming expectations regarding the trends of chemical reactions indicated by the phase diagram. It should be recalled that the leucite phase does not favor the mechanical flexural strength due to the spherical shape of its crystals.

Figure 7.6 shows the graph with the X-ray diffraction pattern of sintered MB+5R2 and MB+15R2 samples. In MB+5R2 sample, diffraction peaks related to quartz and mullite phases were identified. In MB+15R2 sample, diffraction peaks related to quartz, leucite, and anorthite phases were identified. The presence of leucite and anorthite phases is due to the increase of residue R2 in the ceramic

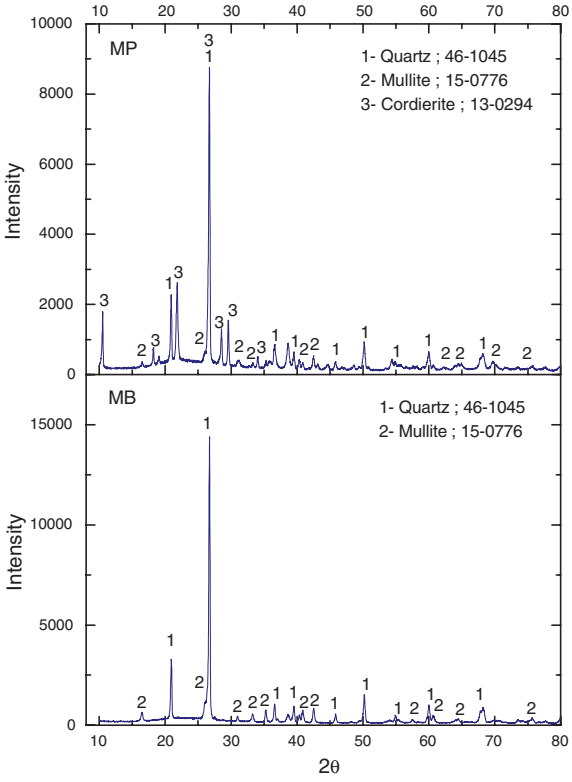

Fig. 7.4 X-ray diffraction pattern of sintered MP and MB samples

mass, confirming the trends shown by the phase diagram. According to the XRF results shown in Table 5.8, the key elements present in residue R2 are K_2O (31.00 %) and CaO (28.18 %). However, positioning formulations in the phase diagram considered the sum of K_2O, CaO, Na_2O, and MgO elements as equivalent to K_2O. Then, the displacement to the leucite vertex when adding residue R2 to the mass indicates not only the formation of leucite, but also of anorthite, since anorthite is located at the same region of the diagram, but in the $CaO–SiO_2{\cdot}Al_2O_3$ system, as can be seen in Chap. 8, Annex III, ray diffraction pattern of sintered MB+4R1 and MB+12R1 samples.

Figure 7.7 shows the graph with the X-ray diffraction pattern of sintered MB+10F sample. The presence of diffraction peaks related to quartz and mullite phases can be observed. This result was expected as the trends shown by the phase diagram.

7.2.2 Open, Close and Total Porosity

AP is the amount of pores interconnected with the outside of the ceramic mass. The AP results of sample residues R1 and R2 are shown in Fig. 7.8. It was observed

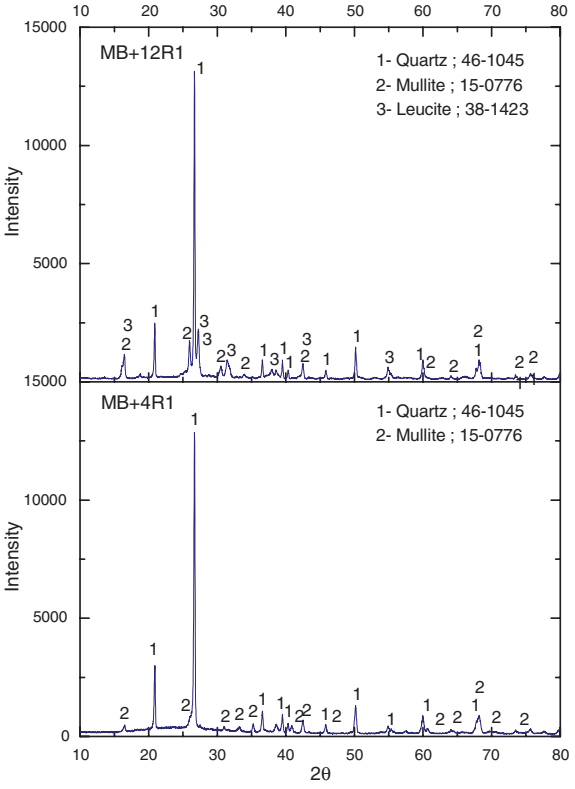

Fig. 7.5 X-ray diffraction pattern of sintered MB+4R1 and MB+12R1 samples

that the percentage of residue R1 that yielded the lowest AP results is between 7 and 9 % of added residue. Observing the phase diagram shown in Fig. 6.1, it could be seen that formulations with R1 percentages between 7 and 9 % are located in the compatibility triangle region, potassium feldspar–SiO_2–Mullite in the primary field of mullite, in a more favorable location, since this compatibility triangle has an invariant point at 985 °C, temperature at which, for these formulations during heating, the first signs of presence of the liquid phase appear. Formulations with R1 percentages above this range are outside the primary field of mullite and, considering formulations with 12 and 14 % residue R1, besides this feature, they go beyond the boundary line of the compatibility triangle potassium feldspar–SiO_2–mullite, from this point belonging to the compatibility triangle leucite–potassium feldspar–mullite, whose invariant point is at temperature of 1,140 °C.

For samples containing residue R2, AP values were lower compared to results of samples with residue R1. The lowest AP values were obtained for MB+10R2 and MB+15R2 samples, with 0.68 and 0.16 %, respectively.

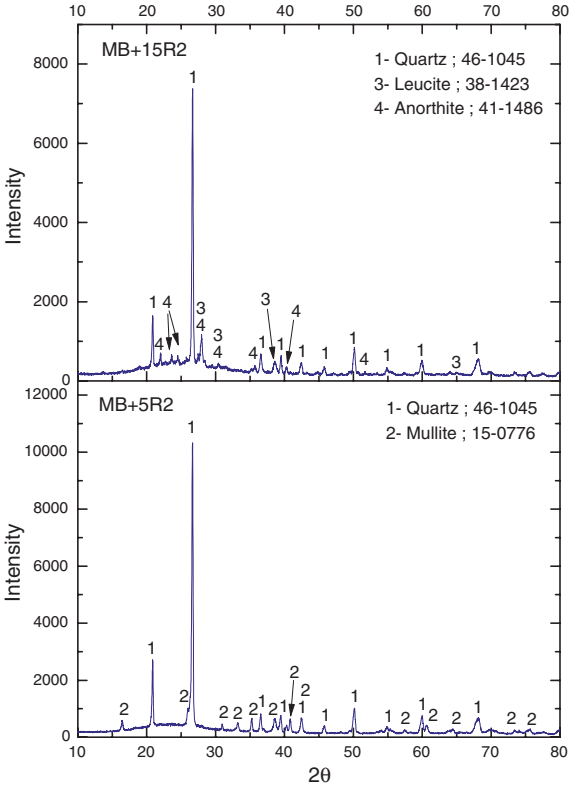

Fig. 7.6 X-ray diffraction pattern of sintered MB+5R2 and MB+15R2 samples

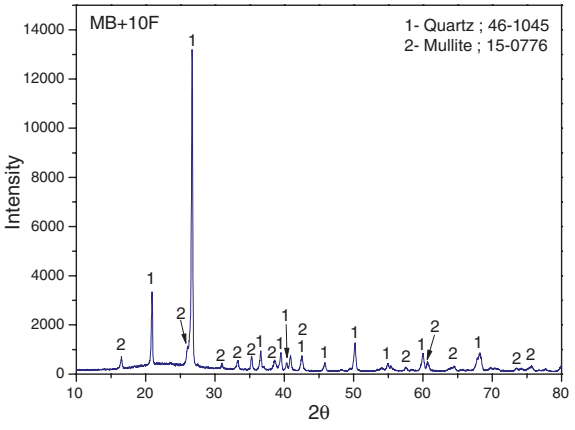

Fig. 7.7 X-ray diffraction pattern of sintered MB+10F sample

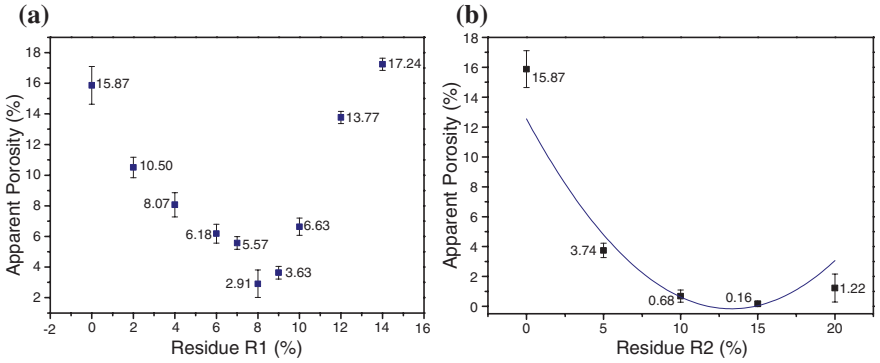

Fig. 7.8 AP results of samples containing R1 (**a**) and R2 (**b**)

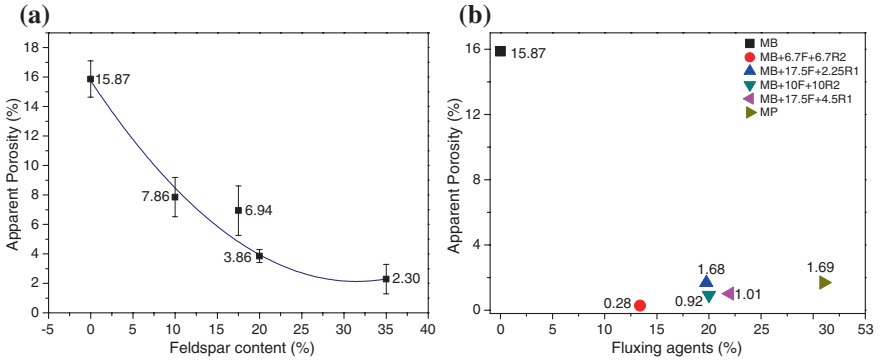

Fig. 7.9 AP results of samples containing feldspar (**a**) and association of residue + feldspar (**b**)

Figure 7.9 shows the AP results of samples added to feldspar and samples with association of residue + feldspar. For samples containing only feldspar as flux, the AP values decrease as the amount of feldspar is increased, that is, the greater the amount of feldspar in the ceramic mass, the lower the AP value of the sintered body.

Masses with associated fluxes (residue R1 + feldspar and R2 + feldspar residue) obtained low AP values, highlighting MB+6.7F+6.7R2 mass that showed 0.28 % AP.

Table 7.1 shows the AP and CP values of masses whose properties obtained positive or negative highlighting. According to Noni et al. (2010), the microstructure of the porcelain tile should have AP and CP below 10 %.

In porosity tests, AP was determined using the Archimedes principle, whereas TP was determined as a function of the fired body absolute density. Then, the CP is the difference between TP and AP. In MB sample, all porosity is of open type, whose pores communicate with the outside part. Analyzing the other results, it could be observed that samples with addition of R1 obtained a slight decrease in

Table 7.1 Total, open, and closed porosity of sintered samples

Formulation	Total porosity (%)	Open porosity (%)	Closed porosity (%)
MB	16.00	16.00	0
MP	8.52	1.69	6.83
MB+4R1	13.36	6.94	6.42
MB+8R1	7.96	2.91	5.04
MB+12R1	17.97	1.77	4.20
MB+5R2	11.30	3.74	7.56
MB+10R2	15.14	0.68	14.56
MB+15R2	21.21	0.16	21.05
MB+10F	11.71	7.86	3.85
MB+17,5F	10.26	6.94	3.32
MB+35F	5.97	2.30	3.68
MB+17.5F+2.25R1	7.49	1.68	5.81
MB+17.5F+4.5R1	8.81	1.01	7.80
MB+6.7F+6.7R2	9.80	0.28	9.52
MB+10F+10R2	21.89	0.92	20.97

CP due to the addition of residue. This may be related to the low viscosity of the liquid formed during firing because the potassium oxide, as a strong flux, produces a low-viscosity liquid during heating. With this feature, the liquid formed has less ability to trap gases released in chemical reactions, favoring the emergence of AP in relation to CP as observed in the results shown in Table 7.1.

In samples added to residue R2, it was observed that for percentages between 5 and 15 % of R2, a reduction in AP was observed as a function of the increase in the percentage of residue added. In contrast, the CP increased for higher percentages of R2. This suggests that the liquid formed showed viscosity high enough to promote the trapping of gases released during heating, favoring the emergence of CP in relation to AP. This increase in CP according to the percentage of residue R2 also occurs in masses with association of residue + feldspar.

The MB+6.7F+6.7R2 mass showed CP equal to 9.52 % while in MB+10F+10R2 mass, the CP increased to 20.97 %. Indeed, this increased CP was caused by the increase in the amount of residue R2 in the mass, as feldspar little contributed to the increase in the CP due to its good stability with respect to the mass loss during heating, as can be seen in Thermal Analysis shown in Fig. 5.11.

7.2.3 Water Absorption

As seen in Table 2.2, NBR-15463 states that the WA value for glazed porcelain tile should be equal to or below 0.5 % and for technical porcelain tile it should be equal to or below 0.1 %. By comparing the AP results with the WA results, an

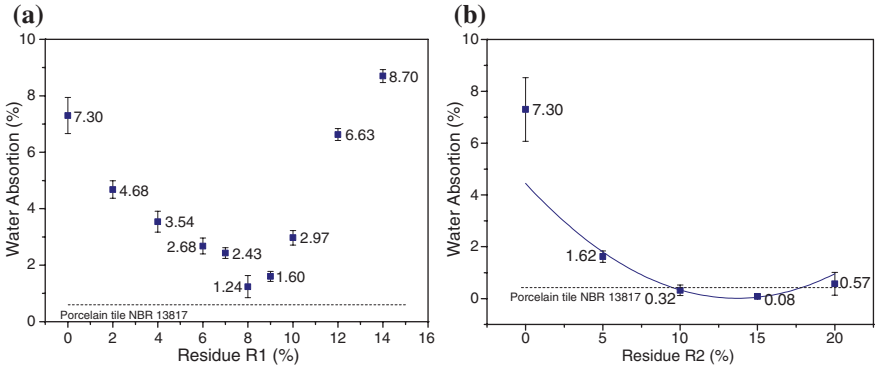

Fig. 7.10 WA results of samples containing R1 (**a**) and R2 (**b**)

analogical behavior of samples with respect to these two properties was observed. This analogy is expected, since both properties are associated with the existence of pores that have interconnection with the outside part.

Figure 7.10 shows the graph with the WA results in function of the addition of residues R1 and R2. The analysis shows that the addition of up to 8 % residue R1 contributes to lower WA, reaching a minimum value of 1.24 %. For more than 8 % addition of residue R1, the WA values tended to increase. It is noteworthy that none of the samples containing only residue R1 as flux obtained WA values within specifications for manufacturing ceramic tiles. Other factor that may have contributed to higher WA levels is the lower viscosity of the liquid formed due to the significant presence of K_2O in the material. Increased amount of fluid with lower viscosity certainly increased AP and therefore WA, since the liquid with such characteristics cannot trap the released gases, which migrate more easily to the surface region of the part.

Regarding residue R2, WA decreased with the addition of residue up to 15 %, and from this content, the WA values tended to increase. Figure 7.11 shows the WA results in relation to the addition of feldspar, as well as samples with association residue R1 with feldspar and R2 with feldspar.

The addition of feldspar also contributed to decrease the WA as expected, and according to results, a trend of decreasing WA as the percentage of feldspar increases is observed. The lowest WA value for samples containing only feldspar as flux was 0.97 % for sample with 35 % feldspar. This WA value is considered high in relation to the minimum standards for the manufacture of porcelain tiles.

Regarding the WA results of samples added to feldspar associated with residues, in general, low WA values were obtained. The best result was obtained by the MB+6.7F+6.7R2 sample (with 6.7 % residue R2 + 6.7 % feldspar), showing 0.12 % WA. This value can be considered excellent, considering the small presence of fluxes in the mass. It is noteworthy that the MB sample, free of fluxes, showed 7.30 % WA, or the addition of residue R2 and feldspar as flux in the respective proportions of 6.7 % provided a decrease of 98.36 % in the WA value.

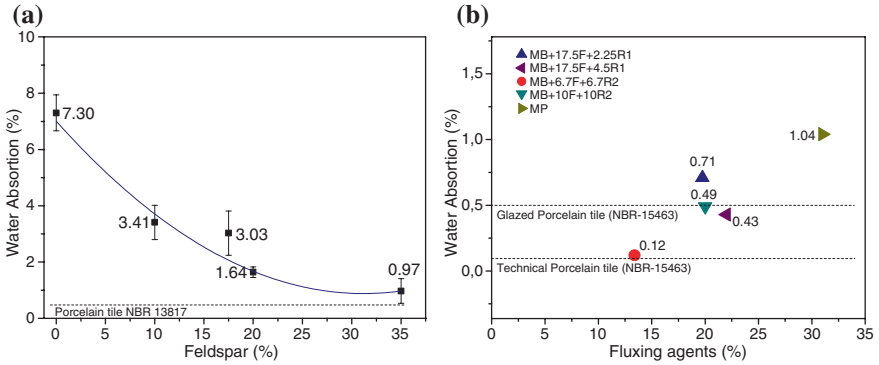

Fig. 7.11 WA results of samples containing feldspar (**a**) and residues + feldspar (**b**)

The MB+10F+10R2 sample obtained WA value equal to 0.49 %, i.e., greater than the value obtained by the MB+6.7F+6.7R2 sample. Analyzing the WA results of residue R2 and feldspar separately (Figs. 7.10b and 7.11a), it was observed that the addition of amounts greater than 15 % caused an increase in WA, whereas for feldspar, no significant increase in WA due to the increased amount of this flux was observed. Then, it could be inferred that the higher WA value in MB+10F+10R2 sample in relation to the MB+6.7F+6.7R2 sample is related to the greater amount of residue R2.

MB+17.5F+2.25R1 and MB+17.5F+4.5R1 samples with addition of residue R1 and feldspar obtained WA values of 0.71 and 0.43 %, respectively. Analyzing the WA results of samples containing feldspar as flux (Fig. 4.43a), it was observed that for addition of 17.5 % feldspar, WA was approximately 3 %. It was also observed that the addition of 2.25 and 4.5 % residue R1 in mass containing 17.5 % feldspar caused a decrease in WA of 76.33 and 85.67 %, respectively.

7.2.4 Linear Firing Shrinkage

LSf is the comparison between length (longest dimension) of the specimen before and after firing expressed as percentage. High retractions are unwanted as they can cause defects in specimens after sintering, for example, warping and microcracks. On the other hand, a very low linear shrinkage (up to 3 %) is an indication of little densification and hence lower porosity reduction. According to Biffi (2002), for porcelain type ceramic plates, LSf must reach from 7.0 to 9.0 %. Figure 7.12 shows graphs containing the LSf results in relation to the addition of residues R1 and R2. According to the results, the maximum LSf related to residue R1 was obtained with the addition of residue in the range from 6 to 8 % and the highest value among the formulations tested was 7.82 %. Regarding the MB sample free of fluxes, the LSf value increases with the increase of R1 to approximately

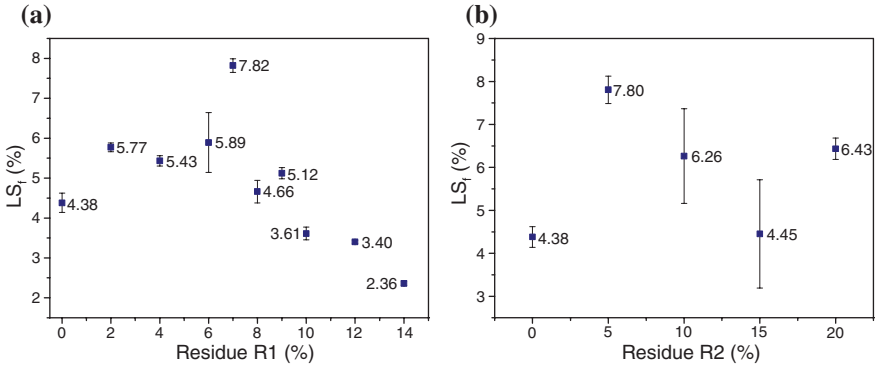

Fig. 7.12 Linear Shrinkage value (LSf) results of samples containing R1 (**a**) and R2 (**b**) residues and feldspar

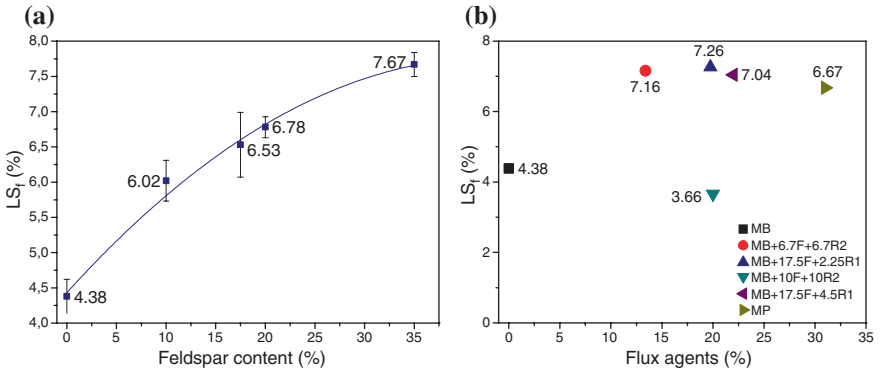

Fig. 7.13 Linear Shrinkage (LSf) results of samples containing feldspar (**a**) and residue + feldspar (**b**)

7 % of added residue (MB+7R1). For larger amounts of residue R1, LSf tends to decrease up to value of 2.36 % related to the sample containing 14 % R1 (MB+14R1).

Regarding residue R2, it was observed that the highest linear Shrinkage (LSf) was obtained with the addition of 5 % R2 (MB+5R2). By increasing the percentage of residue, lower LSf values were obtained. This decrease is associated with increased closed porosity of specimens with 10 and 15 % R2, as results of porosity tests shown in Table 7.1. Figure 7.13 shows the graphs showing the LSf results in relation to the addition of feldspar and samples with residue R1 in association with feldspar and residue R2 with feldspar.

For feldspar, there is a clear trend of increasing LSf value as the percentage of this flux increases. The highest LSf value was obtained with the addition of 35 % feldspar (MB+35F).

MB+17.5F+2.5R1 and MB+17.5F+4.5R1 samples obtained LSf values of 7.26 and 7.04 %, respectively. The MB+6.7F+6.7R2 sample obtained LSf value of

7.16 %, within the usual range indicated by Biffi (2002); however, MB+10F+10R2 sample MB obtained LSf value of 3.66 %, far below recommendations for ceramic tile. LSf value presented by MB+10F+10R2 sample is associated to the higher closed porosity observed in samples with higher amounts of residue R2.

The LSf values achieved by the samples under study are within the specified range for ceramic tiles, with the exception of MB+10F+10R2 sample.

7.2.5 Apparent Specific Mass (ASM) and Real Specific Mass (RSM)

The ASM value of fired bodies provides a notion on the material densification after firing. Figure 7.14 shows the ASM values of samples added to residues R1 and R2. Analyzing the ASM values of samples added to residues R1, it can be seen that the maximum value achieved (2.36 g/cm^3) coincides with the percentage of residue that obtained the lowest water absorption (8 % residue R1), suggesting that for this composition, densification was higher. This same analogy between ASM results and WA can also be observed for samples added to residue R2, where the percentage of 5 % residue R2 obtained the highest ASM value. This fact was expected and indicates the amount of R1 or R2 residues that resulted in higher densification. For additions above this lower percentage, lower ASM values were obtained.

Figure 7.15 shows the graph with the ASM results of samples added to feldspar and samples added to residues R1 and R2 associated with feldspar.

Samples with addition of feldspar obtained increasing ASM values as the percentage of flux addition increases. Thus, it was possible to establish a trend curve for these results, suggesting that the densification of the ceramic body increases as the percentage of feldspar in the mass increases. Samples with associated residue R1 and feldspar obtained ASM values close to that of MP sample. When comparing the ASM values of MB+17.5F sample with the results of MB+17.5F+4.5R1 and MB+17.5F+2.25R1 samples, it can be seen that the addition of residue R1 did

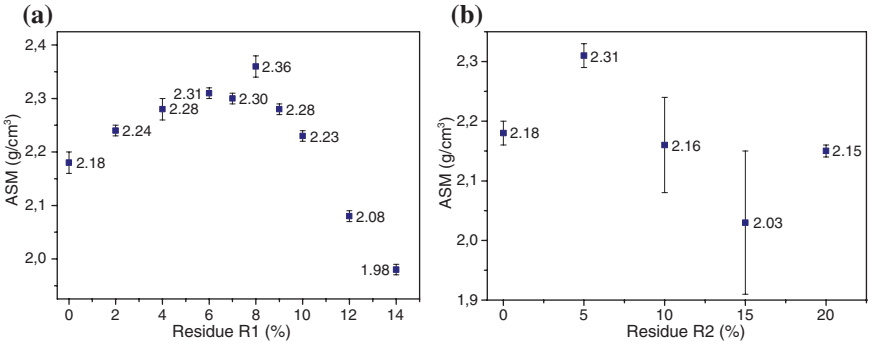

Fig. 7.14 Results of the ASM values of samples containing R1 (**a**) R2 (**b**)

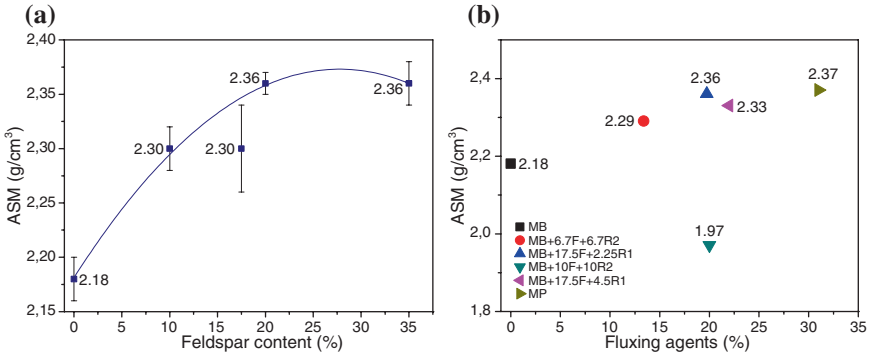

Fig. 7.15 ASM results of samples containing feldspar (**a**) and association of residue + feldspar (**b**)

not affect significantly the ASM results, remaining between 2.33 and 2.36 g/cm^3, respectively.

The MB+6.7F+6.7R2 sample obtained ASM values a little below the aforementioned sample and MB+10F+10R2 sample obtained a value even lower, 1.97 g/cm^3. In this case, comparing the ASM value with the green density value (Table 7.1) of MB+10F+10R2 sample, it can be inferred that after heat cycle, the apparent density value did not change substantially. Possibly, considering the thermal cycle to which it was submitted, the MB+10F+10R2 sample has surpassed the maximum densification point, where from this, the appearance of pores (in this case, closed) increased and the body became less dense or with higher amount of internal voids. The RSM values of the fired body were determined in order to calculate the total porosity as procedures specified in item 3.6.8. Table 7.2 shows the RSM values of some samples, whose properties had positive or negative highlighting.

The RSM/ASM ratio is the compactness, which for sintered bodies gives a comparative view of the material densification. The higher the compactness value, the greater the densification of the ceramic body. According to the results, it can be seen that samples with feldspar (no residue) obtained increasing compactness values as the addition of feldspar is increased. Sample with the addition of 5 % residue R2 achieved higher compactness than MB sample, free of fluxes, indicating increased densification, and for higher percentages of residue R2, the compactness values decreased. The same effect can also be observed when comparing the compactness results between MB+6.7F+6.7R2 and MB+10F+10R2 samples, where compactness values decreased from 0.90 to 0.78, respectively.

7.2.6 Bending Rupture Tension (BRT)

BRT is an important property for ceramic coating. In porcelain tiles, the minimum BRT must be 37 MPa for glazed porcelain tiles and 42 MPa for technical porcelain

Table 7.2 RSM, ASM values, and compactness of sintered samples

Formulation	RSM (g/cm^3)	ASM (g/cm^3)	Green compactness
MB	2.56	2.18	0.85
MP	2.60	2.37	0.91
MB+4R1	2.62	2.27	0.86
MB+8R1	2.56	2.36	0.92
MB+12R1	2.53	2.08	0.82
MB+5R2	2.61	2.31	0.88
MB+10R2	2.54	2.16	0.85
MB+15R2	2.57	2.03	0.79
MB+10F	2.61	2.30	0.88
MB+17.5F	2.56	2.30	0.90
MB+35F	2.51	2.36	0.94
MB+17.5F+2.25R1	2.55	2.36	0.92
MB+17.5F+4.5R1	2.55	2.33	0.91
MB+6.7F+6.7R2	2.54	2.29	0.90
MB+10F+10R2	2.52	1.97	0.78

tiles as described in Table 2.2. Figure 7.16 shows graph containing the BRT results for samples with the addition of residues R1 and R2.

It was observed that samples with the addition of residue R1 (as single flux) showed, in general, BRT values far below the minimum recommended for porcelain tiles.

For masses with the addition of residue R2 (as single flux), it was observed that the addition of 5 % residue contributed to increased BRT from 25.99 to 30.54 MPa. For residue percentage between 10 and 15 %, no significant increase in BRT was observed. The BRT of a ceramic sample is inversely proportional to porosity, or for the same material, more porous bodies tend to be less resistant. Comparing the total porosity values (Table 7.1) of specimens containing percentages between 5 and 15 % of residue R2, it can be observed that even with a trend of decreased AP, there was a significant increase in CP. This explains the fact that even with very low AP and WA values, ceramic tiles have not reached higher BRT values. For higher levels of addition of residue R2, a decrease in BRT values was observed.

Figure 7.17 shows the BRT results of masses containing feldspar and association of residue + feldspar.

The BRT results referring to masses with the addition of feldspar (as single flux) indicate increasing trend of BRT due to the increasing content of feldspar in the mass. In general, the addition of feldspar promoted good behavior in relation to the mechanical strength of specimens, especially MB+35F sample with the addition of 35 % feldspar, which achieved BRT of 43.57 MPa.

Samples with associated residue R1 and feldspar (MB+17.5F+2.25R1 and MB+17.5F+4.5R1) showed decreased BRT values compared to MB+17.5F sample with 17.5 % feldspar. When 2.25 % of residue R1 was added to the mass with 17.5 %

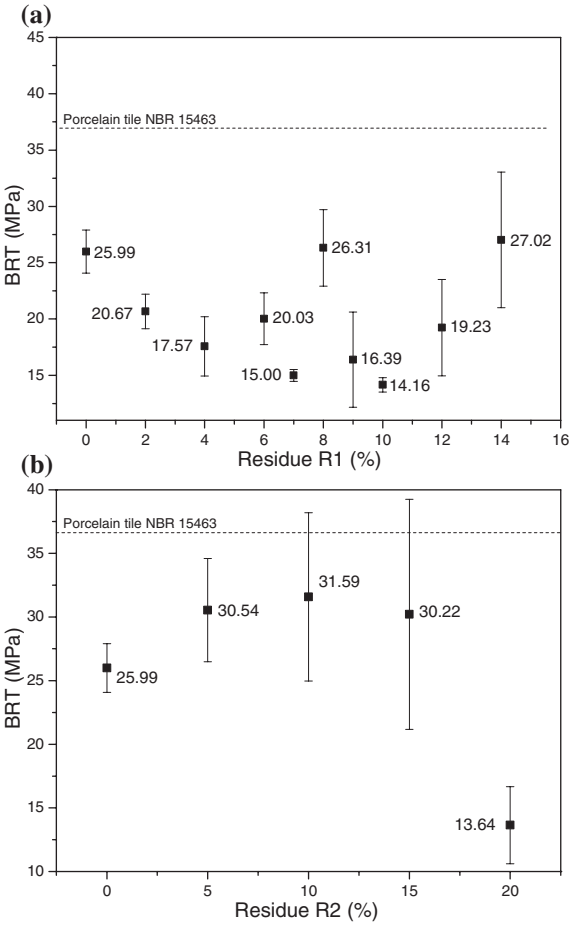

Fig. 7.16 Results of samples containing R1 (**a**) R2 (**b**)

feldspar, the BRT decreased from 37.79 to 25.19 MPa. With the addition of 4.5 % of residue R1 to the mass with 17.5 % feldspar, the BRT decreased from 37.79 to 19.12 MPa. The analysis of these results showed that residue R1 contributed to the decrease of the BRT. This effect may be due to the high mass loss of residue R1, seen in the TGA curve shown in Fig. 4.24, along with the lower viscosity of the liquid formed during firing.

Among the samples with associated residue R2 and feldspar (MB+6.7F+ 6.7R2 and MB+10F+10R2), MB+6.7F+6.7R2 sample showed BRT value of 46.03 MPa. It should be recalled that this sample obtained WA value of 0.12 % and therefore can be included in the range of porcelain tile classification established by NBR-15463. The BRT and WA results become very interesting considering the percentage of flux added to the MB+6.7F+6.7R2 mass. For comparison purposes, the MB+35F sample containing only feldspar as flux in the ratio of 35 % obtained WA of 0.97 % and BRT of 43.57 MPa. It was verified that the association

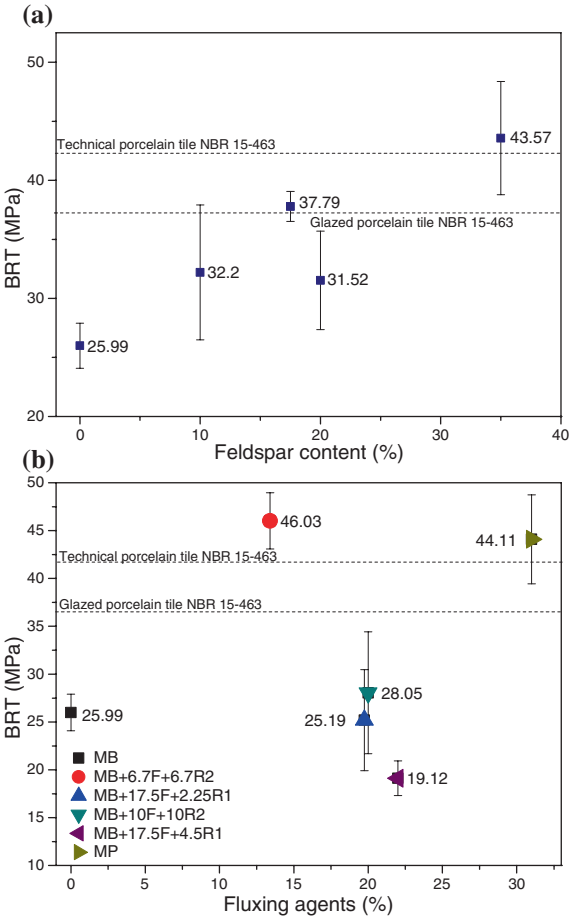

Fig. 7.17 BRT results of samples containing feldspar (**a**) and association of residue + feldspar (**b**)

of residue R2 with feldspar as flux is interesting from the point of view of reducing costs of raw materials and from the point of view of technical properties.

7.2.7 Vitrification Curve

The vitrification of ceramic materials is the measure of microstructure evolution of the material during firing. The vitrification curve used in ceramic tiles illustrates the thermal behavior of the material as a function of temperature. Normally, it is represented by two parameters: porosity and sintering. Porosity can be measured by water absorption (simplest and most widely used method) or by mercury porosimetry, whereas sintering is measured by the linear shrinkage (most used), or thermal expansion (Sanchez-Muñoz et al. 2002).

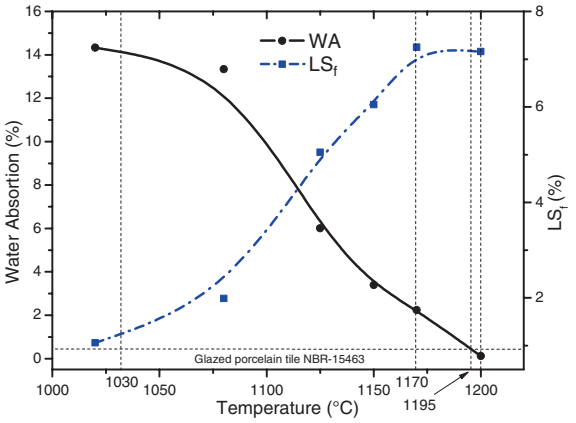

Fig. 7.18 Vitrification curve of MB+6.7F+6.7R2 sample

Of all masses used in this work, MB+6.7F+6.7R2 sample was the only one that, after sintering, obtained WA and BRT results within the specified range for the manufacture of porcelain tiles. Therefore, the behavior of the microstructure using the vitrification curve was investigated. Figure 7.9 shows the vitrification curve of MB+6.7F+6.7R2 mass.

The WA curve follows a decreasing trend up to temperature of 1,200 °C, while the LSf curve follows an increasing trend, with a trend of stabilization from temperature 1,170 °C. According to Sánchez-Muñoz et al. (2002), the temperature corresponding to beginning of the decrease of WA and increase of LSf is the temperature of formation of the melting phase, which in the case of the heating cycle of MB+6.7F+6.7R2 is below the lowest temperature investigated at 1,020 °C. Upon reaching this temperature, all clay transformations, i.e., dehydration and dehydroxylation have occurred, as well as the partial transformation of kaolinite into mullite and the appearance of early stages of molten material and the material develops WA smaller and LSf increasingly higher. This process is known as sintering. According to the authors, sintering progresses up to the optimum firing temperature, which is characterized by being the temperature at which the lowest WA value occurs, and this should coincide with the highest LSf.

In the MB+6.7F+6.7R2 mass cycle, LSf increased up to temperature of 1,170 °C, where constant values tended to occur. For MB+6.7F+6.7R2 mass, the optimum firing temperature was 1,200 °C. However, for the manufacture of glazed porcelain tiles, NBR-15463 recommends WA $\leq$ 0.5 % and it could be observed that, for this WA value, there is a possibility of the firing temperature to be slightly below 1,200 °C, resulting in decreased operating costs. The graph of Fig. 7.18 highlights the temperature of 1,195 °C, for which, according to the results obtained, the WA value is 0.5 %.

References

Biffi GO (ed) (2002) Grês Porcelanato: manual de Fabricação e Técnicas de Emprego. Faenza Editrice do Brasil, São Paulo

Noni JRA, Hotza D, Soler VC, Vilches ES (2010) Influence of composition on mechanical behaviour of porcelain tile. Part I: microstructural characterization and developed phases after firing. Mater Sci Eng A 527:1730–1735

Sanchez-Muñoz L, Cava SS, Paskocimas CA, Cerisuelo E, Longo E, Carda JB (2002) Modelamento do Processo de Gresificação de Massas Cerâmicas de Revestimento. Revista Cerâmica 48(308):217–222

Chapter 8
Mullite and Leucite Formation

Abstract In this chapter will be discussed the formation of mullite and leucite by scanning electron microscopy (SEM) and their consequence on the properties of CBA incorporated materials. SEM images of the fracture surface were presented showing both the crystalline phases.

Keywords Mullite · Leucite · SEM analyzes

In this chapter will be discussed the formation of mullite and leucite by scanning electron microscopy (SEM) and their consequence on the properties of CBA incorporated materials.

8.1 Scanning Electron Microscopy (SEM)

SEM analysis has become an essential tool for evaluating the microstructure of ceramic tiles. In ceramic coating, the fracture surface is usually investigated by SEM in order to assess the presence and characteristics of pores (shape, size) of the glass matrix and of crystalline phases. The analysis of the mullite phase in fired bodies gains particular importance in SEM images, since it is possible to make a distinction as to the form of the crystal, clearly defining if the observed mullite is primary (volumetric shape) or secondary (acicular morphology). The geometric shape of mullite crystals directly influences the mechanical performance of parts. According to Restrepo and Dinger (2003), mullite with acicular or needle shape reinforces the vitreous matrix the same way as fibers reinforce composites. Figures 8.1 and 8.2 show the SEM images related to the fracture surfaces of MP samples with magnifications of 100, 500, 3000 and 8000×, respectively. The rectangles marked in the images indicate the magnified region shown in the following images:

Figure 8.1b shows the existence of pores, mostly with spherical shape, characteristic of closed porosity in the presence of liquid phase. Figure 8.2 shows in

W. Acchar and E.J.V. Dultra, *Ceramic Materials from Coffee Bagasse Ash Waste*, SpringerBriefs in Applied Sciences and Technology,
DOI 10.1007/978-3-319-15281-3_8

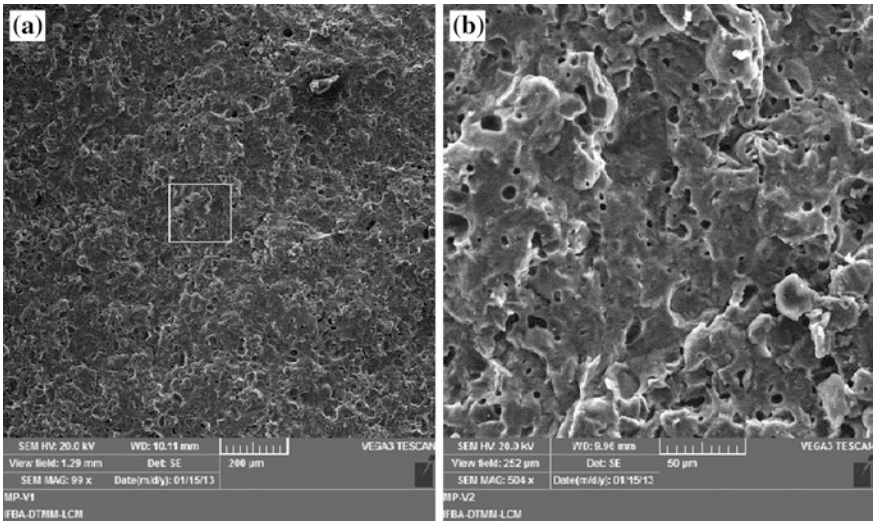

Fig. 8.1 SEM of fracture surface of MP sample with magnification of 100 (**a**) and 500× (**b**)

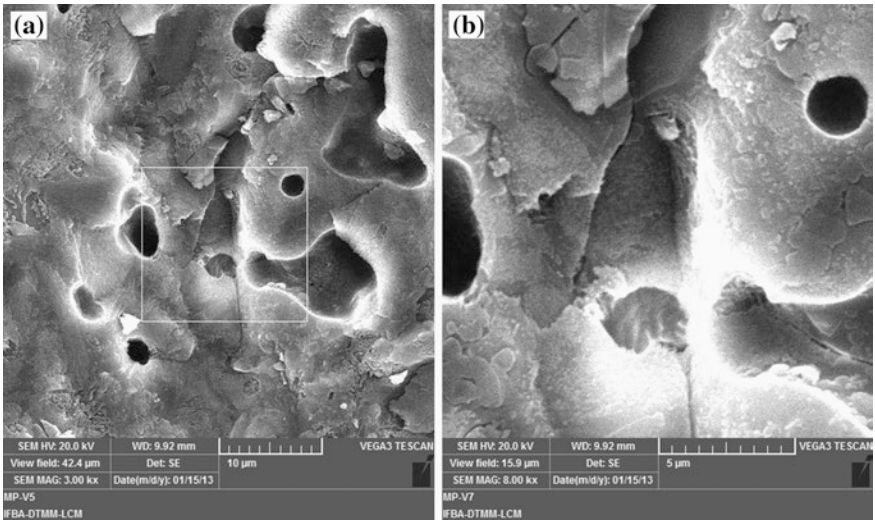

Fig. 8.2 SEM of fracture surface of MP sample with magnification of magnification of 3,000 (**a**) and 8,000× (**b**)

greater detail the size and shape of pores. Figure 8.2b shows small cracks possibly as a result of thermal contraction.

Figure 8.3 shows the SEM images of the fracture surface of MB sample (free from fluxes), with magnification of 100 and 500×. In XRD tests of the fired body, quartz and mullite phases were identified in the MB sample.

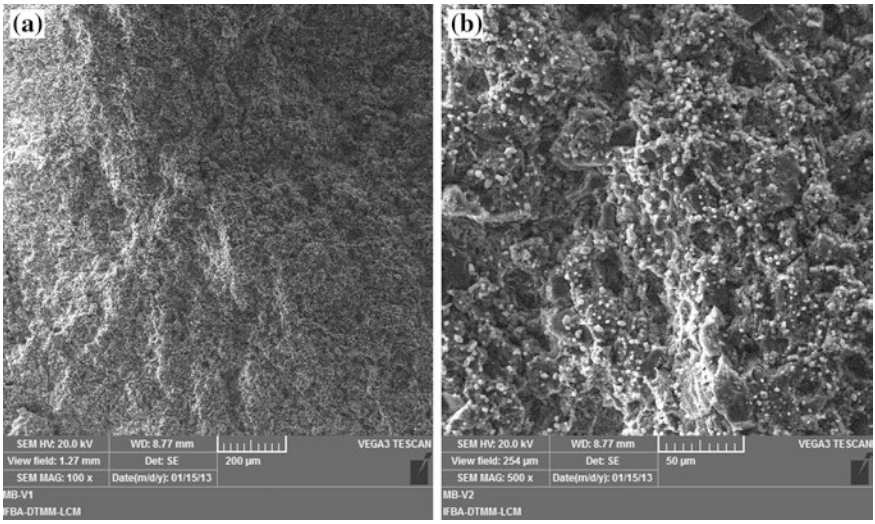

Fig. 8.3 SEM of fracture surface of MB sample with magnification of 100 (**a**) and 500× (**b**)

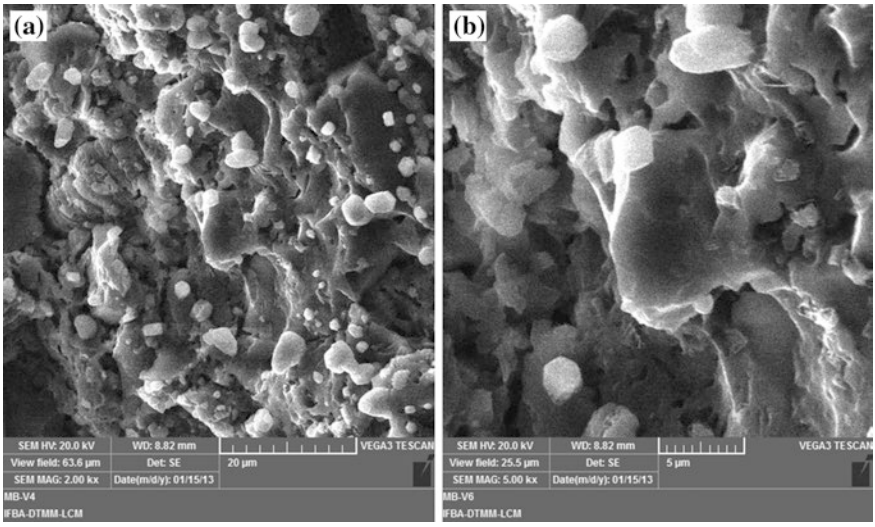

Fig. 8.4 SEM of fracture surface of MB sample with magnification of 2,000 (**a**) and 5,000× (**b**)

Figure 8.4 shows SEM images of the fracture surface of MB sample with magnification of 2,000 and 5,000×. The existence of cavities of irregular shape can be observed, confirming the existence of AP. According to the porosity results, MB sample showed no CP, or any existing porosity was open type. Figures 8.4b and 8.4a show the presence of primary mullite crystals.

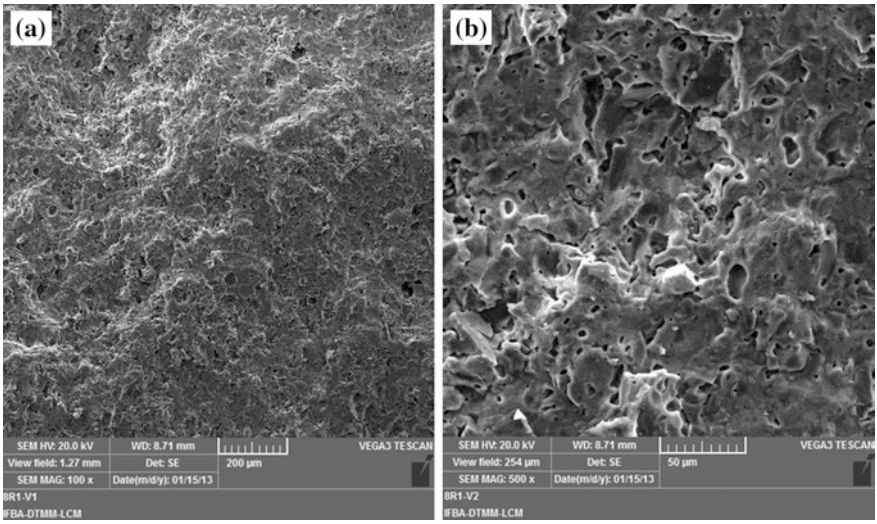

Fig. 8.5 SEM of fracture surface of MB+8R1 sample with magnification of 100 (**a**) 500× and (**b**)

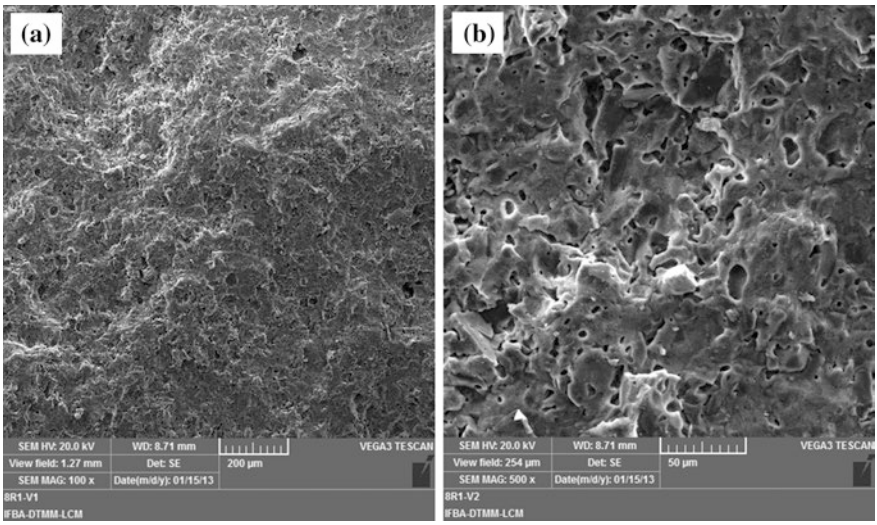

Fig. 8.6 SEM of fracture surface of MB+8R1 sample with magnification of 2,000 (**a**) and 5,000× (**b**)

Figure 8.5 shows the SEM images of the fracture surface of MB+8R1 sample, with magnification of 100 and 500×. Cavities and irregular pores can be identified, confirming the existence of AP in the sample.

Figure 8.6 shows the SEM of fracture surface of MB+8R1 sample with magnification of 2,000 and 5,000×.

It is possible to identify some cracks of thermal origin, possibly caused by differences in contraction during cooling. Quartz particles, generally smaller than 10 μm immersed in the glassy phase can be observed.

Figure 8.7 shows SEM images of the fracture surface of MB+12R1 sample with magnification of 100 and 500×. Figure 8.7a shows a pore with size of about 100 μm and of irregular shape.

The addition of residue R1 as single flux did not promote the growth of acicular-shaped mullite crystals. It is possible that the lower viscosity liquid formed has no influence on the thermodynamic conditions for the growth of secondary mullite crystal during firing. This may be one of the factors that explain the low flexural mechanical strength achieved by samples manufactured with added residue R1. The presence of leucite also contributed to reduced mechanical performance of MB+12R1 sample. The appearance of the fracture surface of MB+12R1 sample, shown in Fig. 8.7a, b suggest that there was little densification of the ceramic body, confirming the results of porosity and ASM tests, where the sample obtained TP equal to 17.97 %, of which 13.77 % of these pores were characterized as open, and ASM equal to 2.08 g/cm^3.

Figure 8.8 shows the SEM images of the fracture surface of MB+5R2, MB+10R2, and MB+15R2 samples with magnification of 100×.

Analyzing images in a comparative way, it was observed that in the range from 5 to 15 % of addition of R2, TP increased significantly as the percentage of residue increased. It was verified that, in most cases, pores are isolated and show spherical shapes, which indicates the presence of CP. Figure 8.8 confirmed the results of porosity tests, which pointed to the presence of CP, and in quantitative terms, tests indicated increased porosity as the percentage of residue R2 increased. This significant increase of closed pores within the ceramic body surely

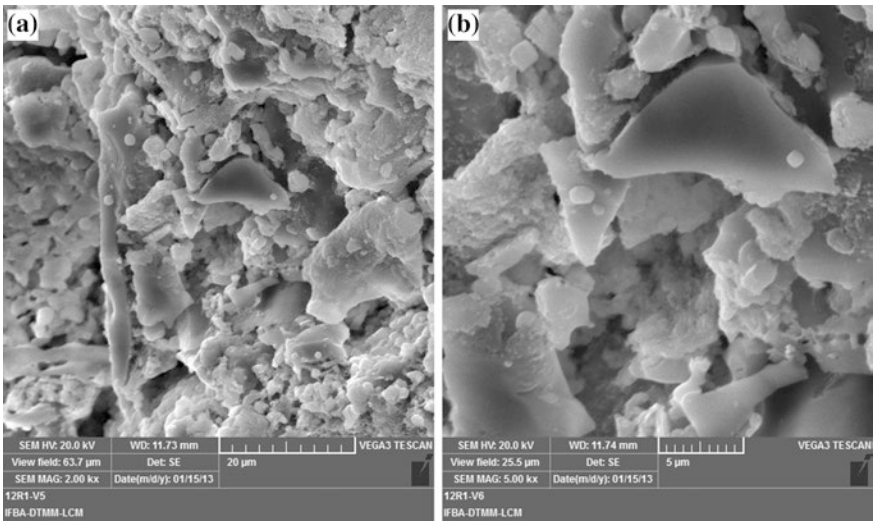

Fig. 8.7 SEM of fracture surface of MB+12R1 sample with magnification of 2,000 (**a**) and 5,000× (**b**)

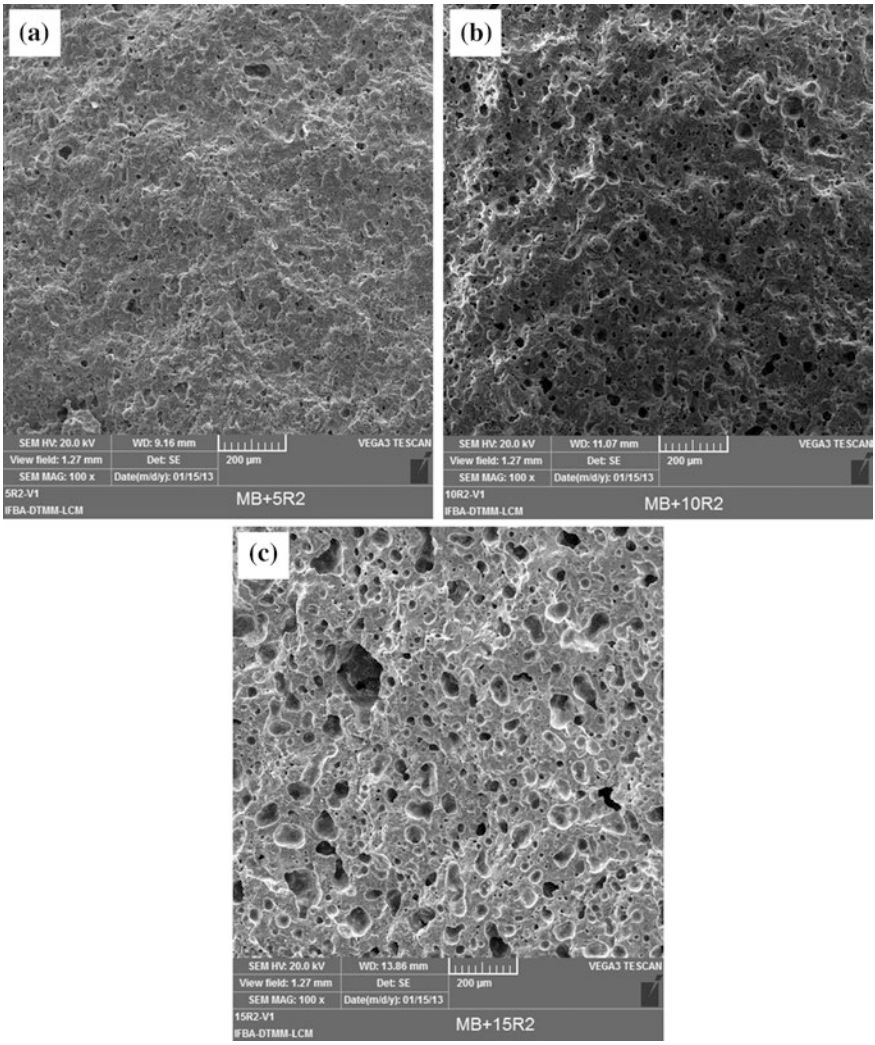

Fig. 8.8 SEM of the fracture surface of MB+5R2 (**a**), MB+10R2 (**b**), and MB+15R2 (**c**) sample with magnification of 100×

hampered the physical properties of LSf, ASM, and BRT as previous reviews. The images also showed that, besides the significant increase in the number of pores, the pore size also increased dramatically as the percentage of R2 increased. Higher porosity, along with increased pore size certainly influenced the mechanical performance of parts. It is noteworthy that each pore present within a ceramic body can act as a stress concentrator and cause the early onset of cracking, leading to the rupture of the material. The presence and characteristics of pores explain the fact that despite having extremely low AP and WA levels, parts with higher levels of R2 do not show high flexural strength.

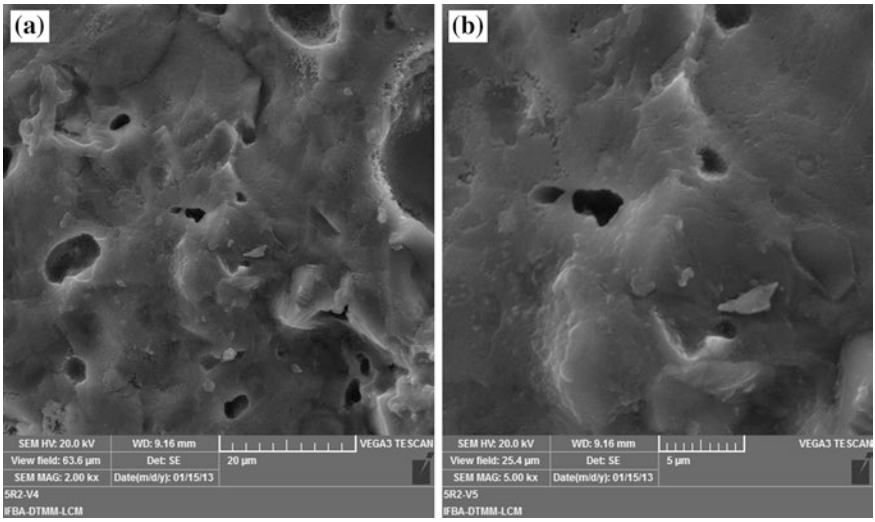

Fig. 8.9 SEM of the fracture surface of MB+5R2 sample with magnification of 2,000 (**a**) and 5,000× (**b**)

Although it is clear that the addition of residue R2 to ceramic mass causes increase in CP, when comparing the technical properties between MB and MB+5 R2 masses, it was observed that adding 5 % R2 decreased TP (24.2 %), decreased WA (77.8 %) and increased BRT (17.5 %), i.e., the addition of 5 % residue R2 resulted in improvements in key technical properties.

Figure 8.9 shows SEM images of the fracture surface of MB+5R2 sample with magnification of 2,000 and 5,000×. It is possible to observe in detail the presence of closed and isolated pores.

Figure 8.10 shows the SEM images of the fracture surface of MB+5R2 sample with magnification of 15,000×. The acicular mullite crystals can be easily identified. The existence of needles of maximum size of 2 μm can be observed. The existence of these secondary mullite crystals suggest that the amount and viscosity of the liquid phase formed during firing promoted not only the filling of pores, but established thermodynamic conditions favorable to the nucleation and growth of mullite needles. These two characteristics should be taken into consideration when evaluating a flux material, as the filling of pores reduces WA and TP, while the mullite needles reinforce the glassy matrix, contributing to the mechanical strength. It is worth mentioning that the porcelain tile must necessarily exhibit low water absorption (≤0.5 %) and high mechanical strength (≥37 MPa).

Figure 8.11 shows SEM images of the fracture surface of MB+10R2 sample with magnification of 2,000 and 5,000×.

In the image of Fig. 8.9, it is possible to observe a crack, possibly of thermal origin, due to the contraction difference during cooling. Similarly to MB+5R2 sample, acicular crystals were identified; however, of maximum size of 4 μm, that

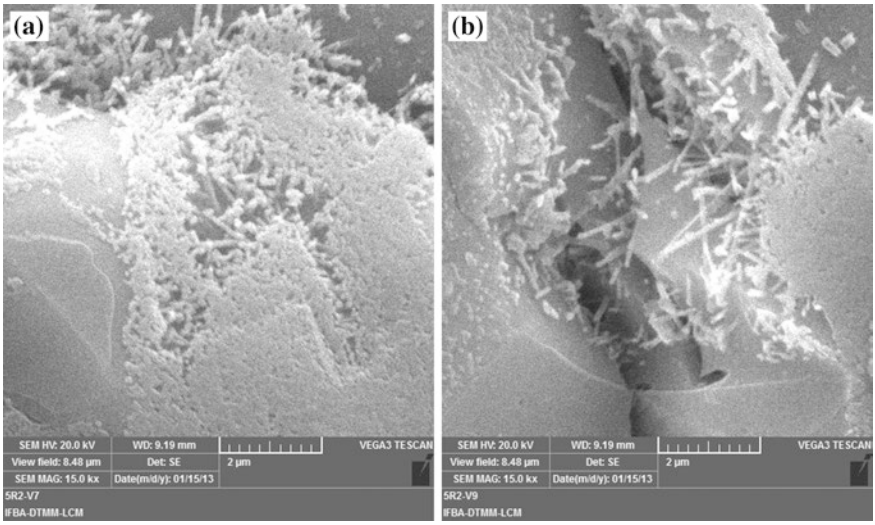

Fig. 8.10 SEM of the fracture surface of MB+5R2 sample, with magnification of 15,000× (**a**) and (**b**)

is, higher than those observed in Fig. 8.10. Theoretically, larger acicular crystals would reinforce the glassy matrix; however, the BRT results contradict this claim, as compared to the MB+5R2 sample, the MB+10R2 sample showed no significant increase in mechanical strength. Certainly, the highest closed porosity of MB+10R2 sample negatively affected performance in relation to the mechanical flexural strength (Noni et al. 2010). Another factor that surely influenced the lower mechanical performance of MB+10F+10R2 sample was the presence of the leucite phase, as in Fig. 8.11, it is possible to verify the presence of spherical crystals whose geometry is characteristic of leucite, according to trend indicated by the phase diagram shown in Fig. 6.3.

Figure 8.12 shows SEM images of the fracture surface of MB+15R2 sample with magnification of 2,000 and 5,000×. According to the XRD results, the crystalline phases present in MB+15R2 sample were quartz, leucite, and anorthite.

Based on the analysis of results, the addition of residue R2 as single flux should be of 5 % of added residue, as for larger amounts, the closed porosity tends to increase and negatively influence the mechanical performance of parts.

Figure 8.13 shows SEM images of the fracture surface of MB+7.5F+2.25R1 sample with magnification of 100 and 500×.

According to the image in Fig. 8.13b, the existing pores are mostly irregularly shaped.

Figure 8.14 shows SEM images of the fracture surface of MB+17.5F+4.5R1 sample with magnification of 100 and 500×. Some pores, viewed in the image of Fig. 8.14a, have spherical shape, with maximum size of about 50 µm. In Fig. 8.14b, irregularly shaped pores can be identified.

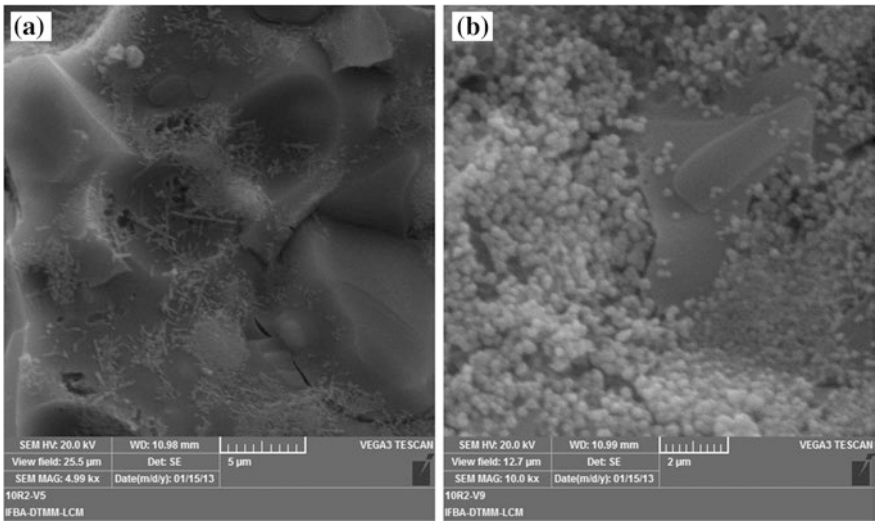

Fig. 8.11 SEM of the fracture surface of MB+10R2 sample with magnification of 5,000 (**a**) and 10,000× (**b**)

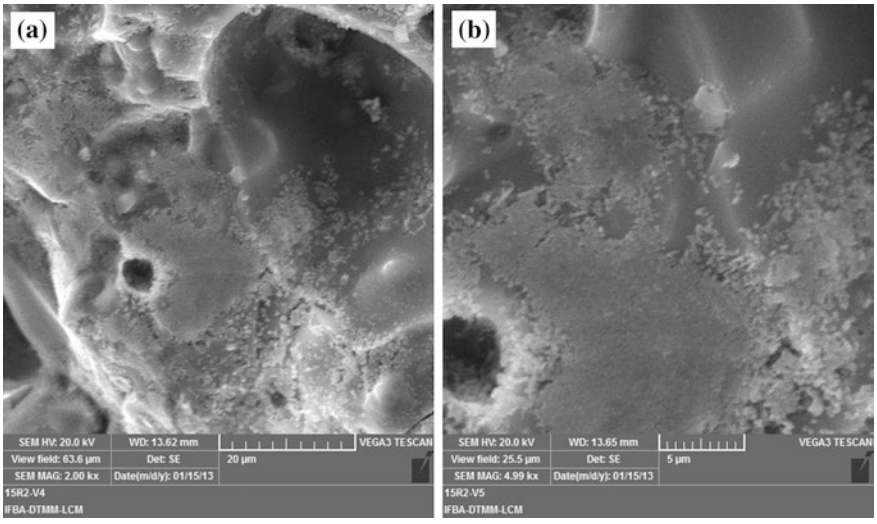

Fig. 8.12 SEM image of the fracture surface of MB+15R2 sample with magnification of 2,000 (**a**) and 5,000× (**b**)

Figure 8.15 shows SEM images of the fracture surface of MB+17.5F+2.25R1 and MB+17.5F+4.5R1 samples with magnification of 5,000×. Discrete acicular crystals of secondary mullite can be viewed, mostly less than 1 µm in size.

The addition of residue R1 plus feldspar as flux in MB+17.5F+2.25R1 and MB+17.5F+4.5R1 samples contributed to the formation of a microstructure with

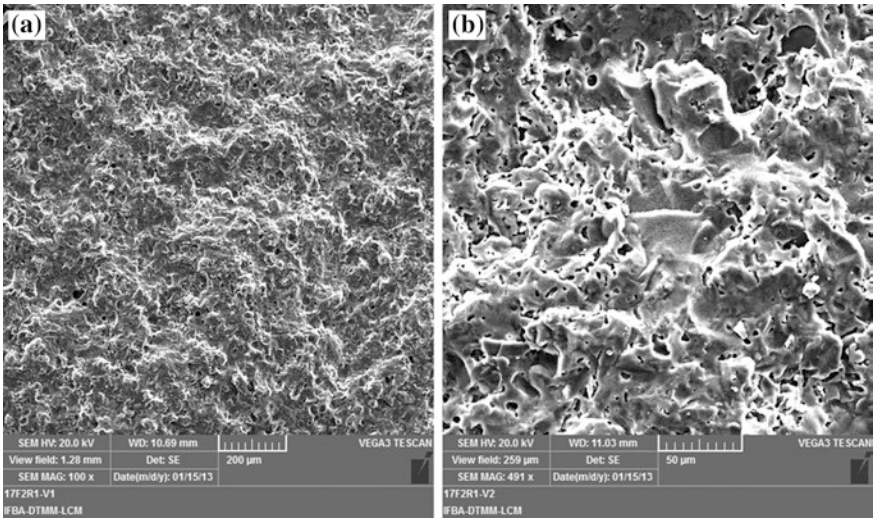

Fig. 8.13 SEM of the fracture surface of MB+17.5F+2.25R1 sample with magnification of 100 (**a**) and 500× (**b**)

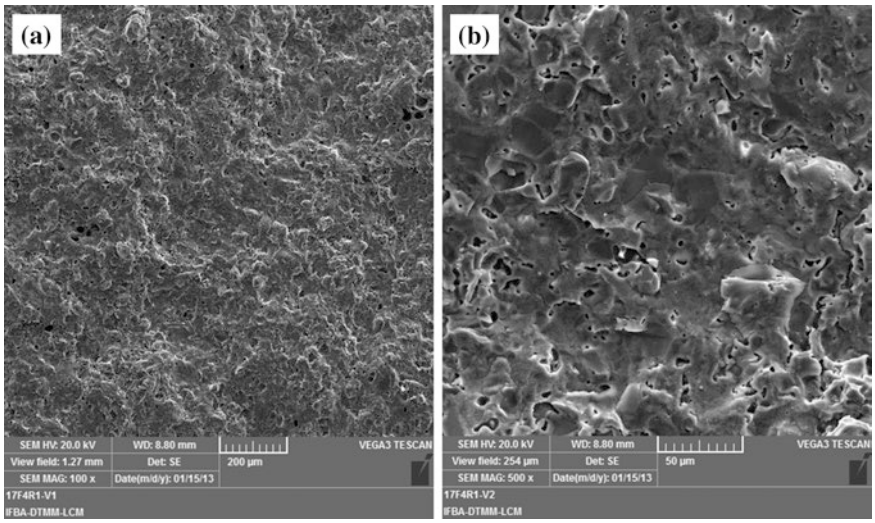

Fig. 8.14 SEM images of the fracture surface of MB+17.5F+4.5R1 sample with magnification of 100 (**a**) and 500× (**b**)

pores of irregular shape and little formation of secondary mullite (Segadães 2006). The acicular crystals viewed had maximum dimensions of about 1 µm, and according to the BRT results, even with the presence of crystals of secondary mullite, the mechanical strength was lower for MB+17.5F+2.25R1 and MB+17.5F+4.5R1 samples when compared to MB+17.5F sample.

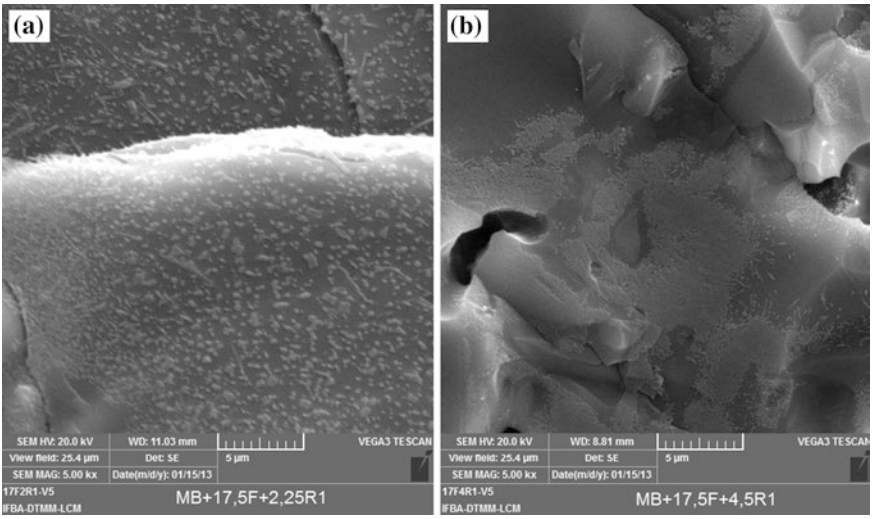

Fig. 8.15 MEV da superfície de fratura das amostras MB+17.5F+2.25R1 (**a**) e MB+17.5F+4.5R1 (**b**), com ampliação de 5,000×

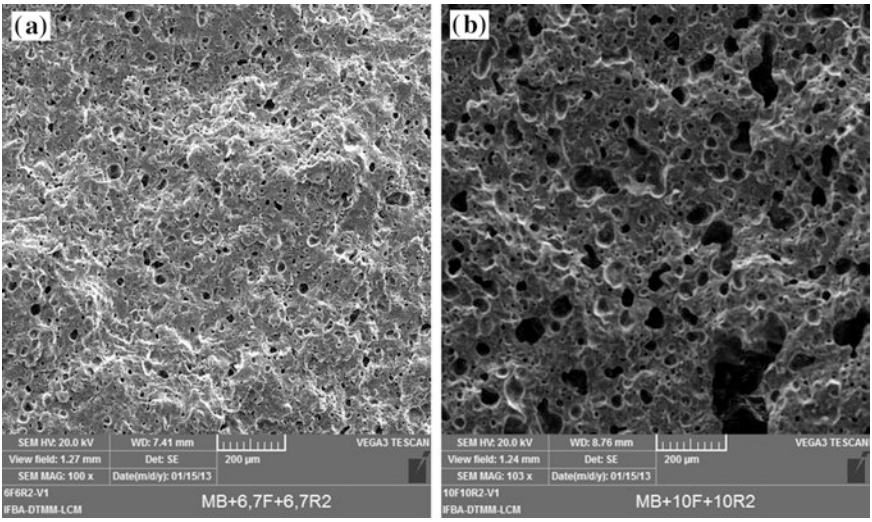

Fig. 8.16 SEM images of the fracture surface of MB+6.7F+6.7R2 (**a**) and MB+10F+10R2 (**b**) samples with magnification of 100×

Figure 8.16 shows SEM images of the fracture surface of MB+6.7F+6.7R2 and MB+10F+10R2 samples with magnification of 100×. Again, it could be observed that the internal porosity in MB+10F+10R2 sample was higher when compared with MB+6.7F+6.7R2 sample, confirming that higher addition of

residue R2 contributed to increase the CP of parts. The images confirmed the results of porosity test, where the MB+6.7F+6.7R2 sample showed TP equal to 9.80 % and CP equal to 9.52 % (both within the usual range for porcelain tiles), while MB+10F+10R2 sample obtained TP equal to 21.89 % and CP equal to 20.97 %, according to porosity tests shown in Table 7.2. As previously mentioned, porosity with these characteristics arises mainly due to the release of gases resulting from chemical reactions and also, the liquid formed during firing must necessarily have viscosity high enough to trap these gases inside the ceramic body.

Secondary mullite crystals were found in all regions investigated of the MB+6.7F+6.7R2 sample (Fig. 8.17). As previously mentioned, the appearance of secondary mullite crystals suggests that the amount and viscosity of the liquid phase formed during firing determine the thermodynamic conditions for nucleation and growth of mullite needles. This feature is important in the microstructure of porcelain tiles, because acicular mullite in format reinforces the glassy matrix resulting in ceramic bodies with higher mechanical strength.

Figure 8.18 shows the SEM images of the fracture surface of MB+10F+10R2 sample with magnification of 2,000 and 5,000×. Acicular crystals of secondary mullite can be observed.

Despite the presence of secondary mullite, MB+10F+10R2 sample showed no satisfactory BRT value (28.05 MPa) and obtained results far below the minimum established by NBR-15463 (≥37 MPa). The effects of excessive porosity were

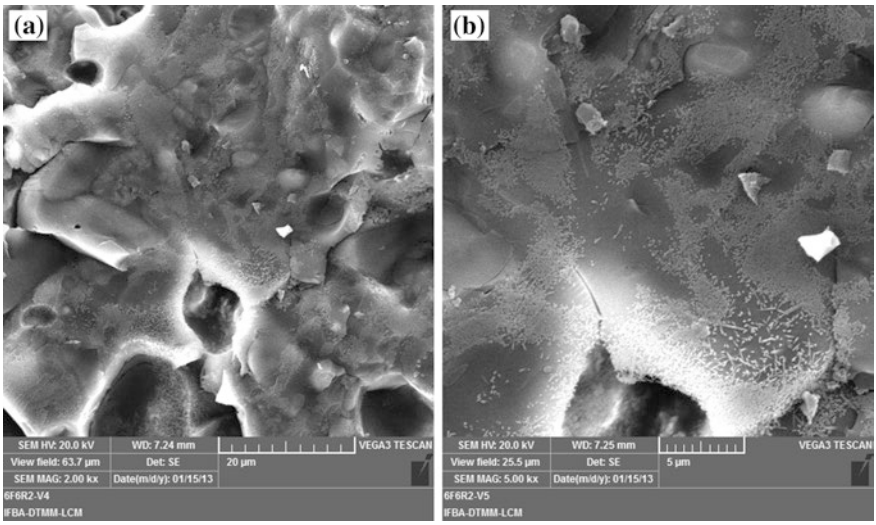

Fig. 8.17 SEM images of the fracture surface of MB+6.7F+6.7R2 sample with magnification of 2,000 (**a**) and 5,000× (**b**)

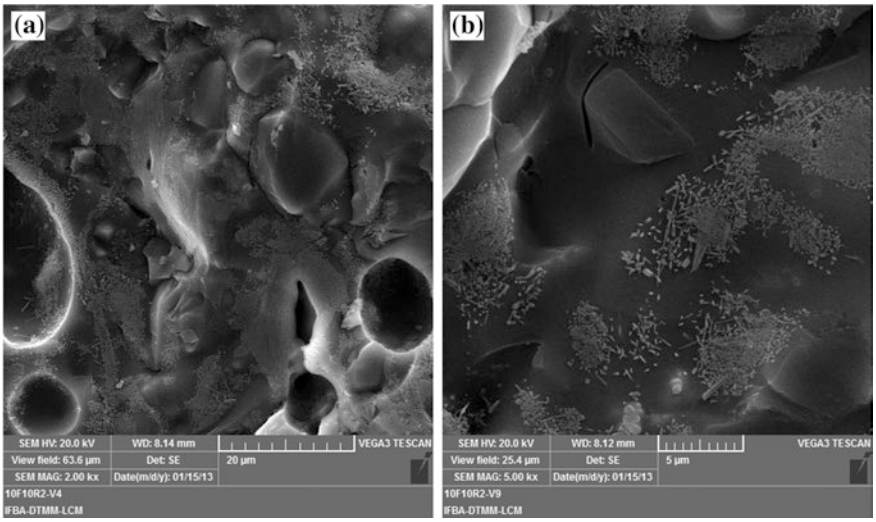

Fig. 8.18 SEM images of the fracture surface of MB+10F+10R2 sample with magnification of 2,000 (**a**) and 5,000× (**b**)

crucial for the BRT results of the MB+10F+10R2 sample, since the presence of secondary mullite was not enough to ensure good results.

References

Noni JRA, Hotza D, Soler VC, Vilches ES (2010) Influence of composition on mechanical behaviour of porcelain tile. Part I: microstructural characterization and developed phases after firing. Mater Sci Eng A 527:1730–1735

Restrepo JJ, Dinger DR (2003) Controle da Deformação Piroplástica em Massas de Porcelanas Triaxiais Usando a Análise Dilatométrica. Revista Cerâmica Industrial 8(4):37–48

Segadães AM (2006) Use of phase diagrams to guide ceramic production from wastes. Adv Appl Ceram 105(1):46–54